



THE HONG KONG
POLYTECHNIC UNIVERSITY

香港理工大學

Pao Yue-kong Library

包玉剛圖書館

Copyright Undertaking

This thesis is protected by copyright, with all rights reserved.

By reading and using the thesis, the reader understands and agrees to the following terms:

1. The reader will abide by the rules and legal ordinances governing copyright regarding the use of the thesis.
2. The reader will use the thesis for the purpose of research or private study only and not for distribution or further reproduction or any other purpose.
3. The reader agrees to indemnify and hold the University harmless from and against any loss, damage, cost, liability or expenses arising from copyright infringement or unauthorized usage.

If you have reasons to believe that any materials in this thesis are deemed not suitable to be distributed in this form, or a copyright owner having difficulty with the material being included in our database, please contact lbsys@polyu.edu.hk providing details. The Library will look into your claim and consider taking remedial action upon receipt of the written requests.

The Hong Kong Polytechnic University
Department of Civil and Structural Engineering

**MEASUREMENT OF ATMOSPHERIC
PEROXYACETYL NITRATE (PAN)
AND THE IMPLICATIONS TO PHOTOCHEMICAL
POLLUTION**

Zhang Jiamin

**A thesis submitted in partial fulfillment of
the requirements for the
Degree of Master of Philosophy**

January 2009

CERTIFICATE OF ORIGINALITY

I hereby declare that this thesis is my own work and that, to the best of my knowledge and belief, it reproduces no material previously published or written, nor material that has been accepted for the award of any other degree or diploma, except where due acknowledgement has been made in the text.

_____ (Signed)

Zhang Jiamin (Name of student)

ABSTRACT

Knowledge of the atmospheric abundance of peroxyacetyl nitrate (PAN) is important for assessing the severity of photochemical pollution and for understanding the chemical transformation of reactive odd nitrogen and its impact on the tropospheric ozone (O₃) budget. Although available monitoring data on O₃ have shown serious photochemical pollution in China, there have been few published continuous measurements of PAN in the country.

In this project, continuous measurements of PAN were made using an automatic GC-ECD analyzer with an on-line calibration device at an urban site in Hong Kong (HK, southern China) and a rural site at Mt. Tai (TS, eastern China), in 2007. O₃ and other trace gases measured as part of TS study were used to support the interpretation of PAN data. Data obtained from previous measurements at a suburban site in Lanzhou (LZ, western China), a remote site at Mt. Waliguan (WLG, western China), and the HK site in 2006 were also analyzed to obtain a more comprehensive picture of PAN in China. The data were examined in terms of time series, statistical analysis, diurnal patterns, correlations between PAN and other species, nitrogen budgets, and regional transport.

Strong photochemical production was found at urban sites, with average PAN mixing ratios of 0.76, 0.74, and 0.94 ppbv in LZ, HK 2006, and HK 2007

studies. Of the two mountain top sites, Mt. Tai, which is situated in the polluted North China Plains, had average PAN concentrations of 1.17 and 0.77 ppbv in spring and summer, whereas the remote WLG site had an average value of 0.44 ppbv, which represents the background level of photochemical pollution in East Asia.

The PAN mixing ratios at the two urban sites (LZ and HK) exhibited strong diurnal variations, with peaks at noon and in the early afternoon. At the polluted mountain top site (TS), PAN levels showed peaks in the afternoon and troughs in the early morning, whereas increased concentrations were observed in the evening at WLG. The correlations between PAN and O₃ were analyzed to shed light on the photochemical processes occurring in different regions. The regression slopes of the daily maximum PAN versus O₃ ranged from 0.091 to 0.020 ppbv ppbv⁻¹ in LZ, HK, and at TS. The differences in slopes are in part due to different compositions of volatile organic compounds in these areas. Nitrogen budgets were computed for Mt. Tai, for which data on individual reactive nitrogen (NO_y) compounds were available, and PAN was found to contribute a small fraction to NO_y compared with nitric acid and particulate nitrate.

Data from the two mountain top sites were also examined to determine the regional transport of air pollution. At polluted Mt. Tai in eastern China, transport of pollutants from different regions to the summit was found using back

trajectory analysis, with a notable impact from Korea and Japan being identified. At remote Mt. Waliguan in western China, backward particle release simulation showed that high-PAN events were mostly associated with the transport of air masses that had passed over Lanzhou.

ACKNOWLEDGMENTS

I would like to thank Prof. Tao Wang, the chief supervisor of this project, for his guidance and support during my research. He provided me with an invaluable opportunity to conduct research as part of several field studies. In overcoming the difficulties of working at rural and remote sites, I acquired precious experience in setting up and operating the most advanced research instruments and developed skills in problem solving and interpersonal communication. In addition to the field study research, the many helpful discussions with Prof. Wang during the analysis of the datasets gave me important insights that shaped my research style and improved my scientific perspective on atmospheric chemistry.

I would also like to express my sincere gratitude to Mr. Steven Poon, Mr. Likun Xue, Dr. Jian Gao, Mr. W.S. Wu, and the staff at the Mt. Waliguan and Mt. Tai Observatories for their assistance with the field studies, and to Dr. Rainer Schmitt for setting up the PAN-Analyzer at Lanzhou. I am also grateful to Dr. Aijun Ding and Dr. Yu Ren for their valuable comments on the project. Special thanks go to Dr. Aijun Ding for conducting the backward Lagrangian particle release simulation. I would also like to thank Prof. Jianmin Chen for his encouragement and support during the development of my research and Dr. Mike Poole for his editing English in this thesis. I thank NOAA Air Resources Laboratory for providing the HYSPLIT model and the Environmental Protection

Department of Hong Kong for providing the O₃ data. Last but not least, I would like to thank my family and my many friends at the Hong Kong Polytechnic University for their support and encouragement throughout my postgraduate study.

This project was funded by a studentship provided by the Hong Kong Polytechnic University. I also acknowledge financial support for the field studies from the Hong Kong Research Grants Council (Project No. PolyU5144/04E), Hong Kong Polytechnic University (Project 1-BB94) and the National Basic Research Program of China (973 program No. 2005CB4422203).

TABLE OF CONTENTS

LIST OF FIGURES	iv
-----------------------	----

LIST OF TABLES.....	vii
---------------------	-----

SECTION I: INTRODUCTION

CHAPTER 1: INTRODUCTION.....	1
------------------------------	---

CHAPTER 2: LITERATURE REVIEW	6
------------------------------------	---

2.1. Definition and importance of PAN as a photochemical air pollutant	6
---	---

2.2. Formation and decomposition mechanisms of PAN.....	9
---	---

2.3. The role of PAN in the photochemical oxidant cycle.....	13
--	----

2.4. Ambient concentrations and characteristics of PAN.....	15
---	----

2.4.1. Ambient concentrations of PAN in North America, South America, and Europe.....	16
--	----

2.4.2. Characteristics of PAN in South America, North America, and Europe	18
--	----

2.4.3. Limited information on PAN in Asia.....	20
--	----

2.5. Photochemical pollution studies in China.....	21
--	----

CHAPTER 3: SIGNIFICANCE AND OBJECTIVES	25
--	----

SECTION II: EXPERIMENTAL SECTION

CHAPTER 4: METHODOLOGY.....	27
-----------------------------	----

4.1. Study areas and measurement sites	27
--	----

4.1.1. Lanzhou.....	30
---------------------	----

4.1.2. Hong Kong	33
------------------------	----

4.1.3. Mt. Tai	35
----------------------	----

4.1.4. Mt. Waliguan.....	39
--------------------------	----

4.2.	Measurement techniques, quality control, and assurance.....	42
4.2.1.	PAN-Analyzer	42
4.2.2.	Instruments for the measurement of other trace gases	48
4.3.	Back trajectory analysis and backward particle release simulation	52

SECTION III: RESULTS AND DISCUSSION

CHAPTER 5: GENERAL DATA DESCRIPTION..... 56

5.1.	Time series.....	56
5.2.	Statistical analysis.....	64
5.3.	Comparison with other locations	70

CHAPTER 6: DIURNAL PATTERNS..... 76

6.1.	Diurnal patterns in urban areas.....	76
6.2.	Diurnal patterns in rural areas	80
6.3.	Diurnal patterns in remote areas	86

CHAPTER 7: RELATIONSHIP BETWEEN PAN AND OTHER GAS

SPECIES..... 89

7.1.	Correlation between PAN and O ₃	89
7.1.1.	Overall results	89
7.1.2.	Correlation between the PAN daily maximum and the O ₃ daily maximum.....	93
7.2.	Relationship between PAN and other gas species.....	98
7.2.1.	Overall results	98
7.2.2.	Nitrogen budget.....	100

CHAPTER 8: REGIONAL TRANSPORT ANALYSIS 104

8.1.	Eastern China.....	104
8.2.	Western China.....	112
8.2.1.	Overall results	112
8.2.2.	Case study of pollution transport to Mt. Waliguan.....	115

CHAPTER 9: CONCLUSIONS.....	121
9.1. Summary of the major scientific findings.....	121
9.2. Suggestions for future work.....	124
 REFERENCES.....	 127

LIST OF FIGURES

Figure 2-1. Formula of peroxyacetyl nitrate (PAN).	6
Figure 2-2. Organic radicals and products in the photooxidation of an organic molecule.....	14
Figure 2-3. Reactive nitrogen compounds in the photochemical oxidant cycle.....	15
Figure 2-4. Peak concentrations of PAN at southern California locations, 1960-1997. Source: Grosjean, 2003.	17
Figure 4-1. Map of China showing the sampling locations.....	27
Figure 4-2. Map showing the location and topography of the LZ site, the WLG site, and surrounding regions. The upper-right corner in the left panel depicts the CO emission intensity (Streets et al., 2006). The urban and industrial (Xigu) areas in Lanzhou are shown in red.	31
Figure 4-3. The LZ site and its surroundings: (a) view to the northwest (rural); (b) view to the east (urban); (c) view to the southwest (industrial). ...	32
Figure 4-4. Overview of the monitoring system in LZ.....	33
Figure 4-5. Map showing the HK study site.....	34
Figure 4-6. Overview of the laboratory in HK PolyU.....	35
Figure 4-7. Map showing the TS study site and surrounding regions.	37
Figure 4-8. The TS site and surroundings.....	38
Figure 4-9. Overview of the monitoring system at TS: (a) sample inlets and catalytic converter boxes; (b) real-time analyzers, calibration and data logging system.	39
Figure 4-10. The WLG site and surroundings.	41
Figure 4-11. Overview of the monitoring system at WLG: (a) sample inlets; (b) catalytic converter boxes; (c) real-time analyzers, calibration and data logging system.	41

Figure 4-12. PAN-Analyzer and Cal-Unit: (a) PAN-Analyzer (above) and calibration unit (below); (b) PAN-Analyzer; (c) calibration unit.	43
Figure 4-13. Oven module of the PAN-Analyzer in two different modes.	44
Figure 4-14. Chromatograms generated by Adam32 v1.42 for (a) an ambient sample with CCl ₄ as the first peak and PAN as the second peak; (b) calibration (PAN peak only).....	47
Figure 5-1. Time series of PAN, O ₃ , CO, and NO _y concentrations measured in LZ from June 18, 2006 to July, 17 2006.....	57
Figure 5-2. Time series of PAN and O ₃ measured in the HK 06 study (a) and PAN in the HK 07 study (b). Cases of strong photochemical pollution events are marked with 1 to 4 in (b).....	58
Figure 5-3. Time series of PAN, O ₃ , CO, NO _y , Total N, NH ₃ *, NO, NO ₂ , and SO ₂ measured at TS in the spring (a) and summer (b) studies.	61
Figure 5-4. Time series of PAN, O ₃ , CO, and NO _y measured at WLG from July 22, 2006 to Aug 16, 2006. Cases of regional transport are marked with 1 to 6.	63
Figure 6-1. Average diurnal patterns of PAN, O ₃ , CO, and NO _y in LZ; the error bars are standard errors.	77
Figure 6-2. Average diurnal patterns of PAN and O ₃ in the HK 06 study, and of PAN in the HK 07 study; the error bars are standard errors.....	79
Figure 6-3. Average diurnal patterns of PAN, O ₃ , CO, NO _y , Total N, NH ₃ *, NO, NO ₂ , and SO ₂ in the TS Spring study; the error bars are standard errors.	82
Figure 6-4. Average diurnal patterns of PAN, O ₃ , CO, NO _y , Total N, NH ₃ *, and SO ₂ in the TS Summer study; the error bars are standard errors.....	85
Figure 6-5. Average diurnal patterns of PAN, O ₃ , CO, and NO _y at WLG; the error bars are standard errors.	87
Figure 6-6. Comparison of the average diurnal patterns of PAN in LZ and at WLG; the error bars are standard errors.	88
Figure 7-1. Scatterplots of PAN versus O ₃ for the LZ (a), HK 06 (b), TS	

Spring (c), TS Summer (d), and WLG (e) studies.	92
Figure 7-2. Scatterplot of the PAN daily maximum versus the O ₃ daily maximum in the LZ, HK 06, HK 07, TS Spring, and TS Summer studies.	94
Figure 7-3. Mean profile of the C ₂ -C ₈ NMHCs measured in the LZ and TS studies.	95
Figure 7-4. Nitrogen budgets in the TS Spring and TS Summer studies. Daytime is defined as 0600 to 1750 BJT for the spring study and 0500 to 1950 BJT for the summer study. Nighttime is defined as 1800 to 0550 BJT for the spring study and 2000 to 0450 BJT for the summer study.	102
Figure 8-1. Examples of the eight types of air masses classified by the back trajectories: (a) south originating passing through eastern China (S) on June 29 at 2100 BJT; (b) west originating passing through central China (W) on Apr 7 at 0000 BJT; (c) continental originating (NW) on Mar 31 at 1200 BJT; (d) north originating (N) on Apr 2 at 0900 BJT; (e) northeast originating passing through the Northeast Plains (NE) on Apr 17 at 0300 BJT; (f) loop trajectories (LP) on July 14 at 1500 BJT; (g) eastern Asia originating (EA) on June 18 at 0000 BJT; and (h) marine originating (ME) on June 20 at 0900 BJT.	107
Figure 8-2. 10-min data for PAN, O ₃ , CO, and NO _y measured at WLG on (a) Aug 6, (b) Aug 7, (c) Aug 8, (d) Aug 9, (e) Aug 10, and (f) Aug 15.	116
Figure 8-3. Back trajectories showing the impact of LZ on WLG in six cases. (HYSPLIT 48-hour trajectory, GDAS data: 100 km, 3-h).....	117
Figure 8-4. Horizontal and vertical distribution of 36-h backward Lagrangian particle plumes at the peak hour of episodes on (a and b) Aug 7, (c and d) Aug 8, and (e and f) Aug 10, 2006. The particles are color-coded by age to show their historical distribution. The left panel shows the results for all vertical levels and the right panel shows the results for altitudes below 1 km (AGL).	119

LIST OF TABLES

Table 1-1. List of abbreviation terms.....	4
Table 2-1. Physical properties of peroxyacetyl nitrate (PAN).	7
Table 4-1. Summary of the field studies at the various sites.....	29
Table 5-1. Summary of the 10-min data from the LZ, HK 06, HK 07, TS Spring, TS Summer, and WLG studies.	65
Table 5-2. Comparison with other sites in polluted areas.	72
Table 5-3. Comparison with other sites in remote areas.	74
Table 7-1. Correlations between PAN and NO _y and between PAN and CO.	99
Table 7-2. Contributions of PAN to NO _y at LZ, TS, and WLG.....	103
Table 8-1. Statistical data on PAN, O ₃ , CO, NO _y , Total N, and SO ₂ in each air mass category captured at Mt. Tai.....	109
Table 8-2. Statistical data on PAN, O ₃ , CO, and NO _y in each air mass category captured at WLG	114

SECTION I: INTRODUCTION

CHAPTER 1: INTRODUCTION

Peroxyacetyl nitrate (PAN) is one of the most important photochemical pollutants in the atmosphere, and acts as an excellent indicator of photochemical air pollution and a reservoir for atmospheric odd nitrogen. PAN is both a reactive nitrogen (NO_y) compound and an organic species, and thus provides a unique link between the reactive nitrogen, hydrogen, and carbon cycles in gas-phase tropospheric chemistry (Prestbo, 1992). NO_y compounds (including nitrogen monoxide, nitrogen dioxide, PAN, nitric acid, particulate nitrate, etc.) are ubiquitous in the troposphere, which are involved in many complicated chemical processes in the atmosphere (Brasseur et al., 1999), and contribute to the formation of ground-level ozone (O₃) and acid rain. Some studies of nitrogen monoxide (NO) and NO_y have been conducted in Asia, but little is known about PAN, another oxidized nitrogen species. Studies of the atmospheric abundance of PAN and its relation with O₃ and O₃ precursors in China, where strong photochemical pollution has been reported in many O₃ studies, are particularly needed to better understand the sources of emission, the relative importance of gas-phase chemical reactions, the O₃ formation potential, and the role of nitrogen in acid deposition.

The lack of data on PAN in China is mainly due to a lack of reliable

instruments to measure it. This project applies a state-of-the-art online technique to measure the atmospheric concentrations of PAN and investigates the extent and mechanisms of photochemical pollution in China. Datasets from urban areas, rural areas, and background areas are presented in this study. Continuous measurements of PAN were conducted at an urban site in Hong Kong (HK) in southern China and at a rural site in Shandong Province (Mt. Tai, TS) in eastern China in 2007. The measurement of PAN at Mt. Tai was part of a comprehensive field study during which many parameters were measured. Trace gas species relevant to the interpretation of PAN were also analyzed in this thesis, including O₃, carbon monoxide (CO), NO_y, total nitrate (Total N, including nitric acid (HNO₃) and particulate nitrate (p-NO₃⁻)), ammonia and ammonium (NH₃^{*}), NO, nitrogen dioxide (NO₂), and sulfur dioxide (SO₂). In addition, data obtained in 2006 by the same atmospheric research team (led by Prof. Tao Wang) were processed and analyzed by the author of this study to provide a more complete picture of the properties of PAN in China. The data include PAN, O₃, CO, and NO_y collected at a suburban site, Lanzhou (LZ), and a remote site, Mt. Waliguan (WLG) in western China. PAN and O₃ data measured in HK in 2006 were also included.

The results on the PAN concentrations, diurnal patterns, and the relationship between PAN and other gas species at the four sites are presented in this thesis. The transport of regional pollution is also investigated with the aid of back

trajectory analysis.

This thesis comprises the following nine chapters.

- 1) Chapter 1 gives a general description of the project background, a brief introduction to the specific study, and an outline of the thesis.
- 2) Chapter 2 presents a comprehensive literature review of PAN's important role in the atmosphere and the mechanisms of its formation and decomposition. Ambient PAN concentrations at different locations, diurnal patterns, and the correlations between PAN and other gases are reviewed, along with previous photochemical pollution studies in areas related to the project.
- 3) Chapter 3 underlines the significance and objectives of the project.
- 4) Chapter 4 illustrates the methodologies adopted, including the selection of sampling sites, a description of the measurement instruments, and the methods used for the back trajectory analysis and backward particle release simulation.
- 5) Chapter 5 shows the general results obtained from the measurements taken at the four sites and presents statistical analysis of the data and comparisons with results from other locations.
- 6) Chapter 6 focuses on the diurnal variations in PAN in the areas under study.
- 7) Chapter 7 discusses the correlations between PAN and O₃ and other gas

species, and examines nitrogen budgets and the contributions of PAN to NO_y.

- 8) Chapter 8 classifies the back trajectories obtained in the TS and WLG field studies and analyses regional transport cases chosen from the datasets obtained during the field studies.
- 9) Chapter 9 provides a summary of the major findings of the project and suggests plans for further research.

Table 1-1 lists all the abbreviation terms in this thesis.

Table 1-1. List of abbreviation terms^a.

Abbreviation	Original Terms
AGL	Above ground level
ARL	Air Resources Laboratory
BJT	Beijing Time
BLC	Blue-light converter
CCl ₄	Carbon tetra-chloride
CG	Carrier gas
CO	Carbon monoxide
ECD	Electron capture detection
EPD	Environmental Protection Department
GAW	Global Atmospheric Watch
GC	Gas chromatographic
HK	Hong Kong
HK PolyU	Hong Kong Polytechnic University
HK 06	Hong Kong 2006
HK 07	Hong Kong 2007
HNO ₃	Nitric acid
HYSPLIT4 model	Hybrid Single-Particle Lagrangian Integrated Trajectory model
JST	Japan Standard Time
LED's	Light emitting diodes

Table 1-1. List of abbreviation terms^a (Continued).

Abbreviation	Original Terms
LPG	Liquefied petroleum gas
LT	Local time
LZ	Lanzhou
MoO	Molybdenum oxide
NH ₃ *	Ammonia and ammonium
NIST	US National Institute of Standards and Technology
NMHC	Non-methane hydrocarbon
NO	Nitrogen monoxide
NOAA	National Oceanic and Atmospheric Administration
NO _x	Oxides of nitrogen
NO _y	Reactive nitrogen
NO _z	Atmospheric oxidation products of reactive nitrogen
NO ₂	Nitrogen dioxide
NPN	N-propyl nitrate
O ₂	Oxygen
O ₃	Ozone
PA	Peroxyacetyl radical
PAN	Peroxyacetyl nitrate
PANs	Peroxyacetyl nitrates
PBL	Planetary boundary layer
PFA	Perfluoroalkoxy
p-NO ₃ ⁻	Particulate nitrate
PRD	Pearl River Delta
RH	Relative humidity
r ²	Correlation coefficient
SO ₂	Sulfur dioxide
Total N	Total nitrate
TS	Mt. Tai
TS Spring	Mt. Tai Spring Phase
TS Summer	Mt. Tai Summer Phase
VOCs	Volatile organic compounds
WLG	Mt. Waliguan
WMO	World Meteorological Organization

^aIn alphabetical order of the abbreviation terms.

CHAPTER 2: LITERATURE REVIEW

2.1. Definition and importance of PAN as a photochemical air pollutant

Peroxyacetyl nitrate (PAN) is the most common one of a homologous series of organic nitrogen compounds known as peroxyacetyl nitrates (PANs). In fact, both peroxyacetyl nitrate (PAN) and peroxyacetyl nitrates (PANs) are misnomers (Roberts, 1990), but have been used since the discovery of these compounds. The correct names are peroxyacetic nitric anhydride for PAN and peroxyacetic nitric anhydrides for PANs (Roberts et al., 2002), but in this thesis the common usage of peroxyacetyl nitrate (PAN) is retained unless otherwise stated. Figure 2-1 shows the formula of PAN.

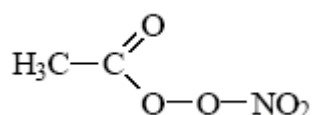


Figure 2-1. Formula of peroxyacetyl nitrate (PAN).

The physical properties of PAN are described in Table 2-1.

Table 2-1. Physical properties of peroxyacetyl nitrate (PAN)^a.

Chemical formula	CH ₃ C(O)O ₂ NO ₂
Physical state at NTP ^b	Colorless liquid
Relative molecular mass	121
Boiling point	No true boiling point, compound decomposes before boiling
Vapor pressure at room temperature	About 2 kPa

^aFrom: US Department of Health, Education and Welfare (1970).

^bNTP = normal temperature and pressure, i.e., 25°C and 101 kPa.

PAN is an important secondary pollutant that is formed by photochemical reactions involving volatile organic compounds (VOCs) and oxides of nitrogen (NO_x). It has received particular interest because of its biological activity as a strong oxidant, which can be toxic to plants and can have deleterious health effects on animals and humans (Gaffney et al., 1989). Exposure to PAN can cause visible damage to agricultural crops when the concentration reaches parts per hundred million levels, eye irritation in the parts per million (ppm) to parts per billion (ppb) range, and has proved lethal to mice at a 2-h exposure at concentrations of 100 to 200 ppm (Stephens, 1969). Some studies have reported that PAN can modify DNA bases (Kligerman et al., 1995; Peak et al., 1969), and that the toxicity depends on three pathways: (1) its oxidizing property, which imitates that of peroxide or peroxyacetyl nitrate; (2) its nitrating and hydroxylating properties, which are similar to those of peroxyacetyl nitrate; and (3) its acetylating property, which resembles that of acetic anhydride (Lin et al., 2000). PAN is also an agent of skin cancer (Lovelock, 1977) and a greenhouse gas (Gaffney et al., 1993).

PAN has also received considerable attention because of its roles in atmospheric chemistry. It serves as an important reservoir for nitrogen oxides during multiday transport of polluted air. Due to its stability at low temperatures and its longer atmospheric lifetime compared with other important NO_y species, PAN can be transported over long distances in winter and in the free troposphere, thereby acting as an agent for the transport of reactive nitrogen (such as NO₂) into other regions of the atmosphere and providing a source of NO_y in regions remote from pollution (Penkett and Brice, 1986). The theoretical basis for this transport is the strong temperature dependent reaction of PAN's reversible thermal decomposition (Spicer et al., 1983), which is further explained in Section 2.2. This reaction is sensitive to the ambient NO₂/NO ratio (Cox and Roffey, 1977). When the NO₂/NO ratio is high, PAN can accumulate and serve as an NO₂ and radical sink. Subsequently, when air containing PAN is mixed with NO-rich air, NO₂ and peroxy radicals are released, thereby contributing to and accelerating downwind troposphere O₃ production and other manifestations of photochemical air pollution (Spicer et al., 1983).

Currently, PAN has no known direct emission source, and is thus an excellent indicator of past photochemical activity involving the formation of O₃ and other secondary air pollutants such as nitric acid and ammonium nitrate (Gaffney et al., 1999; Grosjen et al., 2002). PAN is well known to be a better indicator than O₃, as the background values for PAN are significantly lower than

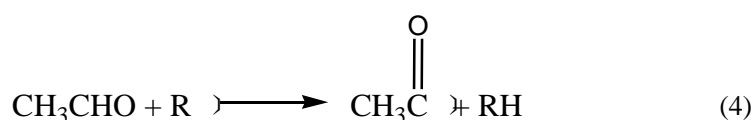
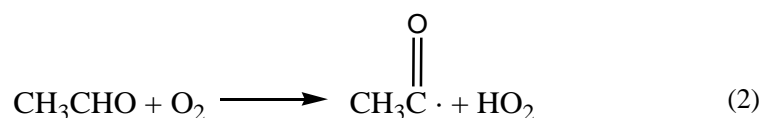
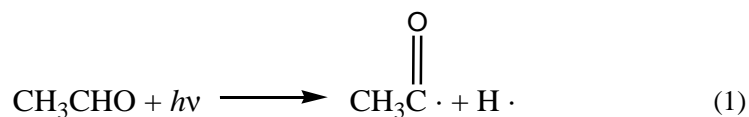
those for O₃ (Rappenglück et al., 1993; Singh, 1987), which are easily raised by the downward transport of free tropospheric air. As it is formed in ambient air only when there are sufficient nitrogen oxides and hydrocarbon precursors, PAN is, therefore, an important indicator of non-methane hydrocarbon (NMHC) driven photochemical air pollution (Rappenglück et al., 2003). Furthermore, because of the great impact of PAN on local peroxy radical levels, measurements of the mixing ratios of PAN are also a useful tool for predicting photochemical O₃ production rates (Gaffney et al., 1999).

2.2. Formation and decomposition mechanisms of PAN

PAN has a wide variety of precursors, including ethane, butane, ethene, isoprene, propane, propene, butenes, acetone, acetaldehyde and biacetyl (Whalley et al., 2004; Williams et al., 2000; Finlayson-Pitts and Pitts, 1986). It exists in a thermal equilibrium with the peroxyacetyl radical (PA), CH₃C(O)O₂ and NO₂, which is both the only source of and the most important sink for PAN (Orlando et al., 1992). The formation rates of PAN are greatest in warm, sunny conditions, but PAN is thermally unstable, and can decompose to form the PA and NO₂ (McFadyen and Cape, 2005).

The production of PAN requires the PA as a specific intermediate (McFadyen and Cape, 1999). Reactions involving acetaldehyde, the source of

which is ethane, can lead to the formation of the radical, CH₃CO (Reactions 1-4), which when subsequently reacted with oxygen (O₂), produces PA (Reaction 5) (Zhang and Tang, 1994).



The final step in the formation of PAN is the three-body reaction of PA with NO₂ (Reaction 6), in competition with the reaction of PA with NO (Reaction 7) (Orlando et al., 1992; Spicer et al., 1983).



In the absence of gases such as NO, which can deplete the PA, PAN remains in the aforementioned reaction equilibrium with the PA and NO₂, as shown in

Reaction 6. In this equilibrium, $k_{6(\infty)} = 4.1 \times 10^{16} e^{-((13600 \pm 350)/T)}$ [s^{-1}] (Orlando et al., 1992) and $k_{-6(\infty)} = 12.1 (\pm 0.5) \times 10^{-12} \times (T/298)^{-0.9 \pm 0.15}$ [molecules $^{-1}$ s $^{-1}$ cm 3] (Bridier et al., 1991). The photochemical production of PAN is very closely linked to that of O₃, as both are initiated by the reaction of hydrocarbons and require the presence of NO_x. In addition, as NO₂ can be produced by the rapid reaction of NO with O₃, high concentrations of O₃ and fresh emissions of NO_x favor longer PAN lifetimes by forcing the equilibrium of Reaction 6 to the right (McFadyen and Cape, 1999).

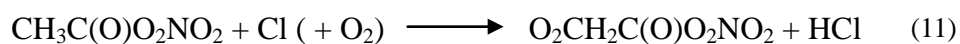
Thermal chemical decomposition is the most important loss mechanism of PAN due to its low rate of reaction with the hydroxyl radical and its low photolysis rate. PAN has a low solubility in water, and therefore its wet deposition rate is also very low (Gaffney et al., 1993). PAN can be decomposed when the equilibrium of Reaction 6 is upset through a reduction in the levels of either PA or NO₂. According to current understanding, the thermal decomposition of PAN primarily occurs through the consumption of the PA, as summarized in Reactions 6, 7, 8, and 9 (Dassau et al., 2004).



NO₂ can be reduced by photolysis or by reaction with O₃ (at night) to form the nitrate radical or with OH to form nitric acid (Gaffney et al., 1993).

According to the aforementioned $k_{-6(\infty)}$ value, the atmospheric lifetime of PAN during thermal chemical decomposition is 0.7 hours at 298 K and 76 days at 255 K, and is thus highly temperature dependent (Dassau et al., 2004).

Decomposition mechanisms other than thermal decomposition occur to a lesser extent, but cannot be neglected. At higher altitudes where thermal dissociation is slow, PAN losses by reaction with OH (Reaction 10, lifetime \approx 200 days; Tsalkani et al., 1988; Talukdar et al., 1995; Dassau et al., 2004) and by photolysis (lifetime \approx 60 days; Senum et al., 1984) represent significant but slow removal processes. Cl oxidation (Reaction 11) must also be considered at low temperatures (Talukdar et al., 1995; Dassau et al., 2004).



Other minor channels for the dissociation of PAN have received some attention. The unimolecular decomposition pathways of PAN have been investigated, and have been found to yield decay products such as CO_2 , CH_2O , methyl nitrate, and NO_3 . The results of these studies, however, indicate that decomposition through these channels occurs at rate constants that are thousands of times slower than that during the decomposition of PAN into the PA and NO_2 (Orlando et al., 1992).

2.3. The role of PAN in the photochemical oxidant cycle

Atmospheric propagation reactions involve hydrocarbon oxidation steps and NO-to-NO₂ conversion reactions. The general mechanism is a propagation chain in which the hydrocarbon molecule RH is converted into the carbonyl RCHO and two NO-to-NO₂ conversions occur, with the OH radical recreated at the end of the set of reactions. The reversible formation of PAN (Reaction 6) is a key termination reaction in tropospheric chemistry. Figure 2-2 summarizes the generalized organic/NO_x system with a focus on the peroxy radicals (RO₂), alkoxy radicals (RO), and acyl peroxyacyl radicals (RC(O)OO) (Seinfeld and Pandis, 1998).

NMHC oxidation is commonly initiated by OH or NO₃[·], followed by reaction with O₂. The RO₂ formed has several possible fates depending on the ambient concentration of NO. When the concentration of NO_x is below about 10 pptv it can react with HO₂ to form ROOH (Calvert et al., 1985), whereas in NO_x-rich environments reaction with NO dominates to generate RO and NO₂. When NO is oxidized to NO₂ by RO₂, the subsequent photolysis of NO₂ produces net O₃ and the NO is recycled to react again. NO may also react with RO₂ to form RONO₂. The RO generated in the above mentioned reaction quickly reacts with O₂ to form RCHO and HO₂. RCHO, including acetaldehyde, then undergoes hydrogen abstraction by OH or NO₃[·], followed by the immediate addition of oxygen to form RC(O)OO. When NO₂ is added directly to RC(O)OO,

PANs are formed to complete the propagation chain (Prestbo, 1992).

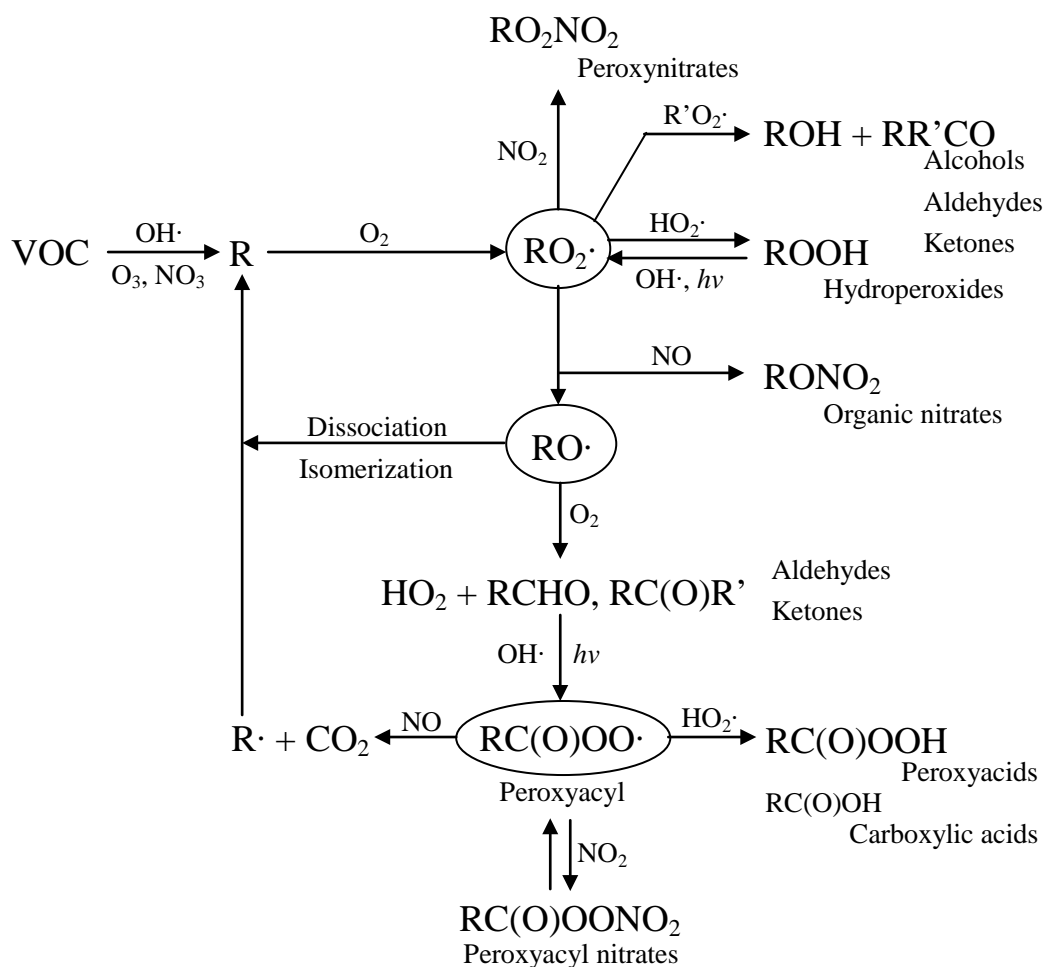


Figure 2-2. Organic radicals and products in the photooxidation of an organic molecule.

From another point of view, concerning NO and NO₂ as the key compounds, the complicated chemical processes in the photochemical oxidant cycle can be summarized as in Figure 2-3, in which PAN also serves as a terminator (Brasseur et al., 1999). NO_y enters the atmosphere as NO_x. The conversion of NO_x results in a decrease in the ratio of NO_x to NO_y with increasing distance from the major anthropogenic sources. The chemical conversion products of NO_x can be

and Volz-Thomas, 1997). It can comprise up to 70-85% of the measured NO_y at higher northern latitudes or higher altitudes (Bottenheim et al., 1993; Muthuramu et al., 1994).

2.4.1. Ambient concentrations of PAN in North America, South America, and Europe

Since its discovery, many measurements of PAN have been taken as part of field studies to investigate the chemistry of the atmosphere. PAN measurements taken in southern California, USA, are the most plentiful. The first quantitative ambient measurements of PAN reported in the literature were conducted by Benzetti and Ryan, who measured ambient PAN in downtown Los Angeles in 1960 (Benzetti and Ryan, 1961) and detected peak PAN concentrations as high as 70 ppbv in August 1960. Ambient levels of PAN in southern California declined between 1960 and 1997 (see Figure 2-4). The peak concentrations ranged from 50 to 70 ppbv in the 1960s, dropped to about 40 ppbv in the 1980s and then to less than 22 ppbv in 1990, 13 ppbv in 1991, and 10 ppbv thereafter. The trends in the 24-hour average and monthly average PAN values are consistent with the peak concentration trend. The highest 24-hour average concentrations were 15 to 20 ppbv before 1980, 5 to 12 ppbv between 1985 and 1991, and 2 to 5 ppbv thereafter. And the monthly averages were 7.0 ppbv in Riverside in 1967-1968, 2.8 ppbv in Tanbark Flat in 1989, and 1 ppbv in Azusa and 0.6 ppbv in Simi Valley in 1997. The major reasons for these declines are increased control of

VOC and NO_x emissions and higher temperatures leading to the greater thermal decomposition of PAN (Grosjean, 2003).

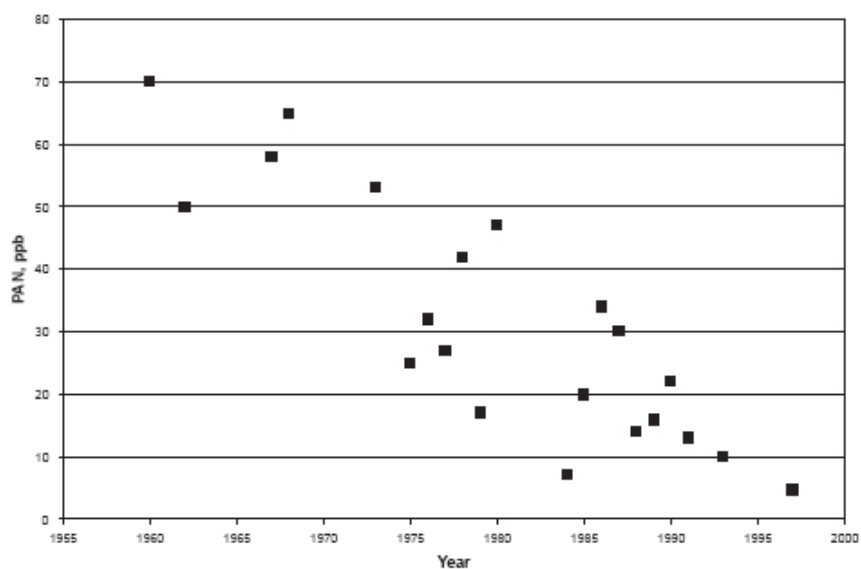


Figure 2-4. Peak concentrations of PAN at southern California locations, 1960-1997. Source: Grosjean, 2003.

Since the measurements taken near Los Angeles in the 1970s, the highest reported level of PAN was observed in Mexico City in 1997, with a daily maximum value exceeding 30 ppbv in five days. However, this value had decreased to a maximum of 8 ppbv in the same city by 2003 (Gaffney et al., 1999; Marley et al., 2007). For more rural areas, long-term measurements were carried out in northern Italy that showed an overall decline in annual average concentrations from 1.5 to 1 ppbv between 1992 and 1995 to less than 1 ppbv in 2000 (Rembges et al., 2001). At high alpine stations such as Jungfrauoch in Switzerland, average mixing ratios of 0.346 ppbv, 0.355 ppbv, and 0.142 ppbv

were observed in spring 1997, summer 1997, and spring 2003, respectively (Zellweger et al, 2002; Whalley et al, 2004). Increasing concentrations of PAN were found in studies at Delft in the Netherlands, with values of 0.2 ppbv in 1973 and 0.8 ppbv in 1986 (Guicherit, 1988), and a long-term trend of increasing concentrations that almost doubled from 0.1 to 0.2 ppbv was reported in measurements taken between 1984 and 1989 in Nova Scotia, Canada (Bottenheim et al., 1999).

2.4.2. Characteristics of PAN in South America, North America, and Europe

In the Mexico City study in 1997, strong diurnal patterns were observed for secondary pollutants, including PAN, PPN, and PBN. On most days, PAN was observed to build up in the morning to reach the levels above 10 ppbv in the early afternoon and then drop to a few tenths of a ppb in the late afternoon. The air flow patterns in Mexico City explain this diurnal behavior of PAN, as they act to lift the pollutant-laden air from the city and transport it into the surrounding regional systems with a minimal recycling of pollutants. The mean ratio of the PAN daily maximum to the O₃ daily maximum of 0.1 ppbv ppbv⁻¹ in the Mexico City study implies photochemical pollution episodes. Moreover, the ratios exceeded 0.2 ppbv ppbv⁻¹ on several days, which were explained by significant PAN precursors in the Mexico City air. At higher levels, PAN holds NO₂ as a reservoir, reducing the O₃ production rate and the subsequent O₃ levels (Gaffney

et al, 1999).

Diurnal variations in PAN similar to those in the Mexico City study in 1997 and in other urban areas were observed between 1996 and 1997 in Porto Alegre, Brazil. Linear least-squares regression of the PAN maximum versus the O₃ maximum yielded the relation $\text{PAN}_{\text{max}} = (0.058 \pm 0.006) \text{O}_{3\text{max}} - (1.200 \pm 0.295)$, $r^2 = 0.707$. Differences in the PAN to O₃ ratios reflect the differences in the chemical composition of the sampled air masses, dry deposition, chemical production, and the chemical removal processes of PAN and O₃ (Grosjean et al., 2002).

In a study at Frijoles Mesa, a remote site in the southwestern USA, from 1987 to 1989, both PAN and O₃ were found to form during daylight hours, showing the expected diurnal variations, with higher levels occurring during periods of photochemical activity. A reasonable correlation between monthly temperature averages and PAN monthly concentration averages was observed as $\text{PAN (ppbv)} = T (\text{°C}) \times (-0.019 \pm 0.001) + (0.329 \pm 0.035)$, $r^2 = 0.76$, which confirms the negative correlation between PAN levels and temperature. Figure 6 in Gaffney et al. (1993) shows an inverse relationship between average monthly concentrations of PAN and O₃ at the Frijoles Mesa site, with the correlation $\text{O}_3 (\text{ppbv}) = \text{PAN (ppbv)} \times (-66.05 \pm 9.08) + (55.9 \pm 2.3)$, $r^2 = 0.80$. In contrast to the positive correlations between PAN and O₃ in the urban atmosphere, this

negative correlation reflects the PAN and O₃ temperature-related characteristics, specifically that O₃ production increases with temperature and the stability of PAN decreases with temperature. This negative correlation also highlights that PAN stores NO₂ in remote areas and that the decomposition of PAN into PA and NO₂ can lead to the photochemical production of O₃ (Gaffney et al., 1993).

Seasonal cycles of PAN were studied at Zeppelin Mountain in the European Arctic between 1994 and 1996. Four distinct features were identified, including a winter concentration plateau, a pronounced spring maximum for the mixing ratios, a summer minimum PAN value, and a small maximum in fall (Beine and Krognes, 2000).

2.4.3. Limited information on PAN in Asia

Very few field measurements of PAN in Asia have been reported in the literature, and most of those were carried out in Japan. At a suburban site near Tokyo, concentrations of PAN were observed to be relatively constant at an annual average of 0.4 ppbv between 1985 and 1994, and results of intermittent surveys of PAN on several Japanese islands have also been reported (Watanabe et al., 1998). Tanimoto et al. (2002) presented 16-month PAN data obtained in 1999-2000 at the remote Rishiri Island in northern Japan, and showed that the transport of polluted Asian continental air masses significantly increased PAN

concentrations at the site, with a springtime peak of ~0.4 ppbv. Diurnal variations in PAN and O₃ were also identified in the field study. From May to June, PAN and O₃ began to increase at 0500-0600 Japan Standard Time (JST) just after sunrise, and reached their maximums at 1200-1400 JST. After peaking, they steadily decreased at a slower rate than the morning build-up. The seasonal variation in PAN was similar to the seasonal cycle at Zeppelin Mountain. PAN exhibited a remarkable springtime peak in April followed by a steep decline toward summer, with a summertime minimum of ~50 pptv and a striking secondary peak being observed in fall (Tanimoto et al., 2002).

PAN levels in the outflow from China were assessed in an aircraft study during TRACE-P measurements in 2001 (Russo et al., 2003), which reported average concentrations of 1225 ± 1014 pptv (<2 km) and 194 ± 69 pptv (2-7 km) for Central China and 207 ± 336 pptv (<2 km) and 142 ± 126 pptv (2-4 km) for Coastal China. These values were higher than those of aircraft studies conducted in other regions. Within China, Zhang and Tang (1994) reported daily maximum PAN concentrations ranging from 1.1 to 6.8 ppbv in urban Beijing in 1990.

2.5. Photochemical pollution studies in China

With its rapid industrialization, photochemical pollution has become a new problem in the ongoing issue of air quality in China. Available data show serious

photochemical O₃ pollution in the major urban and industrial areas of China. For instance, measurements of O₃ and related trace gases between June and July 2005 in a mountain area north of Beijing showed one-hour mixing ratios of O₃ exceeding 120 ppbv on 13 days of the 39 days of observation, with a maximum level of 286 ppbv. O₃ was also strongly correlated with NO_y, with a positive O₃/NO_y correlation slope of 3-6 ppbv ppbv⁻¹, which implies that NO_x plays an important role in the formation of O₃ in emissions from the Beijing urban area (Wang et al., 2006a).

In southern China, three-month measurements of O₃ and other trace gases were carried out at a rural site, the Tai O site, in the southern Pearl River Delta (PRD) between October and December 2001. In the field study, 22 moderately high-ozone episodes (hourly O₃ > 80 ppbv) were observed, and the highest one-hour O₃ mixing ratio was 142 ppbv. Very high concentrations of primary pollutants were also detected at this rural site, with CO levels of about 3,000 ppbv, NO_y levels of about 250 ppbv, and SO₂ levels of about 100 ppbv (Wang et al., 2003). Hourly O₃ concentrations as high as 203 ppbv were observed in autumn 2002 at the same site (Zhang et al., 2007).

In western China, Lanzhou, the capital city of Gansu province, has received great attention as one of the most polluted cities in the world. Although it is not one of the most prosperous cities in China, Lanzhou is highly industrialized, and

its oil refinery, chemical, machinery, and metallurgical industries rank first in China. The large scale of its industry, heavy traffic, domestic exhaust gases, and its special geographical position and topographical conditions all contribute to the photochemical air pollution in Lanzhou (Gao et al., 2004). The Xigu district of Lanzhou, which is an important base for petrochemicals and other major industries, was the first place in China to be recognized as having photochemical smog (Zhang et al., 2000).

In rural areas, the O₃ mixing ratio was reported to be 58 ± 16 ppbv in a 2003 field study conducted at the summit of Mt. Tai on the Shandong Peninsular in the eastern region of China. An examination of the diurnal variations in O₃ revealed a daytime buildup reaching a maximum of about 67 ppbv at 1600 LT (local time), indicating daytime photochemical production, especially in summer. A back trajectory analysis showed that summertime air traveling in the lower troposphere over northern China had the highest concentrations of O₃, implying that the lower troposphere in northern China is significantly polluted in summer (Gao et al., 2005).

Wang et al. (2006b) reported data on O₃ and other trace gases measured at Mt. Waliguan, a remote site in western China. The mixing ratios of O₃, CO, and NO_y were 58 ± 9 ppbv, 155 ± 41 ppbv, and 3.83 ± 1.46 ppbv, respectively, in spring 2003, and 54 ± 11 ppbv, 125 ± 36 ppbv, and 3.60 ± 1.13 ppbv, respectively,

in summer 2003. O₃ was negatively correlated with CO, suggesting that the high-ozone events were mostly derived from the downward transport of the upper tropospheric air and not from anthropogenic pollution.

These studies clearly indicate the presence of photochemical pollution in the major urbanized areas in China. However, there is very limited information on the atmospheric concentrations of PAN in China. The lack of information on the abundance of PAN, whether in polluted or background areas, is an obstacle to the research of photochemical pollution mechanisms and atmospheric chemistry in China and East Asia. This project presents data from continuous ground-based measurements of PAN in three regions of China, offers knowledge about the statistical distribution of PAN concentrations, and helps to explore the source, transport, and chemical processes of PAN in the study areas and the interactions between them.

CHAPTER 3: SIGNIFICANCE AND OBJECTIVES

PAN plays an important role in air quality and atmospheric chemistry, and as a result is of great concern in many countries. However, despite being one of the world's largest emitter of pollutants, China has made limited observations of PAN. This project presents, for the first time, continuous data on PAN concentrations in three regions of China, which should improve our understanding of atmospheric nitrogen chemistry in Asia. The PAN data is used in conjunction with data on O₃ and other gases to deduce the formation mechanisms of photochemical pollution in the western, eastern, and southern regions of China and in urban, rural, and remote areas to fill the knowledge gaps highlighted in Chapter 2. The research findings also provide useful information to support the formulation of strategies to control photochemical pollution in different regions of China.

The major objectives of the project are as follows.

- 1) To take measurements of PAN and supporting gas species and to obtain continuous datasets in urban, rural, and remote areas of China. To calculate the concentrations of the target compounds and compare them with those reported in the literature to determine whether there are differences between regions.
- 2) To investigate the temporal variations in PAN, such as diurnal

variations.

- 3) To analyze the relationships between PAN and other gas species and to infer the formation mechanisms of photochemical pollutants at different sites.
- 4) To investigate the impact of regional pollution in eastern and western China.

SECTION II: EXPERIMENTAL SECTION

CHAPTER 4: METHODOLOGY

4.1. Study areas and measurement sites

Four sampling sites were chosen for the continuous measurements of PAN. These four sites were located at Lanzhou (LZ) in Gansu province (western China), Hong Kong (HK) (southern China), Mt. Tai (TS) in Shandong province (eastern China), and Mt. Waliguan (WLG) in Qinghai province (western China). The sampling locations are shown in Figure 4-1.

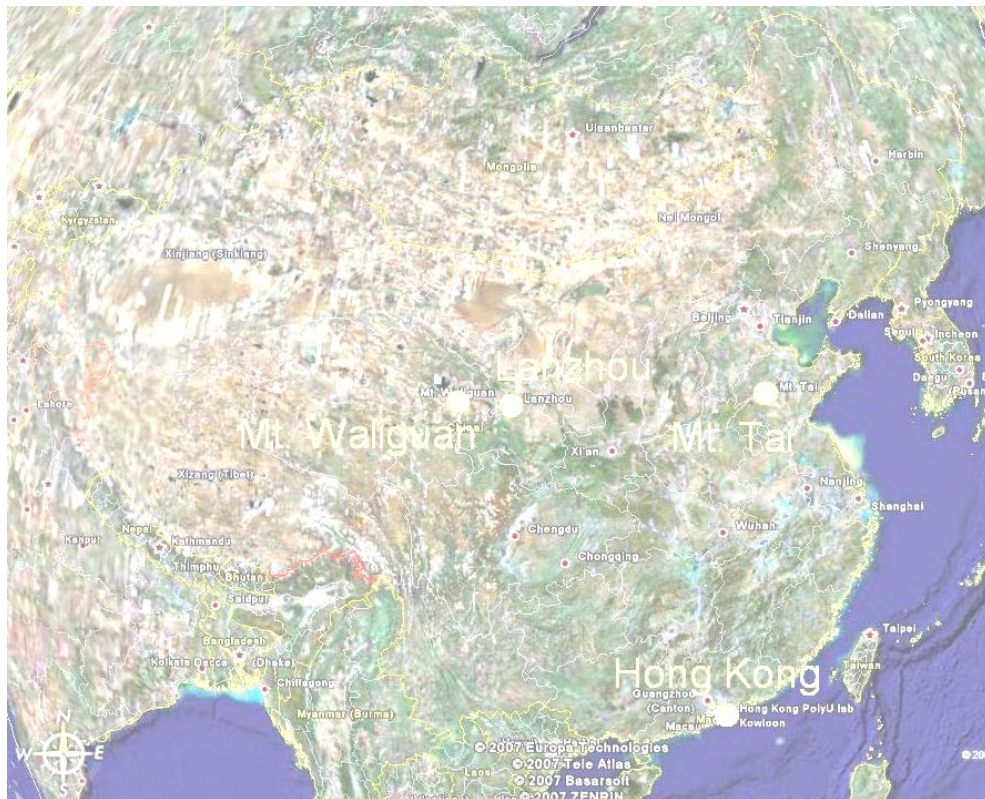


Figure 4-1. Map of China showing the sampling locations.

Table 4-1 lists the site characteristics and six measurement periods for the sampling locations. The sites cover diverse environments and are different in distances from anthropogenic sources. Of the two urban sites, an intensive field study was carried out at Lanzhou in western China, and PAN and O₃ were measured in Hong Kong in southern China. The summit of Mt. Tai was chosen as the location for a two-phase intensive field study to investigate the chemistry and transport of pollution in eastern China, whereas the field study at Mt. Waliguan in western China focused on the chemistry and long-range transport of PAN in the background atmosphere of eastern Asia. As mentioned in Chapter 1, data relevant to the interpretation of the properties of PAN were chosen for analysis from the available datasets obtained in LZ and at TS and WLG. The data used in this study are listed in Table 4-1. In this section, a detailed description is provided of the study areas, the four sites, and the setups of the instruments for measuring the relevant gas species.

Table 4-1. Summary of the field studies at the various sites.

	Period	Site location	Site description	Data used in this study
Lanzhou (LZ)	June 18, 2006 to July 17, 2006 ^a	Western China	Suburban	PAN, O ₃ , CO, NO _y
Hong Kong 2006 (HK 06)	Oct 27, 2006 to Jan 1, 2007 ^a	Southern China	Urban	PAN, O ₃ ^c
Hong Kong 2007 (HK 07)	Oct 3, 2007 to Nov 9, 2007 ^b	Southern China	Urban	PAN
Mt. Tai Spring Phase (TS Spring)	Mar 21, 2007 to Apr 24, 2007 ^b	Eastern China	Rural, mountain top	PAN, O ₃ , CO, NO _y , Total N NH ₃ *, NO, NO ₂ , SO ₂
Mt. Tai Summer Phase (TS Summer)	June 14, 2007 to July 16, 2007 ^b	Eastern China	Rural, mountain top	PAN, O ₃ , CO, NO _y Total N, NH ₃ *, SO ₂
Mt. Waliguan (WLG)	July 22, 2006 to Aug 16, 2006 ^a	Western China	Remote, mountain top	PAN, O ₃ , CO, NO _y

^aThe field studies were conducted before the beginning of this MPhil project, but the data processing and interpretation were performed during the project.

^bField studies conducted as part of this MPhil study, followed by data analysis.

^cO₃ data only available for the period Dec 16, 2006 to Jan 1, 2007.

4.1.1. Lanzhou

Gansu province is situated in the geographical center of China on the middle and upper reaches of the Yangtze River and the Yellow River and at the juncture of the Loess Plateau, the Inner Mongolia Plateau, and the Qinghai Tibet Plateau. The landforms in Gansu are complicated. The eastern part is covered by loess, but the Hexi Corridor on the western fringe of the province features smooth terrain, oases, and desert, including part of the Gobi desert. Seventy percent of the total land area is composed of hilly areas and plateau, and 15% is taken up by desert. Gansu has a dry climate with plenty of sunshine, strong radiation, and large temperature variations between day and night (<http://www.gansu.gov.cn/en/BasicDetail.asp?CID=49>).

Lanzhou (LZ), the capital city of Gansu province, has an area of 13,086 km² and a population of 3.14 million, of which 2.07 million dwell in the central city zone. The city is situated in a narrow valley basin in a mountainous region of western China. LZ is one of the ten most polluted cities in China and the first place where photochemical smog was reported in the 1980s (Zhang et al., 2000). Characterized by a continental climate in the temperate zone, Lanzhou has an annual average temperature of 11.2°C, an annual average precipitation of 327 mm, and an annual sunshine time of 2446 hours (http://www.lz.gansu.gov.cn/about_us.htm). The suburban study site in LZ (36.13°N, 103.69°E, 1631

m above sea level; see Figure 4-2) was located on the top of Mt. Renshou, which is on the southern edge of the mountains surrounding Lanzhou. The site is about 5 km northeast of the Xigu petrochemical district and 15 km northwest of the city center.

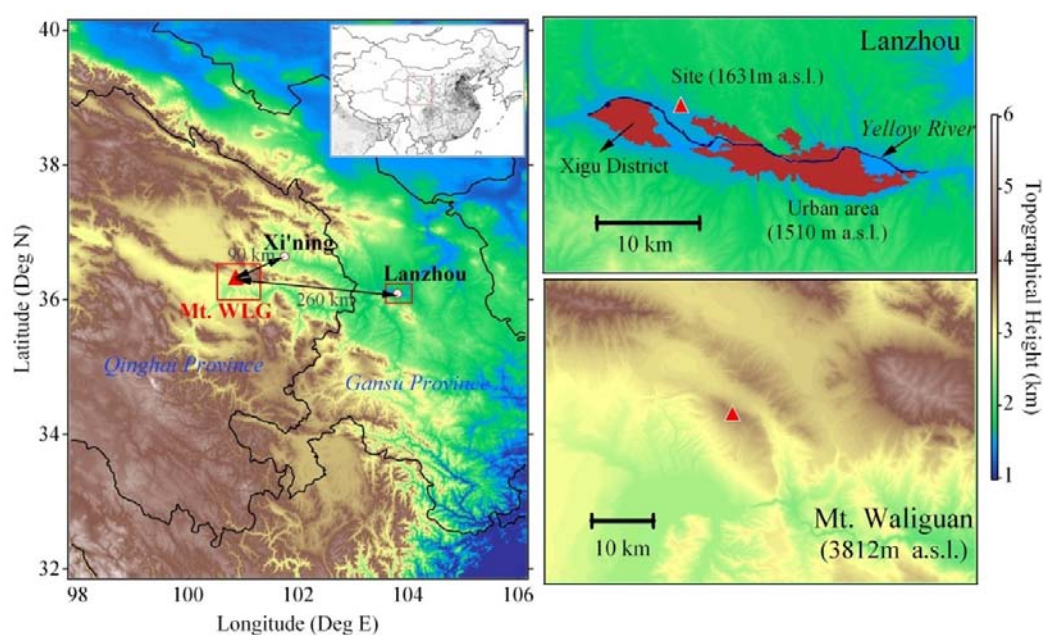


Figure 4-2. Map showing the location and topography of the LZ site, the WLG site, and surrounding regions. The upper-right corner in the left panel depicts the CO emission intensity (Streets et al., 2006). The urban and industrial (Xigu) areas in Lanzhou are shown in red.

The field study at the LZ site was carried out between June 18, 2006 and July 17, 2006. Measurement instruments were placed in a room on the second floor of a cottage (see Figure 4-3), and a portable air-conditioner was used to keep the room temperature under 30°C. Ambient air samples were drawn through a perfluoroalkoxy (PFA) sampling tube (outside diameter, 12.7 mm; inside diameter, 9.6 mm; length, 10.2 m) to a PFA-made manifold inside the room. The

inlet was installed 6.2 m above ground on a separate aluminum scaffold next to the cottage. Bypass pumps were used to reduce the residence time of the sampled air (flow = 10 L/min). The intakes for the PAN, O₃, and CO analyzers were connected to the manifold, and a separate inlet box for the catalytic converter of the NO_y analyzer was installed on the scaffold 5.0 m above ground to give a sampling line length of 10.1 m (flow = 0.8 L/min, inside diameter: 3.2 mm) (see Figure 4-4). Meteorological instruments including a wind sensor, a temperature sensor, and a relative humidity (RH) sensor were also installed on the scaffold next to the sample inlets (6.5 m above ground).



Figure 4-3. The LZ site and its surroundings: (a) view to the northwest (rural); (b) view to the east (urban); (c) view to the southwest (industrial).

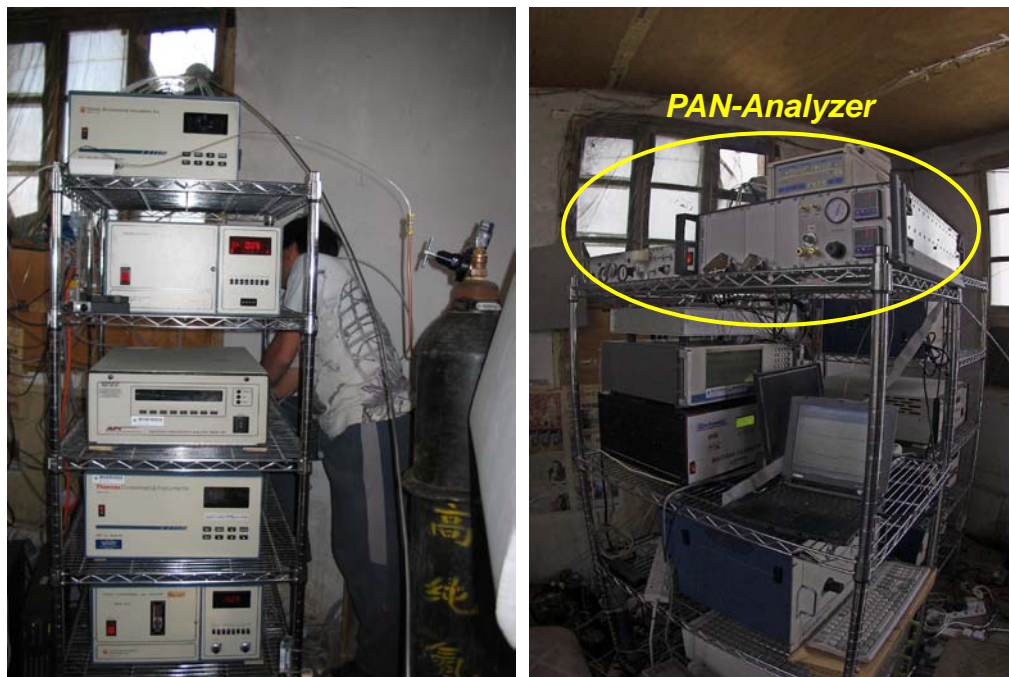


Figure 4-4. Overview of the monitoring system in LZ.

4.1.2. Hong Kong

Hong Kong in southern China is one of the most developed regions in Asia. With more than 6.8 million residents living in a 1,100km² area, this metropolitan region has one of the highest population densities in the world (Louie et al., 2005). Its climate is sub-tropical, tending toward temperate for nearly half the year. The major emission sources in Hong Kong include power plants, vehicles, and industry. Limitations on available land and industrial development have caused high levels of air pollution, which affects the health of Hong Kong citizens, and air quality has become a major concern in Hong Kong (Ho et al., 2002).

The measurements were carried out on the campus of the Hong Kong Polytechnic University (HK PolyU), which is located in the center of the city. The surrounding area is highly populated, with many stores and offices, and is very close to heavily used roads. The HK site (22.31°N, 114.18°E; see Figure 4-5) was a laboratory on the top floor of an eight-storey building in the north-eastern part of the campus with windows facing north.



Figure 4-5. Map showing the HK study site.

The PAN measurements in HK were carried out in two periods: Oct 27, 2006 to Jan 1, 2007 and Oct 3, 2007 to Nov 9, 2007, with supporting O₃ measurements being taken between Dec 15, 2006 and Jan 1, 2007. The PAN and O₃ instruments were placed in the temperature-controlled laboratory (25 ± 2°C), with the sample inlets positioned outside the windows (~1 meter away from the

wall). Two individual PFA tubes (length: 3.5 m; inside diameter: 3.2 mm) were used as sample lines (see Figure 4-6).



Figure 4-6. Overview of the laboratory in HK PolyU.

4.1.3. Mt. Tai

Shandong is one of the 10 coastal provinces of China and, according to the national census in 2006, has an area of 156,700 km² and a population of 93.1 million. The northwestern, western, and southwestern parts of the province are all part of the vast North China Plains. The center of the province is more mountainous, and the east of the province comprises the hilly Shandong Peninsula that extends into the sea and separates the Bohai Sea in the northwest from the Yellow Sea to the east and south. Shandong Province has a temperate

climate, with moist summers and dry, cold winters (<http://www.famouschinese.com/virtual/Shandong#Geography>). Due to the cold climate in winter and early spring, there is a great demand for heat energy during these heating seasons. Continual urbanization and industrialization in the province have increased the demand for energy, and huge amount of pollutants are emitted to the atmosphere from anthropogenic sources, such as power plants and vehicles. This has resulted in the regional deterioration of the air quality in Shandong province and the surrounding areas.

Located in the center of Shandong Province, Mt. Tai covers an area of 426 km². The highest peak of Mt. Tai, Jade Emperor Peak, is the highest point of the province, with a height of 1545 m (<http://www.import.net.cn/info/8/a026bd10.html>). The TS site (36.26°N, 117.11°E, 1534 m above sea level; see Figure 4-7) was located within a meteorological observation station on the summit of Mt. Tai (Riguan Peak), which overlooks the city of Tai'an (population: 500,000) 15 km to the south. The city of Ji'nan (the capital of Shandong province, population: 2.1 million) is situated 60 km to the north. A few villages can also be seen to the north. As a famous tourism spot, Mt. Tai receives a large number of visitors in the summer months, and there are some local emissions from small restaurants and temples. However, the site was situated in the less frequently visited eastern part of the summit (Gao et al., 2005). This rural mountain-top site was selected to best represent the regional air pollution status and to study the exchanges

between the planetary boundary layer (PBL) and the free troposphere.

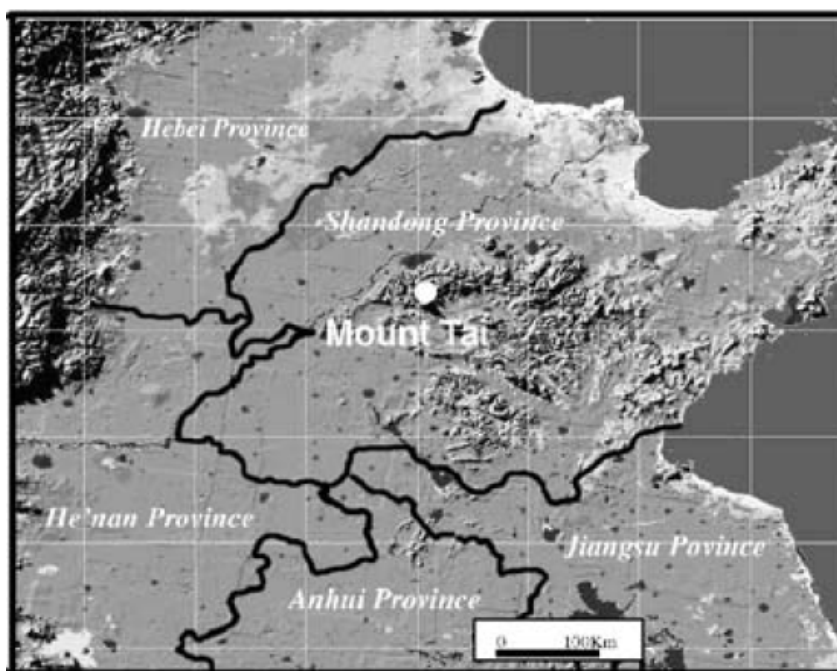


Figure 4-7. Map showing the TS study site and surrounding regions.

Two phases of intensive field study were carried out at the TS site between Mar 21, 2007 to Apr 24, 2007 and between June 14, 2007 and July 16, 2007. The instruments for the measurement of PAN, CO, NO_y & Total N, NH₃^{*}, and NO & NO₂ (only available in the TS Spring study) were placed in a room on the top floor of the meteorological station, and O₃ and SO₂ analyzers were housed in a separate small room nearby (~7 meters to the south of the station) (see Figure 4-8). Ambient air samples were drawn through PFA sampling tubes (inside diameter: 3.2 mm) to the PAN, CO, and NO & NO₂ analyzers, with sampling line lengths of 11.2 m for PAN, 6.7 m for CO, and 7.78 m for NO & NO₂. The inlets for PAN, CO, and NO & NO₂ were installed 7.1 m, 6.6 m, and 6.6 m above

ground, respectively, on a bamboo scaffold above the edge of a terrace outside the main room. The inlet boxes for the catalytic converters of the NO_y & Total N and NH₃* analyzers were installed on the scaffold at a height of 6.4 m and 6.6 m above ground, respectively, with sampling line lengths of 7.5 m for NO_y & Total N and 9.7 m for NH₃* (inside diameter: 3.2 mm). Bypass pumps were used to reduce the residence time of the sampled air for the NO_y & Total N and the NH₃* analyzers (flow = 1.5 L/min) (see Figure 4-9). The intakes of the O₃ and SO₂ analyzers were connected to a manifold, to which air samples were drawn through a stainless steel tube (inside diameter: 10 cm) with the inlet installed at 4 m above ground on the rooftop of the small room.

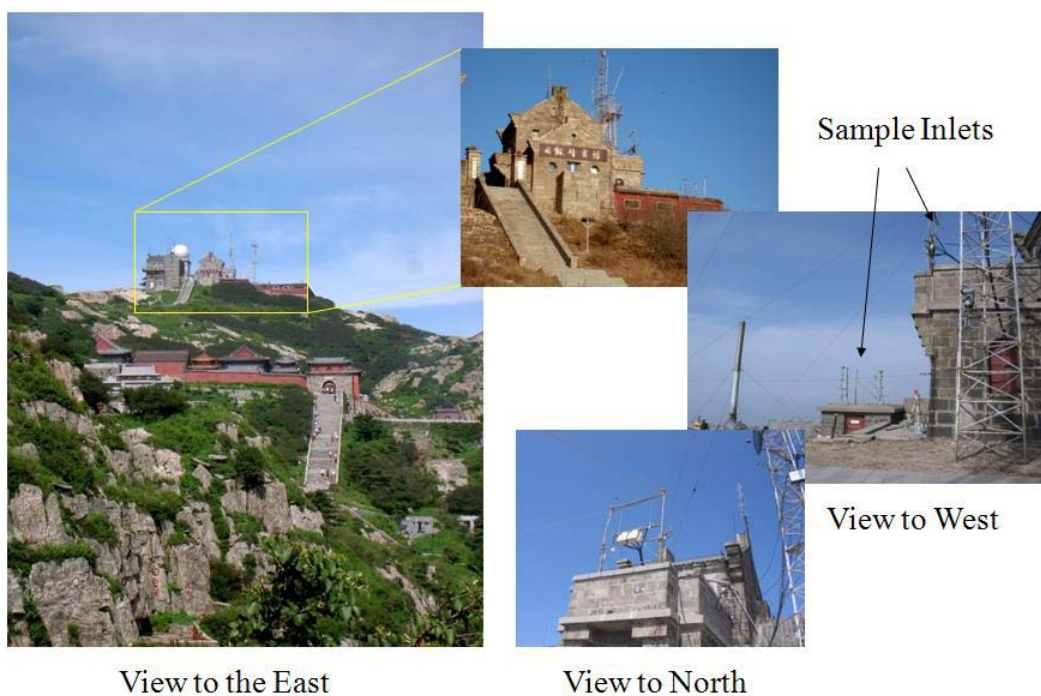


Figure 4-8. The TS site and surroundings.

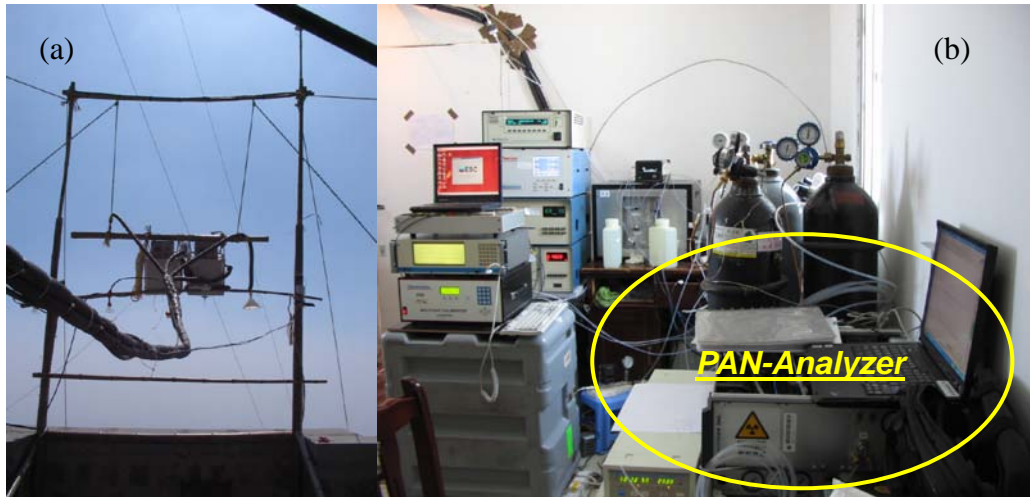


Figure 4-9. Overview of the monitoring system at TS: (a) sample inlets and catalytic converter boxes; (b) real-time analyzers, calibration and data logging system.

4.1.4. Mt. Waliguan

Located in the southern part of northwestern China, Qinghai province is situated on the upper reaches of the Yangtze River and the Yellow River in the northeastern part of the Qinghai-Tibet Plateau. It has an area of 720,000 km² and a population of 5.38 million. The terrain of Qinghai is various and complex. The Kunlun Mountains lie across the whole province, and the Tanggula Mountains, Arjin Mountain, and Qilian Mountain lie to the south and north. The weather in Qinghai is typical of a plateau climate, with low temperatures, dryness, windiness, and a lack of oxygen as the principal characteristics (<http://www.qhwhit.gov.cn/page/NewsShow.aspx?id=287cbde2-8eeb-442e-8043-2c2dbf9d9a3e>).

Mt. Waliguan is situated on the northeastern edge of the Qinghai-Tibetan

Plateau and is isolated from the industrial and populated regions of China. The population density of the surrounding areas is less than 6 people per km² (Zhou et al., 2003). The field site at Mt. Waliguan, the WLG Observatory (36.29°N, 100.90°E, 3816 m above sea level; see Figure 4-2), is one of the World Meteorological Organization's (WMO) Global Atmospheric Watch (GAW) Baseline Stations. It is positioned on an isolated mountain peak that stretches from northwest to southeast, and is about 90 km southwest of Xining, the capital city of Qinghai province, but is separated from the city by several high mountains that are about 4,000 m above sea level, and is 260 km west of Lanzhou (see Figure 4-2). No significant sources of pollutants are present to the west, except for the township of Qiapu Qia (population: 30,000), which is located 26 km to the west but at an elevation of 1,000 m below the station. The surrounding areas are naturally preserved arid/semiarid land and scattered grassland (Wang et al., 2006b).

Measurements were carried out at the WLG Observatory from July 22, 2006 to Aug 16, 2006. The measurement instruments were placed in a temperature-controlled laboratory on the second floor of the observatory ($20 \pm 2^\circ\text{C}$) (see Figure 4-10). The settings for the sampling system were similar to those in LZ, except that the inlet for the PAN, O₃, and CO analyzers and the inlet box for the catalytic converter of the NO_y analyzer were installed at 4.1 m and 2.1 m above the rooftop of the station, respectively (see Figure 4-11). The

settings for the meteorological instruments were essentially identical to those described previously (Wang et al., 2006b).



Figure 4-10. The WLG site and surroundings.

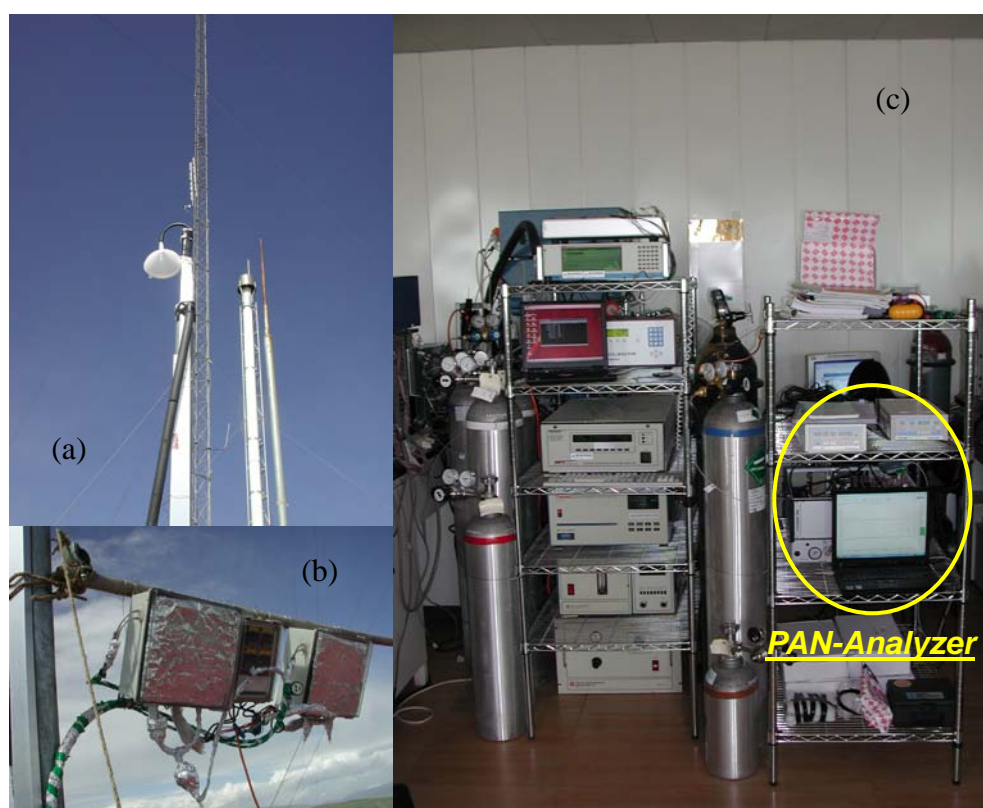


Figure 4-11. Overview of the monitoring system at WLG: (a) sample inlets; (b) catalytic converter boxes; (c) real-time analyzers, calibration and data logging system.

4.2. Measurement techniques, quality control, and assurance

4.2.1. PAN-Analyzer

PAN was measured with a commercially available automatic PAN-Analyzer (see Figure 4-12) equipped with a calibration unit (Meteorologie Consult GmbH). The analytical method was based on gas chromatographic (GC) separation in capillary columns at 16°C with electron capture detection (ECD). The gas mixture sampled (sample loop 2 ml) was transferred to the columns with 5.0 grade nitrogen as the carrier gas. A bypass arrangement for the sample flow provided short residence times in the sample line. The separation was performed in 10-min analytical cycles using pre- and main columns mounted in a compact temperature controlled oven and cooled by Peltier elements. The temperature fluctuations were less than 1 K, and a dual thermostat permitted the operation of the GC over a wide range of ambient temperatures (5-30°C). The pre-column was back flushed after the selected fraction (including PAN) reached the main column to prevent contamination and to reduce the analysis time by preventing substances with long retention times from entering the main column and the detector. The eluates from the main column were analyzed by ECD at 50°C. The detection limits for the instrument are normally 50 pptv and 30 pptv under optimum conditions.



Figure 4-12. PAN-Analyzer and Cal-Unit: (a) PAN-Analyzer (above) and calibration unit (below); (b) PAN-Analyzer; (c) calibration unit.

The sampling, injection, and column switching were accomplished with a pneumatically actuated 10-port valve (VALCO). Figure 4-13 shows the mechanism for switching between the “inject” mode and the “load” mode. In the “inject” mode, carrier gas flow 1 (CG-1) transfers the air sample from the sample loop through the pre-column to the main column. In the “load” mode, the air sample for the next analytical cycle is collected in the sample loop, CG-1 back flushes the pre-column, and carrier gas flow 2 (CG-2) further transfers the air sample through the main column to ECD.

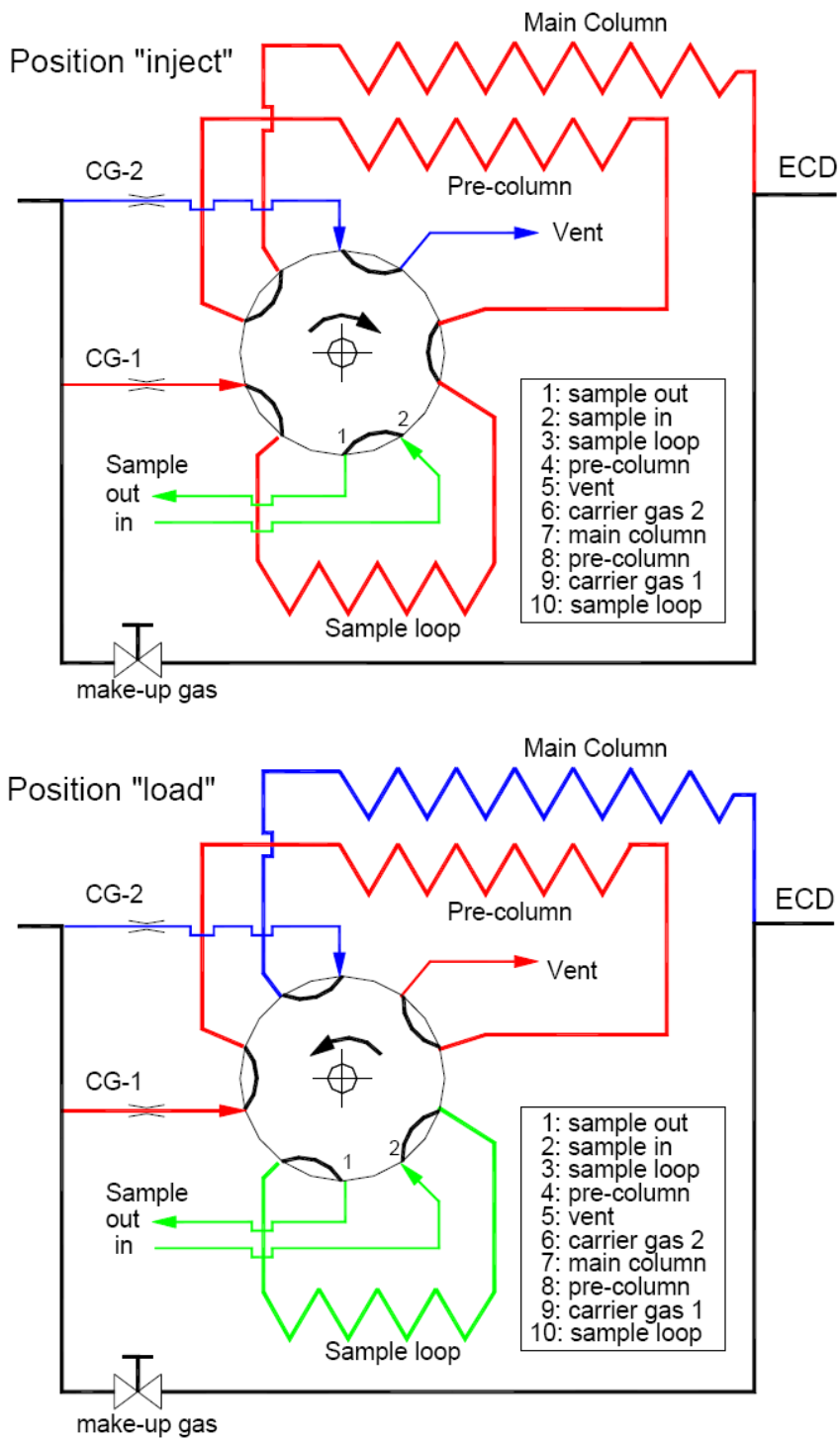
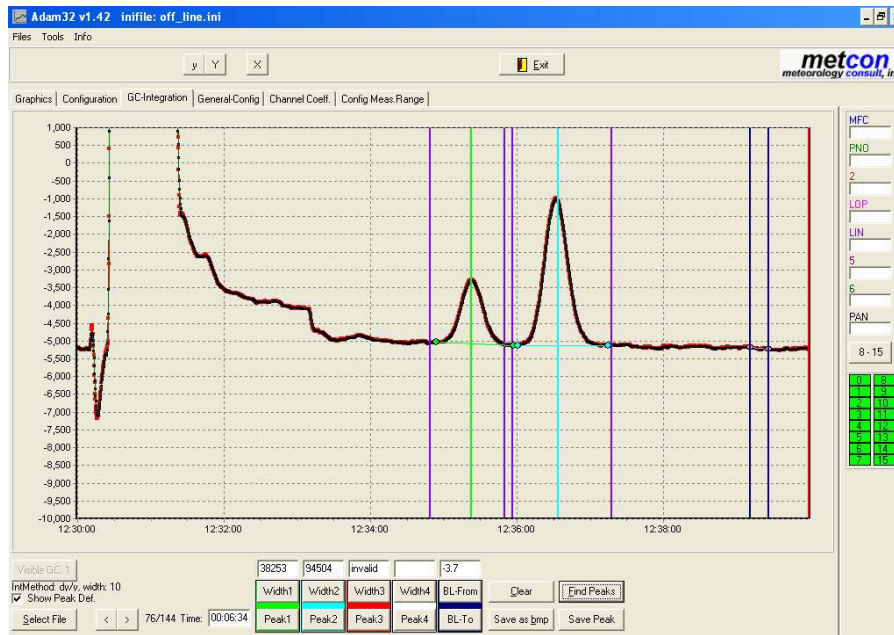


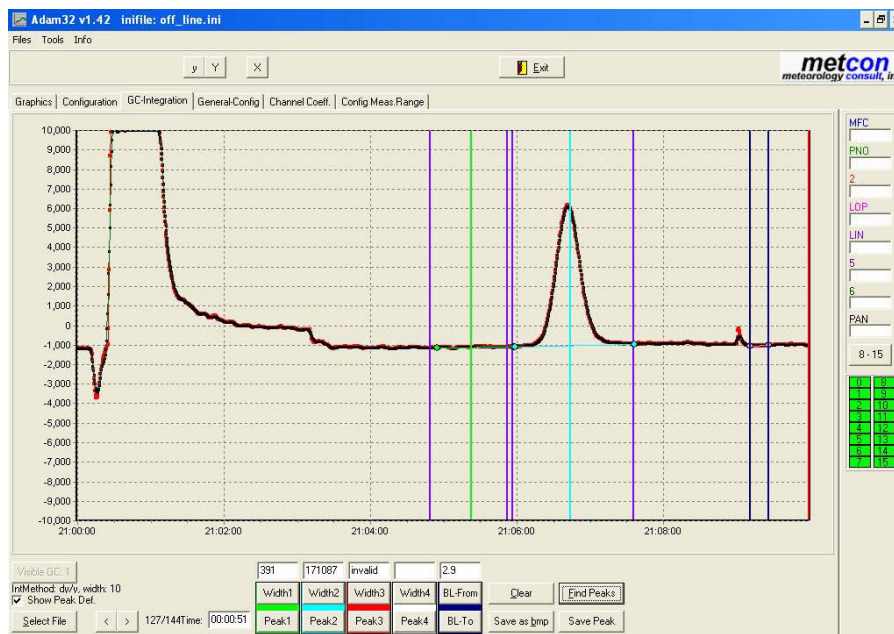
Figure 4-13. Oven module of the PAN-Analyzer in two different modes.

The instrument was calibrated weekly using a calibration unit that produced continuous, stable flows of air with known PAN concentrations. For the LZ, TS, and WLG studies, a US National Institute of Standards and Technology (NIST) traceable NO standard (containing 5.05 ± 0.10 ppmv NO in balance of Nitrogen, purchased from Scott-Marrin Inc., California) with controlled flow was delivered to the PAN calibrator, and excess acetone was photolyzed with a penray lamp in the presence of ultra pure air. The PAN yield was found to be 93% using ion chromatography at FZ-Juelich, Germany by the manufacturer (personal communication, Dr. Rainer Schmitt). The synthesized PAN was diluted to the desired concentration by mixing with scrubbed ambient air (zero air, produced by TEI, Model 111) before it entered the PAN-Analyzer. The concentrations of the generated PAN were therefore directly linked to the flow of the NO standard, and the detector response was determined from the slope of the concentration versus the signal. The calibration for the HK studies was almost the same, except that an NO standard containing $3.00 \pm 2\%$ ppmv NO (purchased from Scott-Marrin Inc., California) was used. In order to reduce the calibration time in the field studies, single point calibration was applied based on the linearity of the sensitivity of the analyzer (personal communication, Dr. Rainer Schmitt). And the calibration concentration range of PAN was dependent on the ambient concentration range at the four sites. In detail, concentrations of 4.04 ppbv, 1.60 ppbv, 1.80 ppbv and 1.20 ppbv were selected for calibrations at LZ, HK, TS and WLG, respectively.

Ten-minute data on PAN were collected using a new PC software package (Adam32 v1.42). Some examples of the chromatograms generated by the software are shown in Figure 4-14. The raw data from the software were in units of peak area, and were transferred into concentrations (ppbv) by multiplying the ratios of known PAN concentrations to peak areas obtained weekly from the calibration. The area of another peak in the chromatograms when sampling ambient air, the carbon tetra-chloride (CCl₄) peak, was used as an internal standard to check the stability of the instrument's sensitivity between calibrations, as the atmospheric concentration of CCl₄ is rather constant.



(a)



(b)

Figure 4-14. Chromatograms generated by Adam32 v1.42 for (a) an ambient sample with CCl_4 as the first peak and PAN as the second peak; (b) calibration (PAN peak only).

4.2.2. Instruments for the measurement of other trace gases

Other trace gases measured at the sites were used to help interpret the PAN data. The instruments for the measurement of these gases are briefly described in the following.

Ozone

O₃ was measured using a UV photometric analyzer (Thermal Environmental Instruments (TEI) Model 49C) with a detection limit of 2 ppbv and a precision of ± 2 ppbv. The analyzer was calibrated by a transfer standard (TEI 49PS) before the commencement of the field studies (Wong et al., 2007).

Carbon monoxide

CO was measured with a gas filter correlation, nondispersive infrared analyzer (Advanced Pollution Instrumentation (API), Model 300) with a heated catalytic scrubber for the baseline determination. The detection limit was 30 ppbv for a 2-min average, with a 2σ precision of about 1% for a level of 500 ppbv and an overall uncertainty of 10% (Wang et al., 2003). Zeroing was conducted every 2 h for 15 min. The CO analyzer was calibrated every two days by injecting zero air and a span gas generated by diluting an NIST traceable standard (containing 151.4 ± 1.5 ppmv CO, 15.12 ± 0.15 ppmv NO and 15.03 ± 0.15 ppmv SO₂, purchased from Scott-Marrin Inc., California).

Total reactive nitrogen

In the LZ and WLG field studies, NO_y was detected with a chemiluminescence analyzer equipped with an externally placed molybdenum oxide (MoO) catalytic converter (TEI, Model 42S). NO_y was converted to NO on the surface of MoO maintained at 350°C, and NO was subsequently measured by chemiluminescent detector. The analyzer had a detection limit of 0.05 ppbv and a 2σ precision of 4% with an uncertainty of about 10% (Wang et al., 2003). In the TS field study, NO_y was measured with a different chemiluminescence analyzer (TEI, Model 42C-Y Trace Level), but the detection principles of the two analyzers are the same (Wang et al., 2006b). In all of the studies, the sensitivity of the NO_y analyzers was checked every two days by injecting zero air and the aforementioned span gas (120 ppbv of NO). The conversion efficiency of the MoO catalyst was checked with an NIST traceable N-propylnitrate (NPN) standard (containing 4.99 ± 0.25 ppmv NPN, Scott-Marrin Inc., California) that indicated the near complete conversion of NPN throughout the study periods. Multipoint calibrations (0 ppbv, 40 ppbv, 80 ppbv, 120 ppbv and 160 ppbv of NO) by diluting the same traceable standard were also conducted at the beginning and end of the studies at each site, and showed the analyzers to have good sensitivity linearity ($r^2 > 0.999$).

Total nitrate

Total N was measured with the same instrument as NO_y (TEI, Model

42C-Y Trace Level) at the TS site, which was also equipped with an externally placed MoO catalytic converter (350°C). The Model 42C-Y Trace Level had two channels for sampling ambient air. One channel was for measuring NO_y as mentioned, and the other channel was almost the same except that one Nylon filter and one Teflon filter were fixed at the beginning of the sample line to filter out HNO₃ and p-NO₃⁻ in the NO_y species. This allowed the concentration of Total N to be obtained from the difference in value between the two channels. The calibration methods were the same as those for NO_y.

Ammonia and ammonium

NH₃^{*} was detected with another chemiluminescence analyzer (TEI, Model 42C-Y) equipped with two externally placed MoO catalytic converters for two different channels. One converter was heated to 350°C and converted NO_y to NO, which was measured by the chemiluminescent detector for one of the two channels on the same principles as the NO_y analyzers. The other converter was heated to 450°C and converted both NO_y and NH₃^{*} to NO. The NO signal detected in this channel was the sum of the concentrations of NO_y and NH₃^{*}. Thus, the concentration of NH₃^{*} was obtained from the difference in value between the two channels. The same calibration methods as those for NO_y were used. The efficiency of the NH₃^{*} conversion on the surface of the MoO was calibrated every three days with an NIST traceable ammonia standard (containing 5.65 ± 0.57 ppmv ammonia, Scott-Marrin Inc., California), and

indicated a conversion efficiency of about 68% during the TS study.

Nitrogen monoxide and nitrogen dioxide

NO and NO₂ were measured with a chemiluminescence analyzer equipped with a blue-light converter (BLC) in the NO_x channel (TEI, Model 42I Trace Level). The BLC uses an array of ultraviolet light emitting diodes (LED's) to photolyze NO₂ to NO. The primary advantages of using BLC includes: 1. Relatively high conversion efficiency; 2. High specificity afforded by narrow spectral output of the LED's, avoiding the absorption cross sections for NO₂ and possible interferential species; and 3. Small size and power requirements. The instrument switched automatically between the NO and NO_x modes. NO was detected by the chemiluminescent detector. NO₂ was converted to NO in the BLC and the NO was subsequently measured. The signal from the NO_x channel was actually the sum of the NO in the ambient air and the NO converted from ambient NO₂. The NO₂ concentration was then obtained from the difference in value between the two channels. The analyzer had a detection limit of 0.05 ppbv and a 2 σ precision of 4% (for NO = 10 ppbv), and the uncertainty was about 10%. The calibration method for the NO and NO₂ analyzer was similar to that for NO_y, except that the conversion efficiency of the BLC was checked every three days with NO₂ synthesized by reaction between NO in the aforementioned traceable standard and O₃ generated by Model 6100 (EnviroNics, Inc.). The conversion efficiency of the BLC was about 46% during the TS study.

Sulfur dioxide

SO₂ was measured by pulsed UV fluorescence (TEI, Model 43C), with a detection limit of 0.06 ppbv and a 2 σ precision of 3% for ambient levels of 10 ppbv (2-minute average). The uncertainty was estimated to be about 9% (Wang et al., 2003). Routine calibrations of the SO₂ analyzer with zero air and span gas and multipoint calibrations at the beginning and end of the field study were conducted in a similar manner as for NO_y, except that the traceable standard was purchased from Jinan DeYang Special Gas Co. Ltd., China.

For all of the trace gases analyzers, a data logger (Environmental Systems Corporation, Model 8816) was used to control the calibrations and to collect data. The CO, NO_y, Total N, NH₃*, NO, and NO₂ data were averaged to 1-min values, the O₃ data collected in LZ, HK and at WLG were taken in 1-min values, and the O₃ and SO₂ data collected at TS were in 5-min values.

4.3. Back trajectory analysis and backward particle release simulation

To learn about the origins and transport pathways of the sampled air masses at TS and WLG, 4-day (for TS) and 7-day (for WLG) back trajectories that terminated at 500 m, 1000 m, and 1500 m above the ground level of the TS and WLG peaks were calculated every three hours during the study periods using the

Hybrid Single-Particle Lagrangian Integrated Trajectory model, Version 4.7 (HYSPLIT4 model) developed by the National Oceanic and Atmospheric Administration (NOAA) Air Resources Laboratory (ARL), which can be accessed via the NOAA ARL Real-time Environmental Applications and Display System website (<http://www.arl.noaa.gov/ready/open/hysplit4.html>). The model settings and physical parameterizations were identical to those described in previous studies (Ding et al., 2004). 48-hour back trajectories with the same settings were also calculated at selected times of chosen cases in the WLG study.

In addition to back trajectory analysis, backward Lagrangian particle release simulation was also conducted for more in-depth analysis of the WLG cases using the Version 4.8 of the HYSPLIT4 model, which is also available from the aforementioned NOAA website. Distinct from the traditional back trajectory method, backward particle release simulation, which considers the dispersion processes, provides a more accurate picture of the history of an air mass (Stohl et al., 2003). The HYSPLIT4 model was run with a 3-D particle method to calculate the dispersion (Draxler and Hess, 1997). During hours of concentration peaks, the model was run 36-hours backward with a total of 5,000 particles released 200 m above the measurement site. The simulation generated hourly positions of all of the 5,000 particles during the 36-hour period. The meteorological data that drove the model were from a GDAS dataset (3 hourly, global and 1° in longitude and latitude; 23 pressure levels; see

<http://www.arl.noaa.gov/ss/transport/gdas1.html> for details). The backward Lagrangian particle release simulation was carried out by Dr. Ding Aijun and the results are used in case studies of air pollution transport.

SECTION III: RESULTS AND DISCUSSION

PAN data obtained at four sites were analyzed to investigate the status, chemistry, and transport of photochemical pollution in different regions of China. In the results and discussion part, time series on PAN and other trace gases measured in the six study periods are presented. The data are analyzed statistically and compared with those obtained from studies in other countries. The diurnal variations in PAN are then characterized for different environments, and the factors affecting the photochemical transformation routes are studied through an analysis of the correlations between PAN and O₃ and an investigation of nitrogen budgets. Finally, the regional transport of air pollution is examined for the two mountain top sites by back trajectory analysis, and cases with elevated PAN concentrations at the WLG site are studied with the help of the HYSPLIT4 model. The structure of each of the following chapters and sections is arranged in a sequence that starts with the data from the urban areas, followed by those from the rural areas, and then those from the remote areas, that is, from LZ and HK, to TS, and finally to WLG.

CHAPTER 5: GENERAL DATA DESCRIPTION

5.1. Time series

Figure 5-1 to 5-4 display the datasets obtained from the four study sites, and show the differing characteristics of gas pollutants among the urban areas, rural areas, and remote areas. All of the data are presented at a resolution of 10 minutes, if not specified otherwise.

Figure 5-1 shows the time series of the mixing ratios of PAN, O₃, CO, and NO_y at the LZ study site. As the figure illustrates, the variation in the concentrations of PAN and other gas species was very significant. The peak concentrations of PAN were as high as ~9 ppbv, but at nighttime the level decreased to lower than 0.5 ppbv. O₃ also showed concentrations spikes every day in a typical pattern of local photochemical production. NO_y, which reached levels as high as ~175 ppbv, and CO, which attained levels of up to ~2500 ppbv, exhibited similar variations in concentrations, which indicates that the study site were frequently influenced by combustion sources.

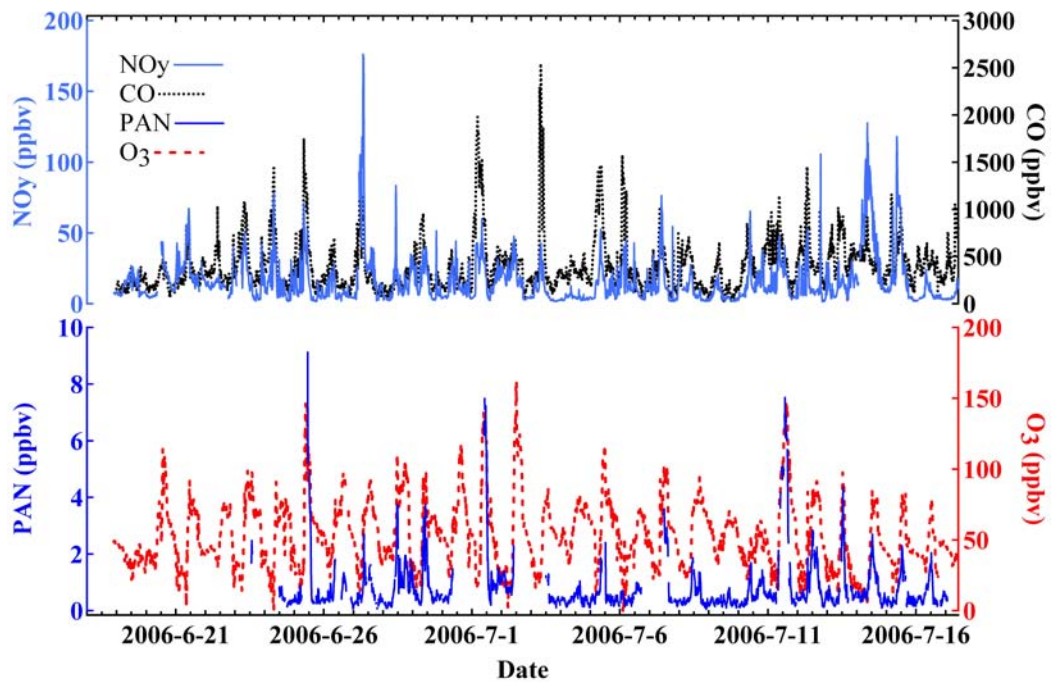
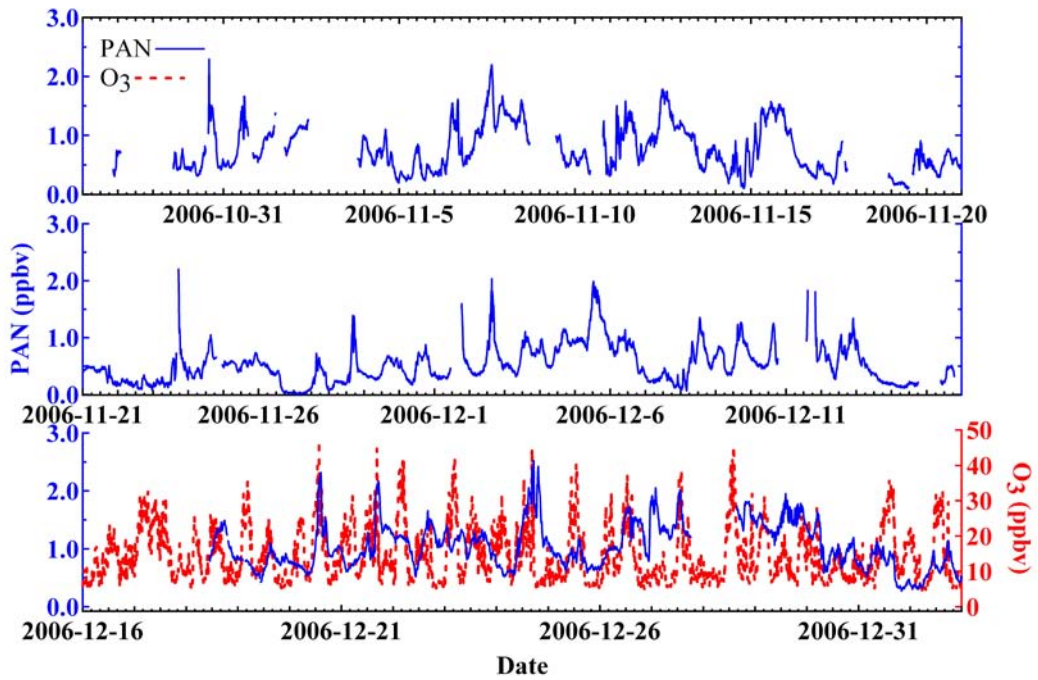
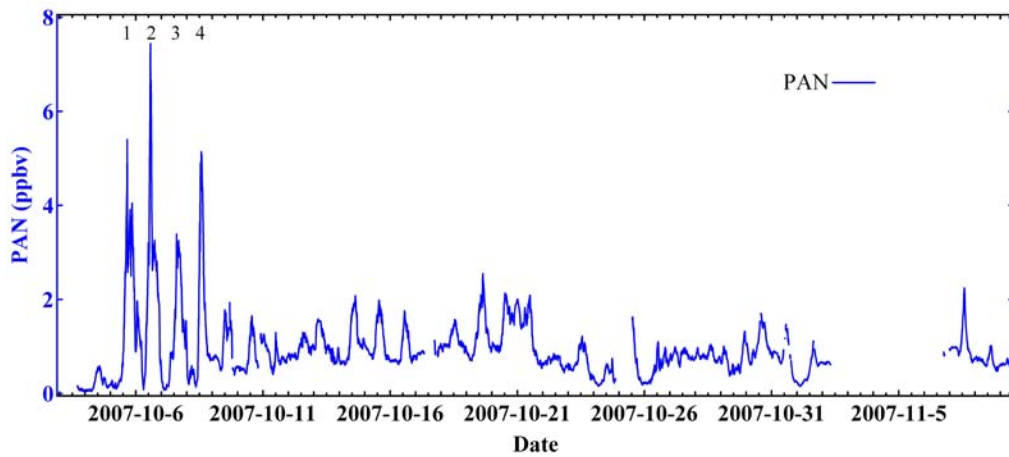


Figure 5-1. Time series of PAN, O₃, CO, and NO_y concentrations measured in LZ from June 18, 2006 to July, 17 2006.

Time series for the other urban site, the HK site, are shown for PAN and O₃ from the 2006 study (HK 06) and for PAN from the 2007 study (HK 07) in Figure 5-2a and b, respectively. In the 2006 study, the highest PAN concentration was lower than 3 ppbv and the O₃ concentrations fell within the range of ~0 to ~50 ppbv, suggesting a moderate photochemical production during that period.



(a)



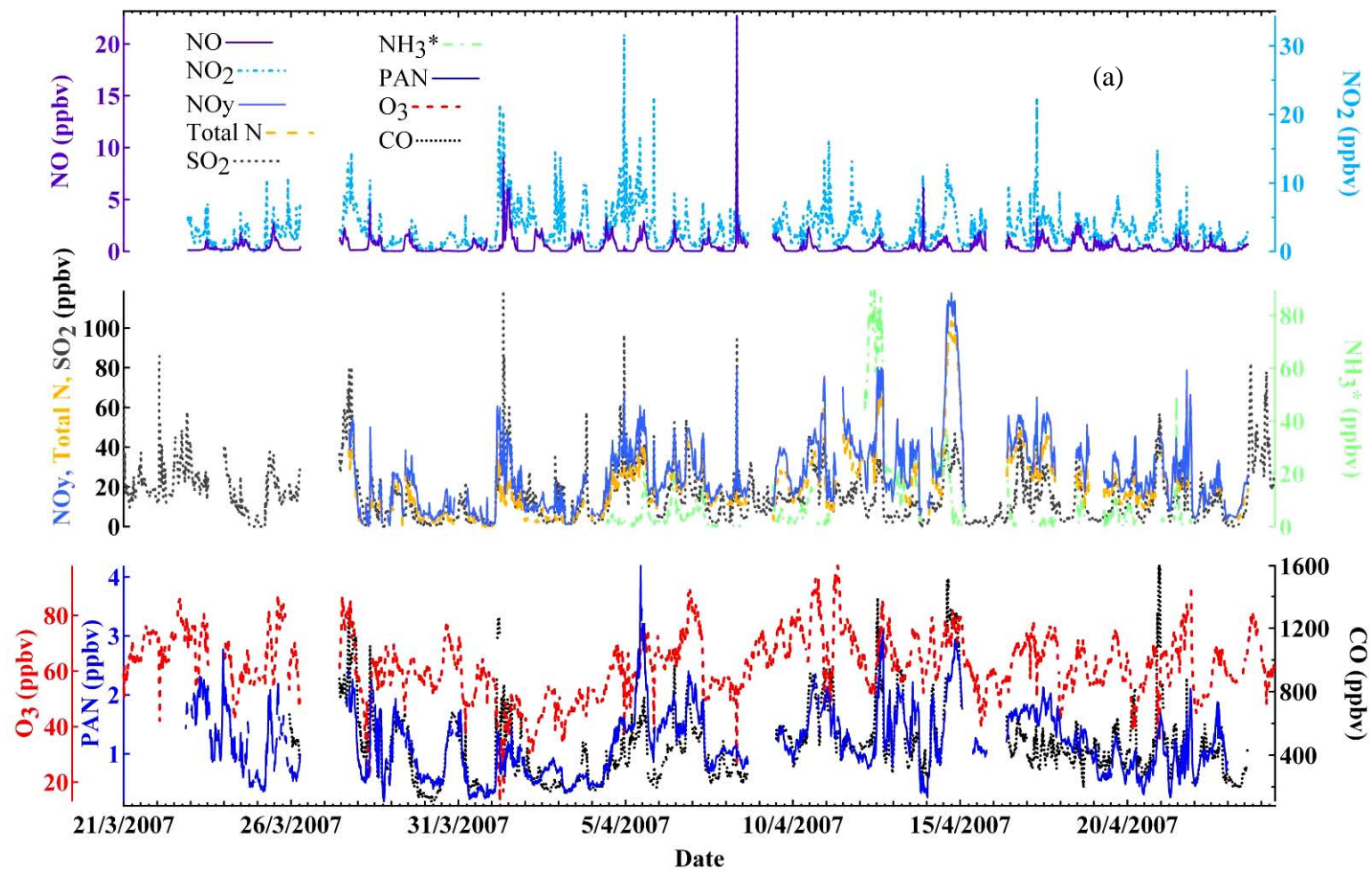
(b)

Figure 5-2. Time series of PAN and O₃ measured in the HK 06 study (a) and PAN in the HK 07 study (b). Cases of strong photochemical pollution events are marked with 1 to 4 in (b).

Figure 5-2b shows that the level of PAN in the HK 07 study was comparable to that in the HK 06 study most of the time, except for the first few days in the study period. Sharp increases in PAN concentrations were detected between Oct 5 and Oct 8, 2007, which are marked with 1 to 4 in Figure 5-2b.

These pollution episodes were associated with the approaching typhoon Krosa, which caused favorable conditions for pollution accumulation and photochemical production, such as calm winds, strong solar radiation, and a suppressed mixing height. Similar cases of photochemical pollution plumes in the autumn have been reported for HK (e.g., Wang et al., 2003), and the detailed regional and local air pollution transport mechanisms by sea-land breezes have been discussed by Ding et al. (2004). Here this study reports PAN measurements at first time in HK, thus further confirm the very strong photochemical production during typical air pollution episodes in typhoon seasons in PRD.

Figure 5-3a and b shows the time series for PAN, O₃, and other trace gases from the TS field studies. In the spring phase, the PAN concentrations ranged between ~0.4 ppbv to ~4 ppbv, with the highest value appearing on Apr 5, 2007, when the primary pollutants NO_y and CO also peaked. All of the gas species exhibited obvious variations in concentrations, indicating the ingress of several kinds of air masses with different sources and photochemical ages to the site.



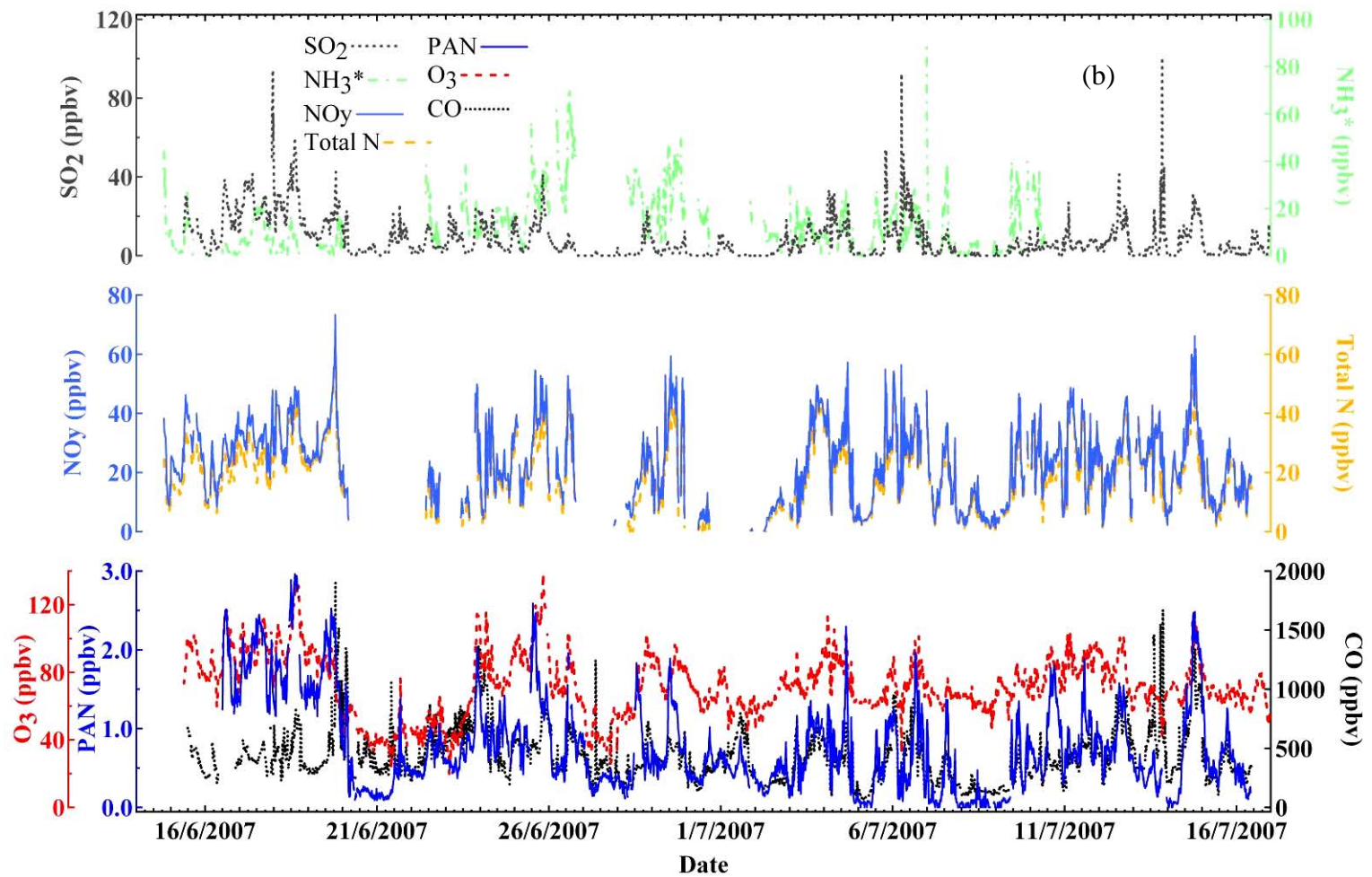


Figure 5-3. Time series of PAN, O₃, CO, NO_y, Total N, NH₃*, NO, NO₂, and SO₂ measured at TS in the spring (a) and summer (b) studies.

In the summer phase, the mixing ratios of PAN were in the range of ~0 ppbv to ~3 ppbv and the PAN concentrations showed larger daily variations than those in the spring phase, indicating stronger photochemical production in summer. Inspection of Figure 5-3b reveals two major periods during which remarkably different types of air masses were sampled. Before June 20, 2007, when there was dense fog, relatively higher levels of PAN and NO_y were maintained both during the day and at night. In contrast, PAN concentrations dropped significantly at night once the fog had lifted on June 20, 2007, and even dropped below the detection limit of the analyzer on July 5, July 7, July 8, July 9, and July 14, 2007. Other gas species such as NO_y and Total N showed similar general patterns to PAN, presumably due to the nighttime downward transport of cleaner air masses from the free troposphere in the summer.

Figure 5-4 shows time series of PAN, O₃, CO, and NO_y at the remote study site of WLG in the summer of 2006. It is worth noting that the ranges for the gas species were much smaller than those at the other sites, indicating less significant variations in the concentrations of these pollutants at WLG. The PAN mixing ratios were in the range of ~0.2 to ~0.6 ppbv, except for the regional transport cases marked with 1 to 6 in the figure, which are discussed in detail in Chapter 8. Both the NO_y and CO (primary pollutants) concentrations were also in very low ranges. Inspection of the figure reveals three major types of air masses sampled during the study period, which are also further investigated with back trajectory

analysis in Chapter 8.

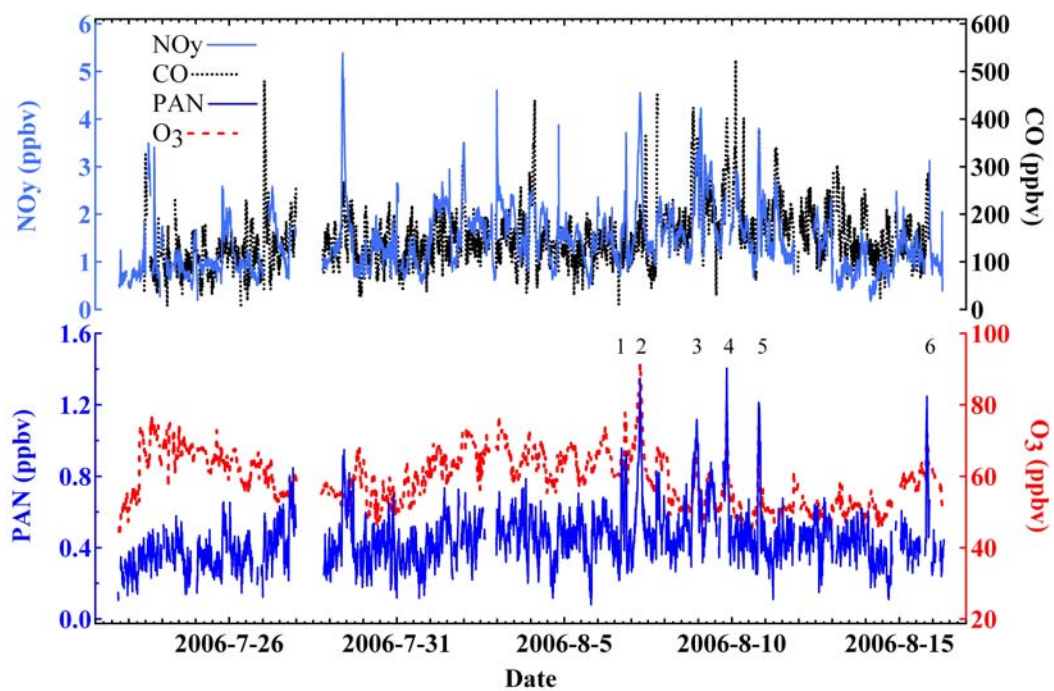


Figure 5-4. Time series of PAN, O₃, CO, and NO_y measured at WLG from July 22, 2006 to Aug 16, 2006. Cases of regional transport are marked with 1 to 6.

5.2. Statistical analysis

Table 5-1 summarizes the statistics for the 10-min average values of PAN and other trace gases at the LZ, HK, TS, and WLG sites, including the mean, standard deviation, median, concentration maximums and minimums, and number of data points. Statistical analysis of the daytime and nighttime parameters was carried out according to different times of sunrise and sunset during the six measurement periods. The data capture rates for PAN were 73.9% for the LZ study, 82.4% for the HK 06 study, 83.1% for the HK 07 study, 85.4% for the TS Spring study, 96.9% for the TS Summer study, and 86.4% for the WLG study after data validation.

Table 5-1. Summary of the 10-min data from the LZ, HK 06, HK 07, TS Spring, TS Summer, and WLG studies^a.

	All data					Daytime ^b					Nighttime ^c				
	Mean	Median	Max	Min	n	Mean	Median	Max	Min	n	Mean	Median	Max	Min	n
<i>LZ</i>															
PAN	0.76 (0.89)	0.47	9.13	0.05	2504	1.01(1.10)	0.67	9.13	0.06	1410	0.44(0.25)	0.39	1.79	0.05	1094
O ₃	53 (24)	49	161	1	4007	62 (25)	63	161	3	2341	40 (15)	41	92	1	1666
CO	404 (280)	332	2544	18	4000	422 (295)	345	2544	24	2349	380 (257)	312	1977	18	1651
NO _y	15.6 (16.5)	10.6	176.2	1.4	3926	18.2 (18.8)	12.6	176.2	1.6	2316	11.8 (11.4)	8.2	105.3	1.4	1610
<i>HK 06</i>															
PAN	0.74 (0.42)	0.66	2.52	n.d. ^d	7844	0.79 (0.46)	0.72	2.52	n.d.	3577	0.69 (0.38)	0.62	2.42	n.d.	4267
O ₃	15 (8)	12	47	5	2448	16 (8)	15	47	5	1122	13 (7)	10	42	5	1326
<i>HK 07</i>															
PAN	0.94 (0.68)	0.80	7.44	0.04	4400	1.08 (0.79)	0.88	7.44	0.05	2142	0.80 (0.50)	0.74	4.05	0.04	2258
<i>TS Spring</i>															
PAN	1.17 (0.56)	1.08	4.19	0.19	3831	1.20 (0.57)	1.12	4.19	0.23	1919	1.14 (0.54)	1.05	2.94	0.19	1912
O ₃	62 (11)	62	98	13	4585	62 (12)	63	98	17	2293	62 (11)	61	94	13	2292
CO	459 (236)	421	1593	108	3291	453 (219)	420	1512	114	1686	465 (252)	422	1593	108	1605
NO _y	26.8 (18.7)	23.3	117.7	0.1	3109	28.3 (18.2)	24.6	117.7	0.6	1687	25.1 (19.1)	21.6	113.7	0.1	1422
Total N	20.9 (16.7)	17.8	103.5	n.d.	2871	21.2 (15.7)	18.4	103.5	n.d.	1639	20.6 (18.1)	16.8	102.5	n.d.	1232
NH ₃ *	11.0 (17.0)	4.3	89.4	n.d.	1417	14.1 (20.2)	6.3	89.4	n.d.	826	6.6 (9.8)	2.6	62.6	n.d.	591
NO	0.46 (0.79)	0.18	22.72	n.d.	4136	0.80 (0.96)	0.57	22.72	0.02	2130	0.10 (0.24)	0.04	6.15	n.d.	2006
NO ₂	3.16 (2.79)	2.40	34.40	0.05	4092	3.37 (2.67)	2.57	34.40	0.27	2087	2.95 (2.90)	2.09	31.67	0.05	2005
SO ₂	15.5 (13.3)	12.7	118.9	n.d.	4563	16.2 (13.1)	13.3	118.9	n.d.	2288	14.8 (13.4)	12.2	96.6	n.d.	2275

Table 5-1. Summary of the 10-min data from the LZ, HK 06, HK 07, TS Spring, TS Summer, and WLG studies^a (Continued).

	All data					Daytime ^b					Nighttime ^c				
	Mean	Median	Max	Min	n	Mean	Median	Max	Min	n	Mean	Median	Max	Min	n
<i>TS Summer</i>															
PAN	0.77 (0.59)	0.61	2.96	n.d. ^d	4176	0.81 (0.63)	0.62	2.96	n.d.	2628	0.69 (0.50)	0.59	2.23	n.d.	1548
O ₃	72 (18)	71	138	20	4480	72 (18)	70	138	23	2838	72 (18)	72	138	20	1642
CO	427 (219)	390	1900	66	3999	434 (202)	405	1900	81	2491	415 (245)	353	1669	66	1508
NO _y	23.1 (12.7)	23.3	73.4	0.2	3375	23.8 (12.7)	23.4	73.4	0.2	2258	21.8 (12.7)	23.1	54.2	0.2	1117
Total N	20.1 (11.5)	19.9	63.8	n.d.	3312	20.4 (11.5)	19.9	63.8	n.d.	2227	19.4 (11.5)	20.0	51.7	0.2	1085
NH ₃ *	13.5 (12.2)	10.5	91.9	n.d.	2120	14.7 (12.7)	11.8	69.5	n.d.	1486	10.7 (10.4)	7.9	91.9	n.d.	634
SO ₂	8.0 (10.0)	4.5	100.6	n.d.	4423	8.4 (10.0)	4.6	92.3	n.d.	2822	7.5 (9.9)	4.0	100.6	n.d.	1601
<i>WLG</i>															
PAN	0.44 (0.16)	0.43	1.40	0.08	3068	0.44 (0.15)	0.43	1.35	0.08	1831	0.45 (0.16)	0.43	1.40	0.11	1237
O ₃	59 (8)	59	91	40	3233	58 (7)	58	91	41	1943	60 (8)	61	86	40	1290
CO	149 (61)	139	524	6	3024	144 (54)	137	451	6	1847	157 (71)	142	524	7	1177
NO _y	1.4 (0.7)	1.3	5.4	0.2	3109	1.4 (0.6)	1.2	5.4	0.3	1886	1.5 (0.7)	1.4	4.6	0.2	1223

^aMean (standard deviation), median, max, and min values are in ppbv; *n* is the number of 10-min data.

^bDaytime is defined as 0600 to 1950 Beijing time (BJT) for the LZ and WLG studies, 0700 to 1750 BJT for the HK 06 study, 0600 to 1750 BJT for the HK 07 and the TS Spring studies, and 0500 to 1950 BJT for the TS Summer study.

^cNighttime is defined as 2000 to 0550 BJT for the LZ and WLG studies, 1800 to 0650 BJT for the HK 06 study, 1800 to 0550 BJT for the HK 07 and the TS Spring studies, and 2000 to 0450 BJT for the TS Summer study.

^dn.d. stands for not detectable or under the detection limit.

For urban areas, the mean values for PAN, CO, and NO_y in LZ were 0.76 ppbv, 404 ppbv, and 15.6 ppbv, respectively. In comparison, the average levels of PAN at HK were 0.74 ppbv in the HK 06 study and 0.94 ppbv in the HK 07 study. These values are typical of urban and suburban sites. The concentrations of these gas pollutants in both LZ and HK were higher in the daytime than at night, reflecting the influence of local photochemical production resulting from a daytime increase in local emissions and solar radiation. The maximums of PAN, O₃, and CO in LZ were 9.13 ppbv, 161 ppbv, and 2544 ppbv, respectively, which indicate strong production of photochemical pollutants from anthropogenic precursors. Peak concentrations of PAN as high as 7.44 ppbv were captured in the HK 07 study, also showing intense photochemical production in the city.

Although the peak PAN value in the HK 07 study was lower than the 9.13 ppbv value detected in LZ, the average mixing ratio of 0.94 ppbv was much higher than that in LZ, and the mean concentration excluding those days with episodes was 0.85 ± 0.41 ppbv, which was also higher than that in LZ, reflecting stronger photochemical activity in subtropical southern China due to the lower latitude. The larger variation in the PAN concentration in LZ (reflected by the larger standard deviation and the larger difference between the daytime and the nighttime data), the higher mean PAN concentration in HK (which in the HK 06 study was similar to that in LZ), and the higher peak value in LZ reflect that LZ is an isolated pollution source with intensive local photochemical production and

located in the relatively cleaner region of western China, whereas HK is affected by both local photochemical pollution and more polluted air masses arriving from the PRD region in southern China. The difference in concentrations between the HK 06 study and HK 07 study was presumably due to year-to-year variations in meteorology.

For the rural site at the summit of Mt. Tai (TS), the mean concentrations of PAN, O₃, CO, NO_y, and SO₂ were 1.17 ppbv, 62 ppbv, 459 ppbv, 26.8 ppbv, and 15.5 ppbv, respectively, in the spring phase, and 0.77 ppbv, 72 ppbv, 427 ppbv, 23.1 ppbv, and 8.0 ppbv, respectively, in the summer phase. The levels of PAN, O₃, CO, and NO_y in both phases of the TS study were much higher than those measured in LZ, reflecting the more severe regional air pollution in eastern China than in the west. The CO concentrations in summer 2007 were similar to those obtained in a previous study at the same site in July 2003, except that the maximums of 1,900 ppbv (10-min average) and 1,456 ppbv (1-h average) were much higher than the 1,175 ppbv detected in 2003. In contrast, the O₃ concentrations in summer 2007 were generally higher than those in July 2003, reflecting the growing amount of photochemical pollution in the North China Plains (Gao et al., 2005). Table 5-1 further shows that the daytime concentrations of these gas pollutants were generally higher than those at night, mainly due to the transport of polluted air masses from the PBL with upslope mountain-valley breezes during the daytime. The exception is CO, which was at a higher level in

the nighttime in the TS Spring study, perhaps reflecting an increase in anthropogenic emissions from combustion sources at night during spring in Shandong province.

The average concentrations of PAN, CO, NO_y, and SO₂ at TS were much higher in the spring phase than in the summer phase. The higher levels in the spring phase may be due to higher anthropogenic emissions, especially from coal consumption in the heating season. Weaker vertical mixing in cold seasons may also contribute to higher pollution within the PBL, which may have been frequently transported to the site by topographical lifting under strong winds during the spring study. Another possible reason for the lower concentrations of PAN in summer is that PAN tends to decompose faster and more thoroughly in the higher temperatures of June and July, which would accord with the low PAN concentrations measured at night. The average mixing ratio of O₃ was higher in summer than in spring, which is typical of the North China Plains and can be attributed to the stronger photochemical production in summer due to more intense solar radiation and higher temperatures (Logan, 1989; Ding et al., 2008).

At the remote mountain top site of WLG, the average concentrations were 0.44 ppbv for PAN, 149 ppbv for CO, and 1.4 ppbv for NO_y, which are typical for remote mountain sites. These values are further reduced to 0.41 ppbv for PAN, 139 ppbv for CO, and 1.3 ppbv for NO_y after the exclusion of data from days

with regional transport cases. The difference between the daytime and nighttime concentrations was not significant. The peak concentrations of PAN, CO, and NO_y were 1.40 ppbv, 524 ppbv, and 5.4 ppbv, respectively. Compared with the urban and rural areas, these levels in the remote area are in a very low range, and thus provide valuable information on the background levels of these gas species in China. The mean value of O₃ at WLG was higher than those in LZ and HK, mainly due to the transport of free tropospheric air to the site at high altitude. This issue is further discussed in Chapter 6.

5.3. Comparison with other locations

To place the levels of PAN observed in this study into a global context, Table 5-2 and Table 5-3 summarize the results of PAN measurements taken elsewhere in the last two decades. For polluted areas (see Table 5-2), the mean PAN values from the field studies in LZ, HK, and at TS, which ranged from 0.74 ppbv to 1.17 ppbv, were all higher than those measured in other polluted areas (urban, suburban, and rural areas: 0.38 to 0.67 ppbv). This reflects the presence of serious photochemical air pollution in western, eastern, and southern China, particularly in the Lanzhou air basin, the North China Plains, and the southern area of PRD. The maximum value of 9.13 ppbv in LZ was higher than the peak value of 8 ppbv observed in 2003 in Mexico City, but lower than the 1997 peak value of 34 ppbv. The reduction in PAN concentrations in Mexico City is mainly

due to the control of VOC emissions since 1997 (Gaffney et al., 1999; Marley et al., 2007). A similar declining trend of PAN concentrations has also been reported in Los Angeles, where the peak level decreased from 70 ppbv in the 1960s to about 10 ppbv in the 1990s (Renzetti and Ryan, 1961; Grosjean, 2003). The highest concentration of 7.44 ppbv in HK was only lower than the peak values in the Mexico City study and in LZ, but was generally higher than at sites in other studies.

Although the TS studies were carried out at a mountain top site, the PAN concentrations measured are not comparable with those from other mountain top studies, as these have mostly been conducted in remote areas (see Table 5-3) but Mt. Tai is surrounded by heavily polluted and industrialized areas. The results are instead compared with those from other flatland sites in polluted areas in Table 5-2. The peak concentrations in the TS studies were comparable to those in these locations, but the average PAN concentrations were generally higher than in previous studies, especially in the spring phase, which suggests the regional abundance of photochemical precursors in the North China Plains.

Table 5-2. Comparison with other sites in polluted areas^a.

	Period	Mean	Max	Latitude, Longitude	Altitude, m asl	Site Description	Ref ^b
Lanzhou	June-July 2006	0.76(0.89)	9.13	36.13°N, 103.69°E	1631	Suburban	1
Hong Kong 2006	Oct 2006-Jan 2007	0.74 (0.42)	2.52	22.31°N, 114.18°E		Urban	1
Hong Kong 2007	Oct-Nov 2007	0.94 (0.68)	7.44	22.31°N, 114.18°E		Urban	1
Mt. Tai Spring Phase	Mar-Apr 2007	1.17 (0.56)	4.19	36.26°N, 117.11°E	1534	Rural, Mountain top	1
Mt. Tai Summer Phase	June-July 2007	0.77 (0.59)	2.96	36.26°N, 117.11°E	1534	Rural, Mountain top	1
Mexico City	Apr-May 2003		8	19.36°N, 99.07°W		Urban	2
Mexico City	Feb-Mar 1997		34	19.49°N, 99.15°W		Urban	2,3
La Porte super site (Houston)	Aug-Sep 2000	0.48	6.5	26.67°N, 95.06°W		Suburban	4,5
Cornelia Fort Air Park (Nashville)	June-July 1999	0.674	2.51	36.19°N, 86.70°W		Suburban	6
Porto Alegre, Brazil	May 1996-Mar 1997	0.40(0.63)	6.67	30.03°S, 51.23°W	10	Rural	7
Eastern Scotland	1994-1998		3	55.87°N, 3.20°W	200	Rural	8
Ichihara, Japan	1985-1994	0.38(0.05)		35.52°N, 140.08°E		Rural	9

^aMeans (standard deviation) and maximums are in ppbv.

^bReferences: 1, this study; 2, Marley et al., 2007; 3, Gaffney et al., 1999; 4, Roberts et al., 2003; 5, Roberts et al., 2001; 6, Roberts et al., 2002; 7, Grosjean et al., 2002; 8, McFadyen and Cape, 2005; 9, Watanabe et al., 1998.

At the remote WLG site, the O₃ and CO levels were comparable to the levels measured at other continental mountain sites (Wang et al., 2006b). Although the mean level of NO_y (1.41 ppbv) at WLG in this study was much lower than that measured in the previous study in 2003 (mean = 3.60 ppbv), it was still higher than the mean NO_y levels measured at remote sites elsewhere (see Table 2 of Wang et al., 2006b). The average PAN concentration (0.44 ppbv and 0.41 ppbv excluding transport cases) was generally higher than previously measured (0.01 to 0.36 ppbv for the other studies in Table 5-3), which leads to the conclusion that the WLG site has a naturally higher level of NO_y species. The maximum PAN value at WLG (1.40 ppbv) is comparable to those measured at European and North American mountain sites but higher than results obtained on the islands of Japan (ranging from 0.37 ppbv to 0.97 ppbv).

Table 5-3. Comparison with other sites in remote areas^a.

	Period	Mean	Max	Latitude, Longitude	Altitude, m asl	Site Description	Ref ^b
Mt. Waliguan	July-Aug 2006	0.44(0.16)	1.4	36.29°N, 100.90°E	3816	Mountain top	1
Jungfrauoch	Feb-Mar 2003	0.142	1.29	46.55°N, 7.98°E	3580	Mountain top	2
Jungfrauoch	July-Aug 1997	0.356(0.194)	0.853	46.55°N, 7.98°E	3580	Mountain top	3
Jungfrauoch	Mar-May 1997	0.346(0.245)		46.55°N, 7.98°E	3580	Mountain top	4
Jungfrauoch	June-Aug 1997	0.355(0.211)		46.55°N, 7.98°E	3580	Mountain top	4
Jungfrauoch	Sep-Nov 1997	0.145(0.124)		46.55°N, 7.98°E	3580	Mountain top	4
Jungfrauoch	Dec 1997-Feb 1998	0.154(0.156)		46.55°N, 7.98°E	3580	Mountain top	4
Rishiri Island, Japan	Jun 1999	0.150(0.112)		45.07°N, 141.12°E	35	Island	5
Rishiri Island, Japan	Jul 1999	0.090(0.083)		45.07°N, 141.12°E	35	Island	5
Rishiri Island, Japan	Aug 1999	0.036(0.020)		45.07°N, 141.12°E	35	Island	5
Nopigia, Greece	May-June 1999		1.9	35.53°N, 23.78°E		Coastal	6
Neumayer	Feb 1999	0.013(0.007)	0.048	70.65°S, 8.25°W		Antarctic	7
Summit, Greenland	Jul 1999	0.074(0.026)		72.33°N, 38.75°W	3210	Mountain top	8
Summit, Greenland	June-July 1998	0.052(0.019)		72.33°N, 38.75°W	3210	Mountain top	8

Table 5-3. Comparison with other sites in remote areas^a (Continued).

	Period	Mean	Max	Latitude, Longitude	Altitude, m asl	Site Description	Ref ^b
Zeppelin Mountain	1994-1996	0.170(0.093)	1.608	78.90°N, 11.88°E	474	Arctic	9
Sado Island, Japan	Nov-Dec 1995	0.13(0.07)	0.37			Island	10
Yakushima, Japan	Dec 1994	0.25(0.11)	0.51			Island	10
Oki Island-2, Japan	Mar 1994	0.34(0.17)	0.97			Island	10
Oki Island-1, Japan	Nov 1992	0.22(0.09)	0.37			Island	10
Tsusima Island, Japan	Oct 1991	0.27(0.24)	0.79			Island	10
Frijoles Mesa, USA	Jun 1988	0.21	1.13	35.88°N, 106.32°W	1950	Mountain top	11
Frijoles Mesa, USA	Jul 1988	0.16	0.52	35.88°N, 106.32°W	1950	Mountain top	11
Frijoles Mesa, USA	Aug 1988	0.17	0.78	35.88°N, 106.32°W	1950	Mountain top	11

^aMeans (standard deviation) and maximums are in ppbv.

^bReferences: 1, this study; 2, Whalley et al., 2004; 3, Zellweger et al., 2000; 4, Zellweger et al., 2002; 5, Tanimoto et al., 2002; 6, Rappenglück et al., 2003; 7, Jacobi et al., 2000; 8, Ford et al., 2002; 9, Beine et al., 2000; 10, Watanabe et al., 1998; 11, Gaffney et al., 1993.

CHAPTER 6: DIURNAL PATTERNS

Diurnal patterns of PAN can be affected by diurnal changes in several factors and processes, including the emission of precursors, photochemical formation conditions, transport and dilution, chemical decomposition, and deposition. Inspection of the diurnal patterns of PAN and other measured gas species at the four sites revealed the different characteristics of the various environments of the measurement locations. This chapter presents the diurnal patterns of PAN and other gases at the different types of sites to show the similarity and differences among urban areas, rural areas, and remote areas.

6.1. Diurnal patterns in urban areas

Figure 6-1 shows the average diurnal mixing ratios (and standard errors) of PAN, O₃, CO, and NO_y in LZ. The primary pollutants CO and NO_y reached their maximum mean values at 0800 BJT, with a CO max of ~750 ppbv and a NO_y max of ~35 ppbv. The enhanced levels of primary pollutants in the morning with very similar diurnal profiles imply the advection of urban plumes to the study site in the morning. The decreased concentrations in the afternoon were partly due to growth of the boundary layer and partly due to the changing wind directions (figure not shown), which brought clean rural air masses in the afternoon and at night. The secondary pollutants, including PAN and O₃, exhibited very strong diurnal patterns. The PAN and O₃ mixing ratios both began

to rise in the morning at 0700 BJT, coinciding with the rise in solar radiation and the increase in CO and NO_y, indicating a local source for the photochemical production of secondary pollutants. PAN reached its highest mean value of ~2.2 ppbv before O₃ at 1100 BJT, and began to decompose in the afternoon because of the high temperature. In contrast, the mean O₃ concentration continued to increase to reach a daily peak of ~80 ppbv at 1500 BJT.

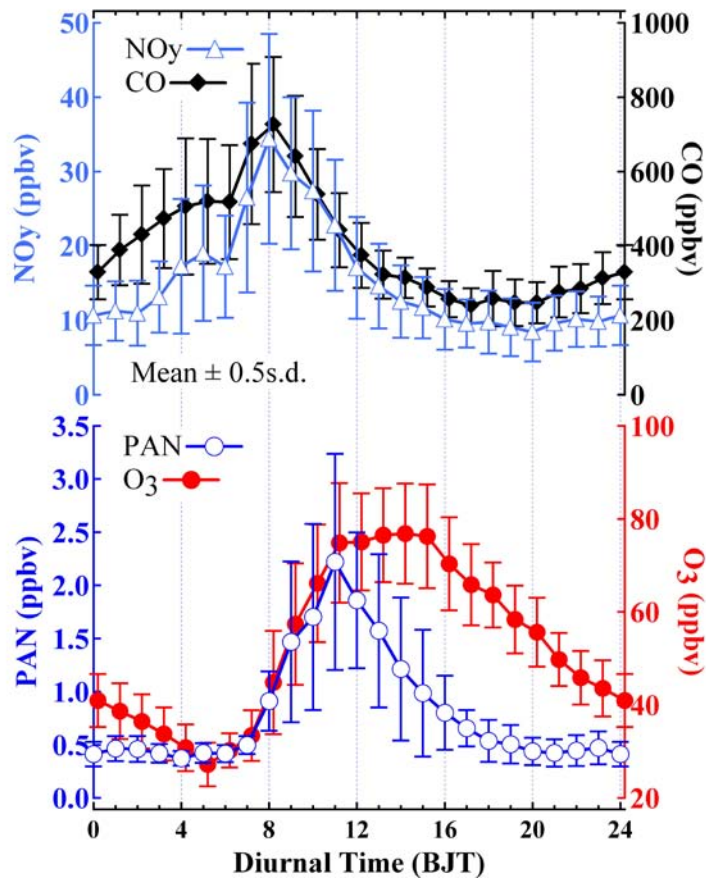


Figure 6-1. Average diurnal patterns of PAN, O₃, CO, and NO_y in LZ; the error bars are standard errors.

Figure 6-2 shows the average diurnal mixing ratios (and standard errors) of PAN and O₃ in the HK 06 study and of PAN in the HK 07 study. PAN exhibited clear diurnal patterns in HK, with relatively stable values (~0.65 ppbv for HK 06 and ~0.75 ppbv for HK 07) from midnight to morning hours and then an increase at 0900 LT. After reaching a maximum of about 0.95 ppbv in the HK 06 study and 1.6 ppbv in the HK 07 study at 1400 BJT the concentration declined in the afternoon. These profiles and the increasing PAN levels in the daytime indicate the photochemical formation of PAN. The daytime increase in PAN was sharper in LZ than in HK, reflecting the more intensive local photochemical production in LZ in the summer, whereas the highest concentrations of PAN in HK appeared 3 hours later than in LZ, indicating that the thermal decomposition of PAN is a less important removal process in HK in the autumn and winter. The higher level of PAN in the nighttime in HK suggests a more polluted regional background level in southern China. The diurnal patterns of PAN in the HK 06 and HK 07 studies were very similar, except that the range of PAN concentrations in the HK 07 study was higher than that in the HK 06 study, which can be attributed to the different meteorological conditions as mentioned in Chapter 5.

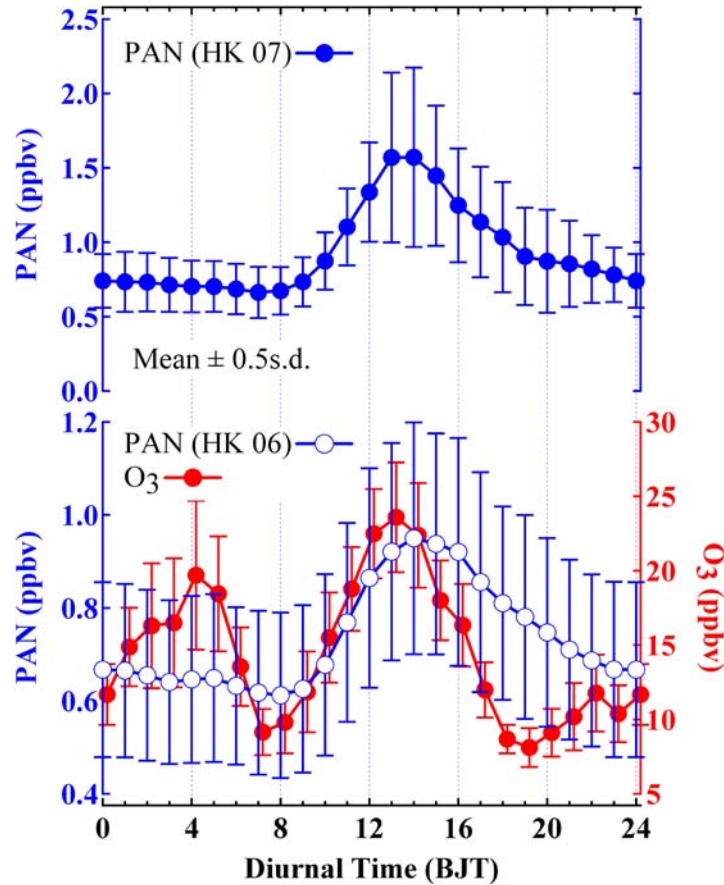


Figure 6-2. Average diurnal patterns of PAN and O₃ in the HK 06 study, and of PAN in the HK 07 study; the error bars are standard errors.

The O₃ mixing ratios in the HK 06 study suggest a large impact from local urban emissions as indicated by a morning trough (~10 ppbv), an afternoon peak (~25 ppbv), and a weak evening trough (~8 ppbv). The two troughs, which correspond to traffic rush hours, were presumably due to chemical titration by freshly emitted NO from the Hung Hom Harbor Tunnel near the HK PolyU sampling site. The afternoon peak indicates the photochemical formation of O₃. Compared with previous studies conducted at four sites in HK and Macau (see Figure 3 of Wang et al., 2003), O₃ exhibited the narrowest peak in this study and

the lowest concentration range. This is mainly due to the larger titration by local NO_x, as the sampling site on the HK PolyU campus was a shorter distance from urban emission sources than the sampling sites in the previous studies.

6.2. Diurnal patterns in rural areas

To obtain useful insights into the factors that might affect the PAN concentrations at different times of a day in the particular environment of the rural mountain top site of Mt. Tai, the diurnal variations in PAN concentrations and other trace gases were explored.

Figure 6-3 shows the average diurnal mixing ratios of PAN, O₃, CO, NO_y, Total N, NH₃*, NO, NO₂, and SO₂ at the TS site in the spring study. The primary pollutants, including CO, NO_y, Total N, and SO₂, all exhibited a broad afternoon peak, with the peak value appearing at about 1400 BJT when the PBL was well developed. The higher mixing ratios of these gas species have been attributed to the transport of pollutants from the PBL by the daytime upslope wind and the growth of the convective PBL (Gao et al., 2005). Secondary pollutants such as PAN and O₃ exhibited very similar diurnal patterns. Both the PAN and O₃ mixing ratios began to rise in the early morning, reaching the highest mean value of ~1.35 ppbv for PAN and ~70 ppbv for O₃ at 1600 BJT, two hours later than the primary pollutants. This indicates the presence of photochemical production

processes in the sampled air masses along with the transport from the emission sources to the summit of Mt. Tai. The similarity of the diurnal patterns of PAN and O₃ indicates similar sources of the precursors of these two species.

It is interesting to note that there was a second PAN peak at 2000 – 2100 BJT at night that corresponded to the highest peaks of CO and Total N at 2100 BJT, of SO₂ at 2000 BJT, and the minor peaks (or increases in concentration) of NO_y at 2000 BJT and of O₃, NH₃*, and NO at 2100 BJT. As the wind direction at the TS site in spring is predominantly southwesterly with a speed of more than 3 m/s (figure not shown), the elevation in the concentrations of these gases at night was probably due to the advection of large urban sources southwest of Mt. Tai, after the strong vertical mixing experienced in the afternoon. As expected, a city group (Jining, Yanzhou, Qufu, and Zhouxian) is located 75 km to 100 km southwest of Mt. Tai, air masses from which can reach the sampling site in about 7 to 8 hours. CO exhibited another peak before sunrise similar to that identified by Gao et al. (2005) in the 2003 study at Mt. Tai. It was explained by possible changes in small- to meso-scale dynamical transport. As no increase in concentration was detected in the other gas species at that time, this CO pattern was perhaps due to some of the closer combustion sources to the site.

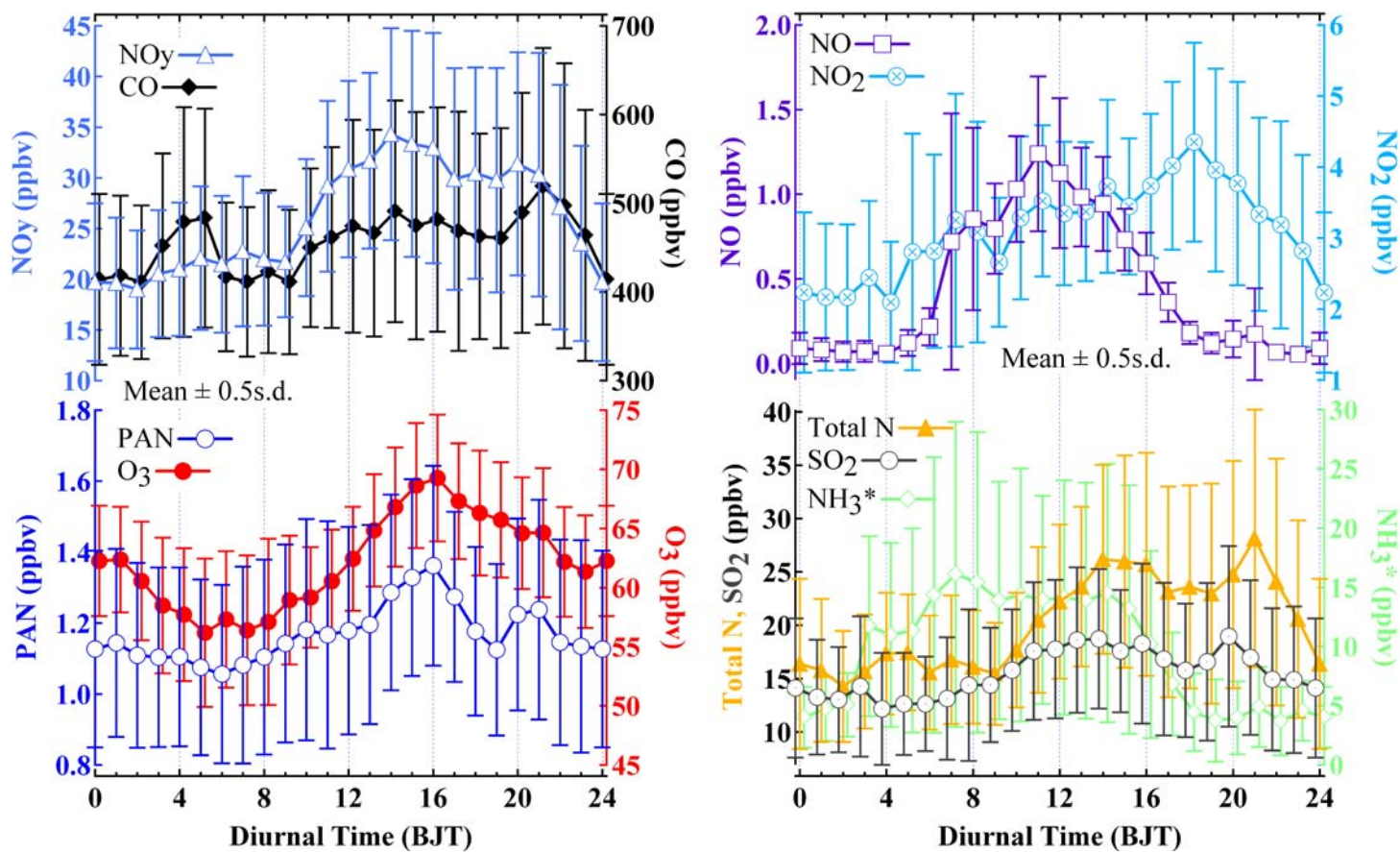


Figure 6-3. Average diurnal patterns of PAN, O_3 , CO, NO_y , Total N, NH_3^* , NO, NO_2 , and SO_2 in the TS Spring study; the error bars are standard errors.

Figure 6-4 shows the average diurnal mixing ratios of PAN, O₃, CO, NO_y, Total N, NH₃*, and SO₂ at the TS site in the summer study. Similar to the spring phase, primary pollutants including CO, NO_y, and Total N showed a broad afternoon peak, still mainly due to the daytime PBL vertical mixing and probably also mountain-valley breezes. SO₂ concentrations were also greater in the daytime, but experienced a small trough in the afternoon (1600 BJT), which may be due to different combinations of pollutants from the emission sources. The concentrations of the secondary pollutants, including PAN and O₃, began to rise in the morning along with the increase in primary pollutants, indicating the presence of photochemical production. The highest value of PAN appeared two hours before that of O₃, presumably for the same reason of PAN's thermal instability as posited for LZ in the summer, and possibly also due to the potential heterogeneous reactions of PAN on aerosol surfaces at TS, as the high aerosol levels at the site may support the heterogeneous loss of PAN (Gaffney et al., 1998). The minor peak of PAN at 2100 BJT could still be seen in the summer, but the minor peaks of the other gas species were no longer detectable.

A comparison of the diurnal patterns of PAN between the rural and urban sites reveals that the summer diurnal pattern of PAN at TS was similar to the pattern in HK, with peak values occurring at 1400 BJT. However, the daily buildup of PAN was stronger in the TS Summer study (~0.7 ppbv) than in the HK 06 study (~0.4 ppbv), reflecting the greater abundance of PAN precursors in

eastern China. The diurnal pattern of O₃ in the TS Summer study was very close to that found in the summer period in the 2003 study (Gao et al., 2005), with the continuous drop in the morning being explained either by the possible break-up of nighttime surface inversions on the mountain slopes or the transport of air masses of different origins.

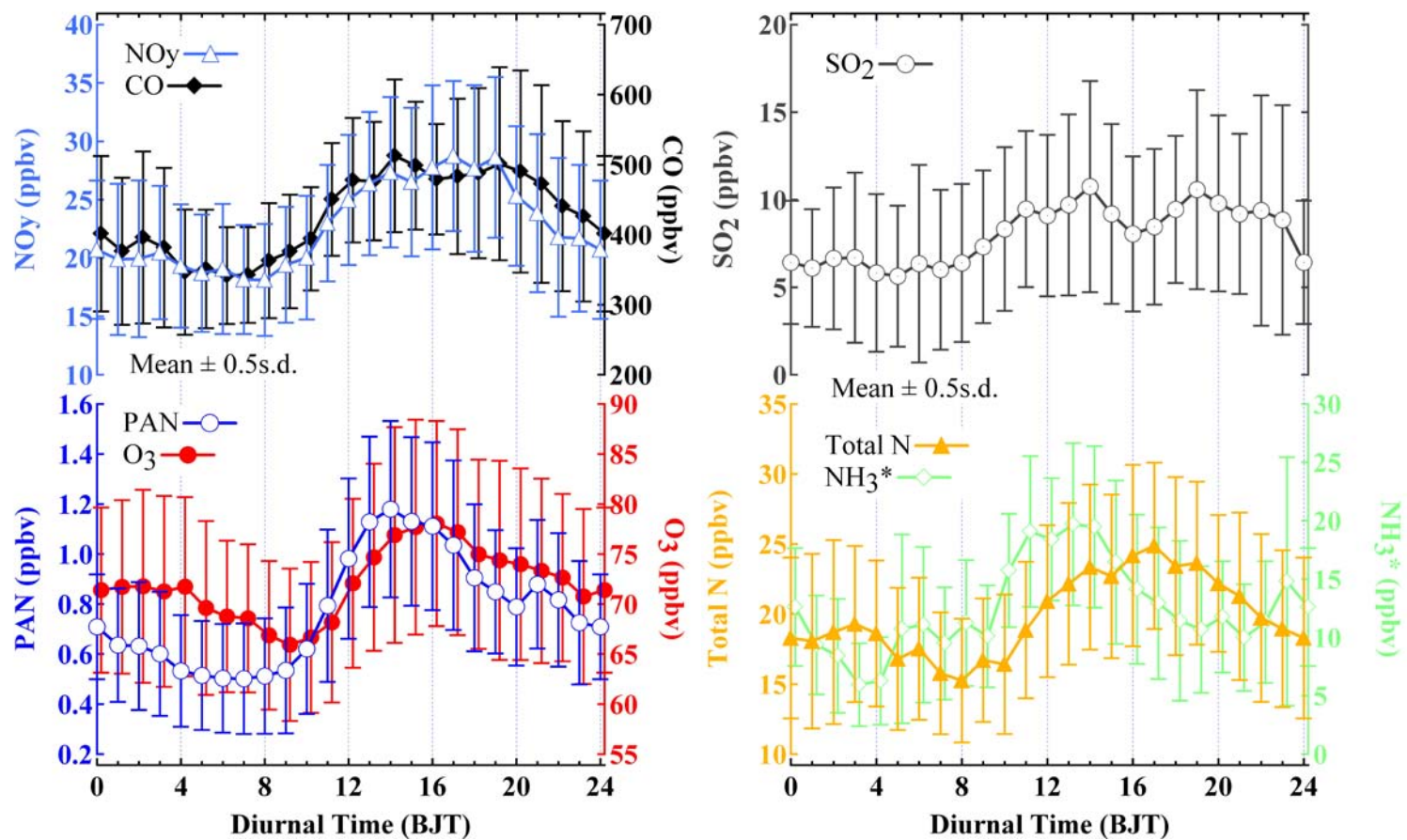


Figure 6-4. Average diurnal patterns of PAN, O₃, CO, NO_y, Total N, NH₃*, and SO₂ in the TS Summer study; the error bars are standard errors.

6.3. Diurnal patterns in remote areas

At the remote WLG site, the diurnal difference in the average concentrations of the trace gases was much less distinct than at the other sites, as shown in Figure 6-5. The mean mixing ratios of NO_y experienced a minimum of ~1.0 ppbv in the afternoon (1600 – 1700 BJT) and enhanced levels in the morning and at nighttime with a maximum of ~1.7 ppbv. CO also showed relatively lower values in the afternoon and higher values in the morning and at night (mean value: 120 – 180 ppbv). Despite the smaller range of mean values, the diurnal profiles of NO_y and CO were similar to those found in the previous study at WLG in 2003 (Wang et al., 2006b), except that the NO_y profile was different from that identified in the summer of 2003. The average PAN mixing ratios showed a similar pattern to that of NO_y, with an afternoon trough that may have been due to an increased mixing height in the afternoon. Higher concentrations of PAN (and of primary pollutants) were noted at night, which, as is shown in detail in Chapter 8, were mainly caused by five plumes transported from the urban areas of Lanzhou and other pollution sources in the east. The average concentrations of O₃ were lower (~57 ppbv) at noon (1000 – 1400 BJT) and higher (~62 ppbv) at night. This is a typical pattern observed at remote mountain top sites that can be explained by mountain-valley circulation, with a down-slope flow at night bringing in O₃-rich air from the free troposphere (e.g., Wang et al., 2006b). A slight increase in O₃ was also observed at the time of the

PAN peak at 2000 BJT, indicating an anthropogenic impact.

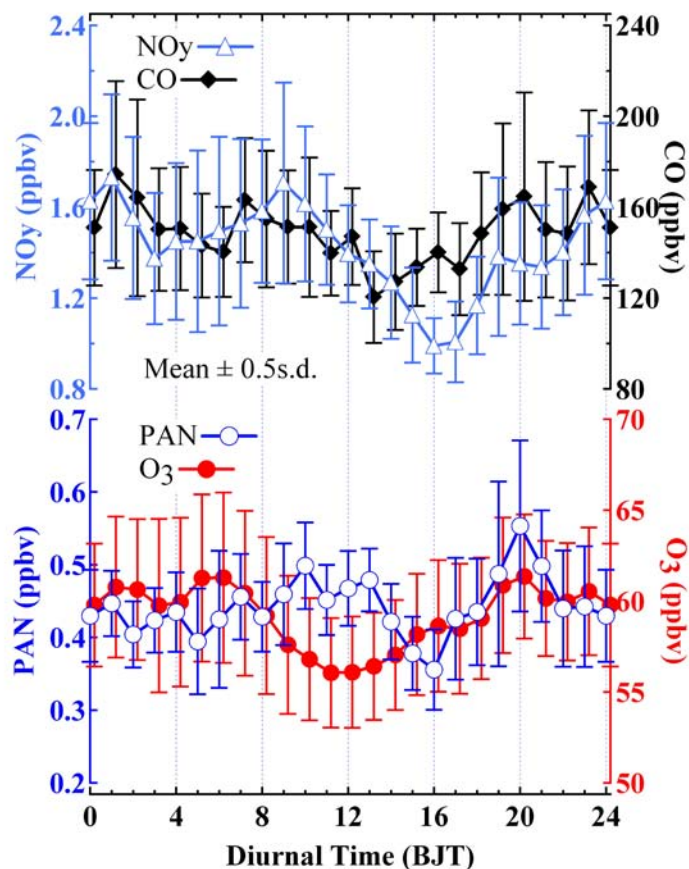


Figure 6-5. Average diurnal patterns of PAN, O₃, CO, and NO_y at WLG; the error bars are standard errors.

A comparison of the diurnal patterns of PAN in LZ and at WLG reveals an interesting phenomenon: the average mixing ratios of PAN at the urban LZ site during the night (2200 – 0600 BJT) were almost identical to those observed at WLG (~0.45 ppbv), as shown in Figure 6-6, indicating that the regional baseline level of PAN was reached at night in LZ with very little carryover of pollutants from day to day. Winds at night in LZ are mostly from the north east and occur at

increasing speeds, which brought in regional background air masses containing similar mean PAN concentrations to those measured at WLG despite the different altitudes of the two sites.

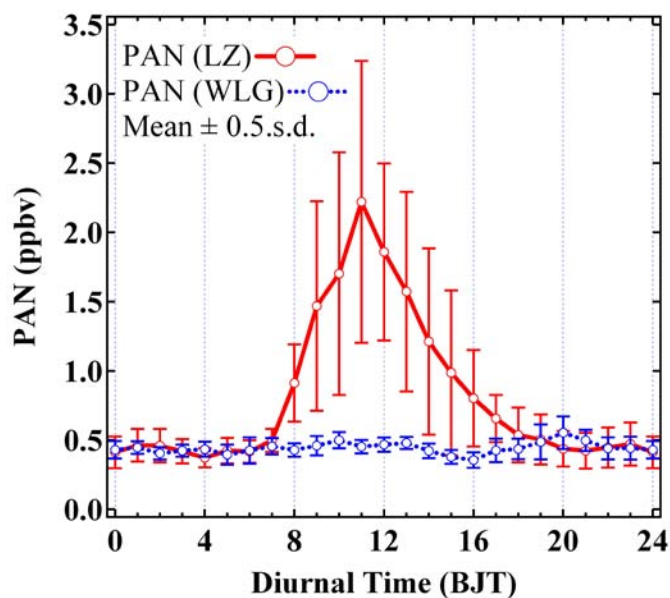


Figure 6-6. Comparison of the average diurnal patterns of PAN in LZ and at WLG; the error bars are standard errors.

CHAPTER 7: RELATIONSHIP BETWEEN PAN AND OTHER GAS SPECIES

7.1. Correlation between PAN and O₃

PAN and O₃ have a common photochemical source involving NO_x and VOCs. Whereas O₃ forms from the oxidation of virtually all reactive VOCs, PAN is produced only from those VOCs that are precursors to the acetyl radical CH₃CO (Grosjean et al., 2002), with aldehydes and olefins being the two main groups of precursors (Gaffney et al., 1999). Therefore, the correlation between the two species can give useful information on the atmospheric loading and composition of VOCs and also shed light on the photochemical processes involved in the formation of PAN and O₃.

7.1.1. Overall results

Figure 7-1 shows the correlations between the concurrent data on PAN and O₃ from the LZ, HK 06, TS Spring, TS Summer, and WLG field studies. The concentrations of PAN and O₃ measured in LZ exhibited a relatively weak overall correlation (correlation coefficient (r^2) = 0.32 for the whole period, figure not shown) due to the titration of O₃ by NO and the thermal decomposition of PAN. Removal of the data points associated with O₃ concentrations of < 50 ppbv improves the correlation, giving a PAN versus O₃ slope of 0.055 ppbv ppbv⁻¹ and

an r^2 of 0.56 (see Figure 7-1a). This is typical for suburban sites where air masses with simultaneous photochemical formation of PAN and O_3 have been sampled. The still moderate r^2 value is mainly due to the different diurnal patterns of PAN and O_3 , as the O_3 maximum persisted longer into the afternoon whereas PAN was thermally decomposed to a level lower than 1 ppbv.

In the HK 06 study, the correlation between PAN and O_3 was only examined in the last 17 days of the study when O_3 levels were measured, that is, between Dec 16, 2006 and Jan 1, 2007 (see Figure 7-1b). As expected, there was almost no correlation between PAN and O_3 ($r^2 = 0.02$) due to the intensive titration of O_3 by NO, the sources of which were very close to the site, and also the weak photochemical production in the winter.

There was a weak correlation between PAN and O_3 in the TS Spring study, with a PAN versus O_3 slope of $0.028 \text{ ppbv ppbv}^{-1}$ and an r^2 of 0.33 (see Figure 7-1c). The slope value was lower than that for the LZ study, indicating a lesser abundance of PAN precursors compared with O_3 at TS than in LZ. The low r^2 demonstrates the complexity of sources of air masses sampled at different times in the field study. In the TS Summer study, PAN and O_3 were more strongly correlated than in the spring study, with a PAN versus O_3 slope of $0.022 \text{ ppbv ppbv}^{-1}$ and an r^2 of 0.48 (see Figure 7-1d). It is worth noting that the slope value was even lower in the TS Summer study than in the TS Spring study, indicating

that the dominant route of photochemical transformation of primary pollutants is to O₃ rather than to PAN in the summer season at this location. Another possible reason is that the thermal decomposition of PAN is stronger in the summer, which resulted in lower concentrations of PAN compared with those in spring. The relatively higher r² value in the summer season shows that photochemical production is a more important factor in hotter weather than other factors that affect PAN and O₃ concentrations.

The PAN versus O₃ slopes of 0.028 ppbv ppbv⁻¹ and 0.022 ppbv ppbv⁻¹ for the TS Spring and TS Summer studies were lower than the corresponding slope for LZ (0.055 ppbv ppbv⁻¹) and higher than that for WLG (0.004 ppbv ppbv⁻¹). These slopes are in accordance with earlier studies, which report a decrease in slope with increasing distance from pollution sources from 0.07 in urban areas to 0.001 in oceanic air masses (Altshuller, 1983; Sirois and Bottenheim, 1995). The results reflect the nature of the TS site as a mountain top site at high altitude but surrounded by polluted areas.

At the remote WLG site, the overall correlation of the concurrent PAN and O₃ data was much weaker than at the urban LZ site and the rural mountain top of Mt. Tai (see Figure 7-1e). Except for a few cases involving the transport of plumes to WLG, the two species were not correlated most of the time, which is consistent with previous studies at WLG that have suggested that summertime O₃

there is significantly influenced by the transport of stratospheric/upper tropospheric air masses (Ding and Wang, 2006; Wang et al., 2006b).

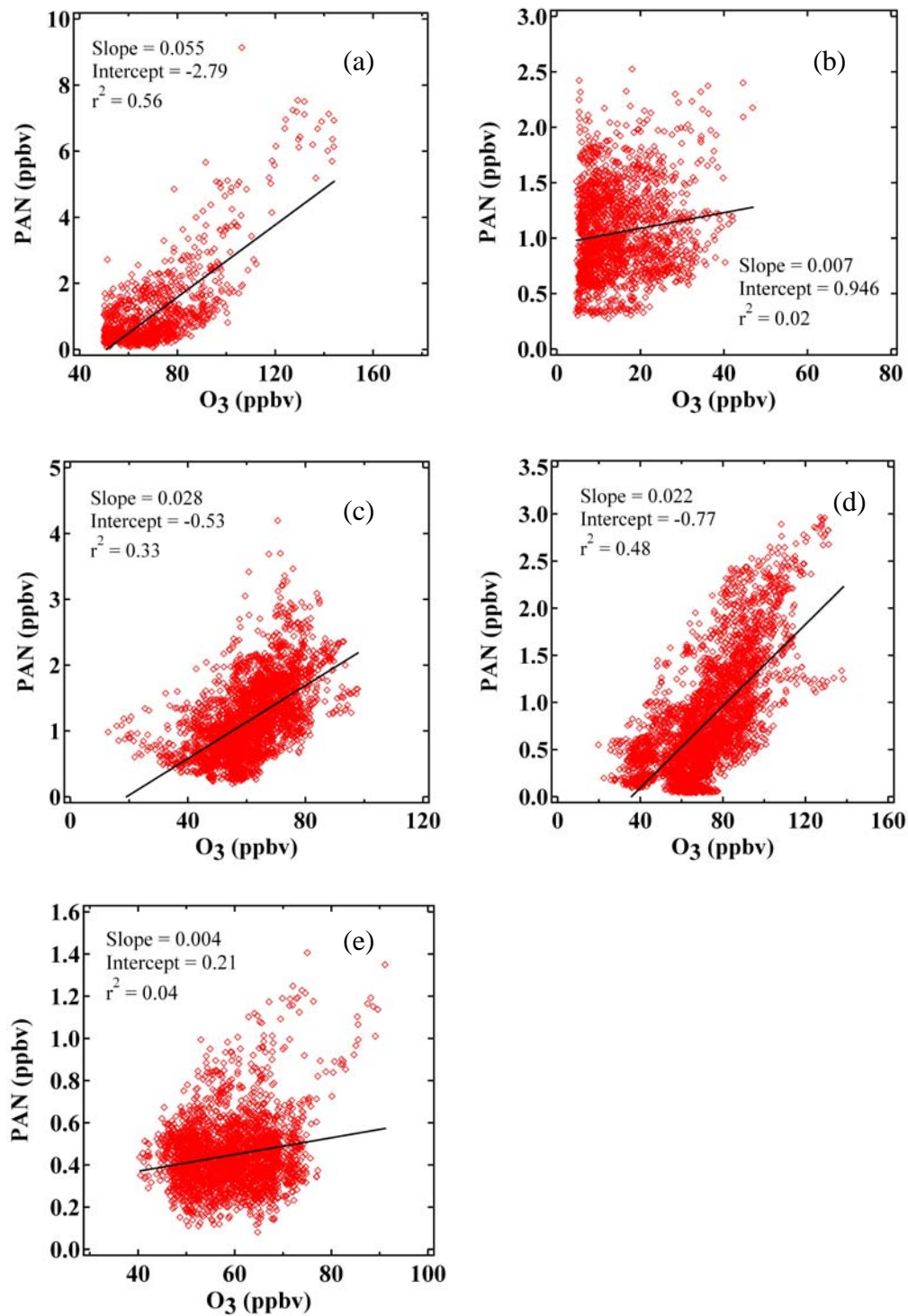


Figure 7-1. Scatterplots of PAN versus O₃ for the LZ (a), HK 06 (b), TS Spring (c), TS Summer (d), and WLG (e) studies.

7.1.2. Correlation between the PAN daily maximum and the O₃ daily maximum

There is usually no simple overall relationship between the concurrent data on PAN and O₃ due to the different VOC sources of the two gases. In addition, PAN is thermally unstable and some O₃ is of stratospheric origin and is transported to the earth's surface without any accompanying PAN. Moreover, O₃ is more affected by local pollution sources of NO than PAN is affected by titration in freshly polluted air (McFadyen and Cape, 2005). To give a clearer picture of the photochemical production processes in which PAN and O₃ are the two destinations for the chemical transformation routes, the correlations between the PAN daily maximum and the O₃ daily maximum are examined to reduce the impacts of other factors on the concentrations of PAN and O₃ in periods of less photochemical formation.

Figure 7-2 shows the correlations between the PAN daily maximum and the O₃ daily maximum during the LZ, HK 06, HK 07, TS Spring, and TS Summer studies. At the suburban LZ site, a strong positive correlation ($r^2 = 0.91$) between the daily maximum values of PAN and O₃ was observed. The regression slope (PAN daily max/O₃ daily max) is 0.091 (ppbv ppbv⁻¹), which indicates that, on average, 9 PAN molecules were produced for every 100 O₃ molecules formed in LZ air during the daytime. The peak ratio of PAN to O₃ in LZ was generally larger than those reported in recent studies in other urban and suburban areas,

such as Mexico City (0.02) (Marley et al., 2007), Porto Alegre, Brazil (0.058) (Grosjean et al., 2002), and Nashville (0.025) (Roberts et al., 2002). A larger ratio of about 0.117 was also observed in Mexico City in 1997 before the comprehensive control of olefins in liquefied petroleum gas (LPG) began in the city (Marley et al., 2007; Gaffney et al., 1999).

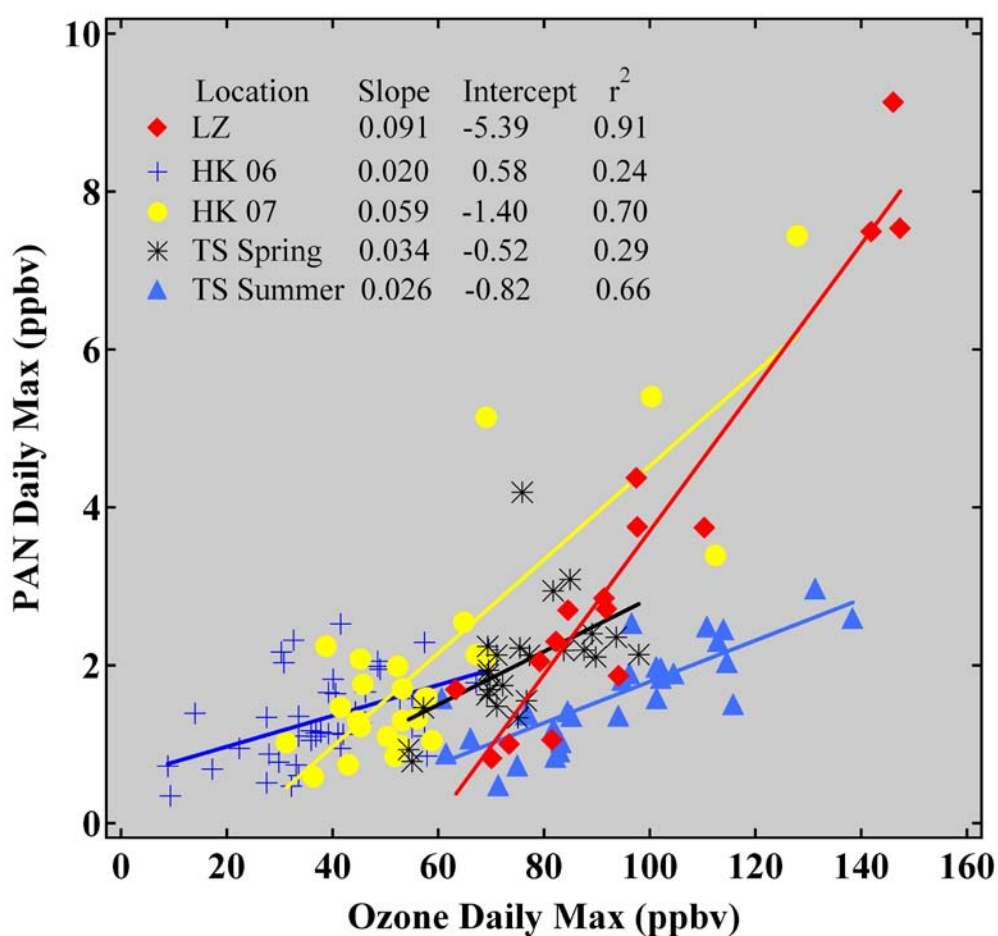


Figure 7-2. Scatterplot of the PAN daily maximum versus the O₃ daily maximum in the LZ, HK 06, HK 07, TS Spring, and TS Summer studies.

The high PAN/O₃ ratios observed in the LZ study imply the presence of relatively more abundant PAN precursors in the VOCs in LZ city. An

examination of the mean profile of the C₂-C₈ NMHCs measured during the study confirms this notion, and reveals that ethene and propene were the dominant NMHCs in LZ (see Figure 7-3). The high concentrations of olefins in LZ can be attributed to the fact that about 60% of the vehicles in the city now burn LPG (with the remaining 40% using compressed natural gas) since the city government introduced the “gas instead of oil” program in 2005 in an attempt to improve the overall air quality of the city (http://news.xinhuanet.com/newscenter/2005-08/23/content_3391563.htm), and also to the emission from the petrochemical plants, the main products of which include ethene and propene (<http://www.lh-resin.com/pages/products.htm>).

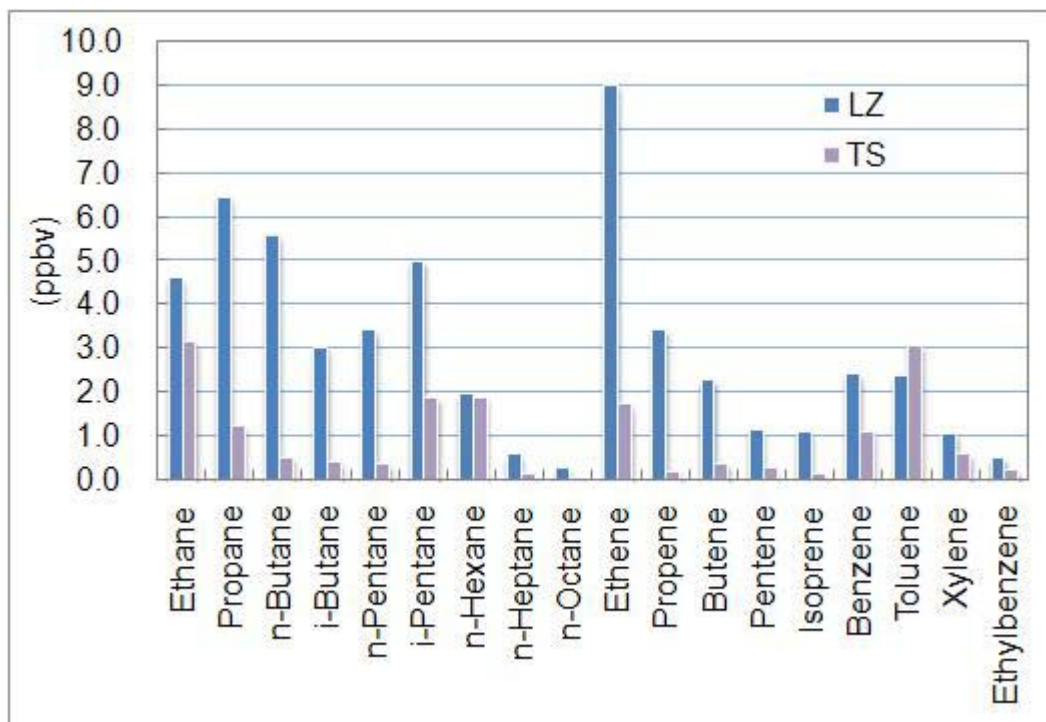


Figure 7-3. Mean profile of the C₂-C₈ NMHCs measured in the LZ and TS studies.

As O₃ data are not available for the HK site for all of the days of the study, hourly O₃ data from the Environmental Protection Department (EPD) of Hong Kong monitored at the Central/Western General Station were used to analyze the correlations between the PAN daily maximums and O₃ daily maximums in the HK 06 and HK 07 studies. These O₃ data can be obtained online (<http://epic.epd.gov.hk/ca/uid/airdata/p/1>). Because of the different resolution of these O₃ data, the peak concentrations of O₃ tend to be lower, resulting in a small increase in the PAN/O₃ ratios in the HK studies.

There is a relatively weak positive correlation ($r^2 = 0.24$) between the daily maximum values of PAN and O₃ in the HK 06 data, with a regression slope (PAN daily max/O₃ daily max) of 0.020 (ppbv ppbv⁻¹). This value is close to those in European and North American cities (Schrimpf et al., 1998; Glavas and Moschonas, 2001). In contrast, a much stronger positive correlation ($r^2 = 0.70$) was found between the daily maximum values of PAN and O₃ in the HK 07 study due to stronger photochemical production in that period. The regression slope of the PAN daily maximum to the O₃ daily maximum was 0.059 (ppbv ppbv⁻¹), higher than that in the HK 06 study, lower than that in LZ, and comparable to the slopes recorded for several South American cities (Rubio et al., 2004; Grosjean et al., 2002), reflecting the moderate level of PAN precursors in Hong Kong.

Figure 7-2 shows the correlations between PAN daily maximum and the O₃

daily maximum in the TS studies, and demonstrates that the value of r^2 in the summer study ($r^2 = 0.66$) was much higher than that in the spring study ($r^2 = 0.29$), implying greater simultaneous production of PAN and O_3 in air masses arriving at the site in summer. The regression slopes (PAN daily max/ O_3 daily max) were $0.034 \text{ ppbv ppbv}^{-1}$ and $0.026 \text{ ppbv ppbv}^{-1}$ for the spring phase and summer phase, respectively. These values are higher than those reported in studies at other rural sites, such as Simi Valley, USA (0.014) (Grosjean et al., 2001) and Edinburgh, Scotland (0.015) (McFadyen and Cape, 2005).

It is interesting to note the large difference in the PAN/ O_3 ratios in LZ and at TS. The peak ratios of PAN to O_3 at TS in eastern China were much lower than those in LZ in western China. It is believed that the primary reason for this is the different atmospheric loads and compositions of the NMHCs in the different regions. The NMHCs present in LZ favor the formation of PAN more than those present at TS. This is confirmed by an inspection of the mean profile of the C_2 - C_8 NMHCs (Figure 7-3), which shows that the overall NMHC level at TS was much lower than that in LZ, although the NO_y concentrations in the TS studies were higher than those in the LZ study, as discussed in Chapter 5. In addition, the key precursors of PAN, such as ethene and propene, constituted a much larger fraction of the total NMHCs in LZ than at TS. The difference in NMHC composition between LZ and TS is presumably due to the different industrial structures of the two places, as power plants are the major emission sources in

the North China Plains where TS is located. It could thus be concluded that the lower ratios of PAN to O₃ at TS are mainly due to the lack of VOC precursors of PAN, which limits the photochemical production of PAN in eastern China.

7.2. Relationship between PAN and other gas species

7.2.1. Overall results

To assess the impact of emissions and atmospheric stability on PAN levels, the correlations between PAN and NO_y and between PAN and CO were analyzed. As summarized in Table 7-1, no simple relationship was identified between PAN and NO_y or between PAN and CO in LZ. The r^2 of PAN and NO_y was 0.05 for the whole period because there were two distinct ratios between PAN and NO_y on different days, suggesting that air masses of different photochemical ages or emission ratios (especially VOCs to NO_y ratios) were sampled. On June 23, 25, 28, and 29 and July 1, 5, 7, 11, and 13, the linear least-squares regression slope of PAN/NO_y was 0.055 ppbv ppbv⁻¹, indicating a significant photochemical transformation from primary pollutants to PAN, whereas on the other days the slope was 0.007 ppbv ppbv⁻¹. The profile of the scatterplot of PAN versus CO for LZ (figure not shown) is similar to that of PAN versus NO_y (figure not shown) with two main groups of data pairs, again indicating that the sampled air masses had different features.

Table 7-1. Correlations between PAN and NOy and between PAN and CO^a.

	PAN versus NOy			PAN versus CO		
	Slope	Intercept	r ²	Slope	Intercept	r ²
LZ	0.011	0.60	0.05	0.0008	0.45	0.04
TS Spring	0.023	0.56	0.57	0.0017	0.40	0.48
TS Summer	0.033	0.12	0.43	0.0013	0.21	0.24
WLG	0.152	0.22	0.45	0.0011	0.29	0.18

^aSlope values are in ppbv ppbv⁻¹, and intercept values are in ppbv.

At TS, moderate correlations between PAN and NOy and between PAN and CO were observed in both spring and summer. The r² values of PAN/NOy and PAN/CO were higher in spring than in summer, possibly implying that PAN and primary pollutants from similar sources were transported to the site in spring, whereas in summer the PAN level was more affected by different regimes of in-situ production. The slopes of PAN/NOy for TS (0.023 and 0.033 ppbv ppbv⁻¹) were lower than those for LZ on the days with significant photochemical production (0.055 ppbv ppbv⁻¹), presumably due to a lower VOC to NOy ratio at TS than in LZ, which is in accordance with the analysis in Section 7.1.2.

PAN and NOy were also moderately correlated in the study at WLG, with a PAN/NOy ratio of 0.152 and an r² of 0.45. The high value of the slope and the moderate value of the r² can be explained by the relatively greater contribution of PAN to NOy at WLG (see Section 7.2.2). The relatively low r² value for PAN and CO indicates that the two gases are not correlated in air masses with background levels due to their different original concentrations.

7.2.2. Nitrogen budget

NO_y is defined as the sum of NO_x (NO and NO₂) and its atmospheric oxidation products, which is abbreviated as NO_z and includes PAN, HNO₃, p-NO₃⁻, HONO, HO₂NO₂, NO₃, and 2N₂O₅ (e.g., Sandholm et al., 1994; Zellweger et al., 2003). NO_x, PAN, and Total N (HNO₃ and p-NO₃⁻) are considered to be the most abundant NO_y compounds in the troposphere, and their contributions to NO_y vary systematically (Jacobi et al., 2000).

The data for the various NO_y compounds measured in the field studies at Mt. Tai were used to analyze the nitrogen budgets. Figure 7-4 shows the results for the spring and summer studies. In the spring study, PAN, Total N, NO, and NO₂ together contributed on average 95.9% to the total NO_y mixing ratio. Total N (78.0%) constituted the major fraction, followed by NO_x (11.8% NO₂ and 1.7% NO), and PAN (4.4%). The relatively small unidentified fraction (4.1%) shows the accurate determination of the NO_y species. PAN contributed a very small fraction to NO_y at TS compared with other studies (e.g., Zellweger et al., 2000; Ford et al., 2002), mainly due to the very high concentrations of NO_y and the significant contribution of Total N to NO_y at the TS site. NO_x also contributed a relatively small fraction of NO_y, which indicates that the air masses sampled at TS had been transported over a relatively long distance. Thus, the high concentration of NO_y and the low fraction of NO_x measured in the TS Spring study indicate severe regional air pollution despite the lack of pollution

sources in the immediate vicinity. The partition of NO_z between PAN and Total N either reflect the predominant role of inorganic chemistry in the atmosphere of the North China Plains or an unknown source of Total N, which deserves further investigation.

Although NO_x data are not available for the summer study, it can be deduced from the spring phase data that NO_x contributed about 70% to the unmeasured part of the NO_y species. Figure 7-4 shows that PAN and NO_x contributed smaller fractions to NO_y in summer than in spring, and that as much as 86.8% of the NO_y was made up of Total N. Although the total NO_y mixing ratio was lower in summer, the analysis reveals the inorganic transformation of NO_x to NO_z to be the more dominant pathway in summer.

In terms of the difference between daytime and nighttime, PAN was present in a slightly larger fraction in the nighttime in spring, probably due to its longer lifetime compared with other NO_y species in low spring temperatures, whereas a smaller fraction was found during the nighttime in the summer study, presumably due to the faster thermal decomposition of PAN in summer. NO_x was present in larger fractions in the daytime in both the spring and summer studies due to the stronger fresh emissions in the daytime.

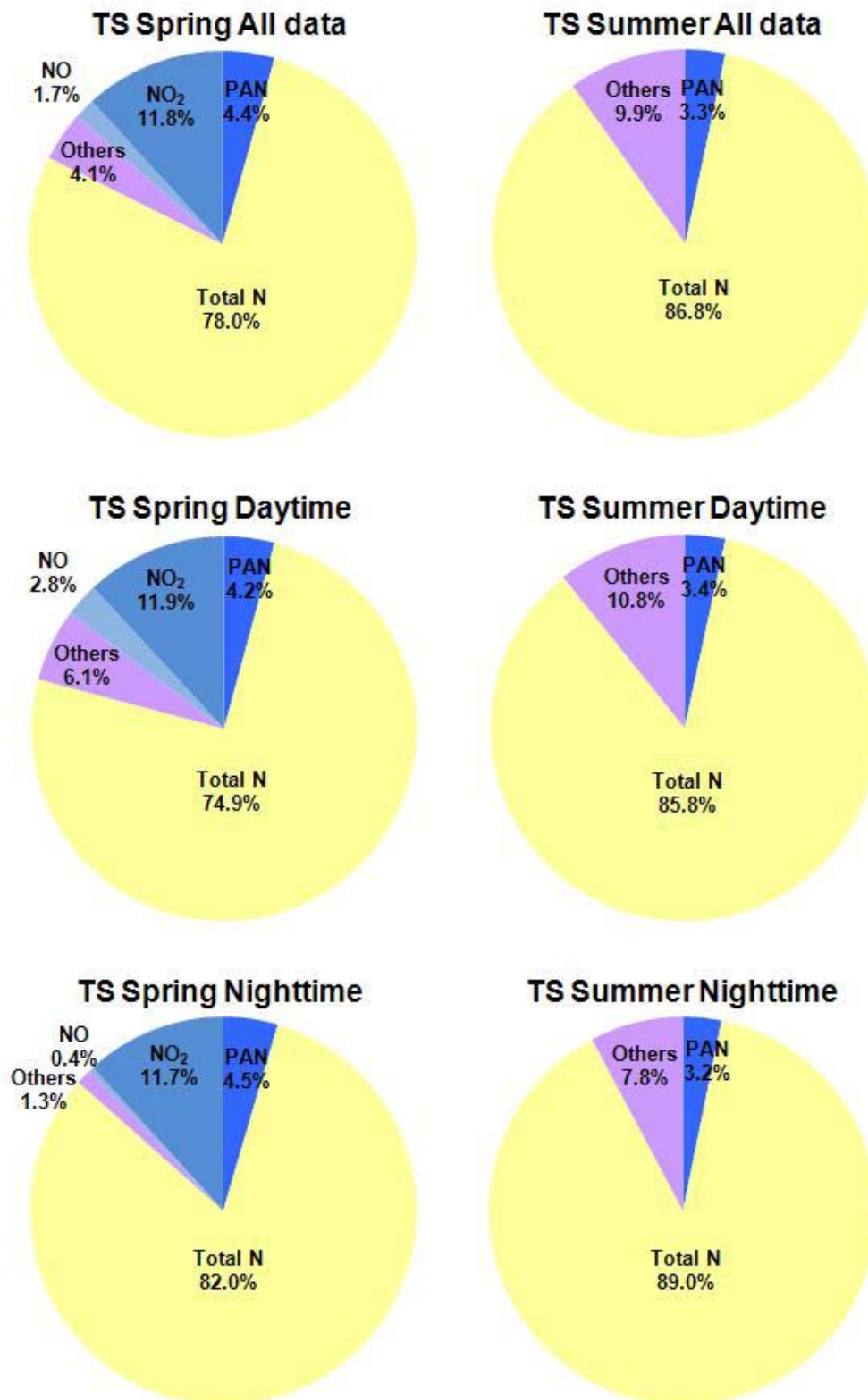


Figure 7-4. Nitrogen budgets in the TS Spring and TS Summer studies. Daytime is defined as 0600 to 1750 BJT for the spring study and 0500 to 1950 BJT for the summer study. Nighttime is defined as 1800 to 0550 BJT for the spring study and 2000 to 0450 BJT for the summer study.

The contributions of PAN to NO_y in the LZ, TS Spring, TS Summer, and WLG studies are summarized in Table 7-2. The fraction of PAN in NO_y in LZ was comparable to that at TS, but for different reasons. As the LZ site is close to anthropogenic pollution sources, it may frequently be influenced by polluted air masses, and thus NO_x can be assumed to contribute significantly to the total NO_y. The PAN fraction of NO_y was larger in the daytime in LZ, reflecting the strong photochemical formation during the daytime at this site. At WLG, the relatively high contribution of PAN to NO_y (31.5%) is in good agreement with other measurements taken at high altitudes over continental areas (Whalley et al., 2004; Ford et al., 2002; Zellweger et al., 2000).

Table 7-2. Contributions of PAN to NO_y at LZ, TS, and WLG.

	All data	Daytime ^a	Nighttime ^b
LZ	4.9%	5.5%	3.7%
TS Spring	4.4%	4.2%	4.5%
TS Summer	3.3%	3.4%	3.2%
WLG	31.5%	32.2%	30.4%

^aDaytime is defined as 0600 to 1950 BJT for the LZ and WLG studies, 0600 to 1750 BJT for the TS Spring study, and 0500 to 1950 BJT for the TS Summer study.

^bNighttime is defined as 2000 to 0550 BJT for the LZ and WLG studies, 1800 to 0550 BJT for the TS Spring study, and 2000 to 0450 BJT for the TS Summer study.

CHAPTER 8: REGIONAL TRANSPORT ANALYSIS

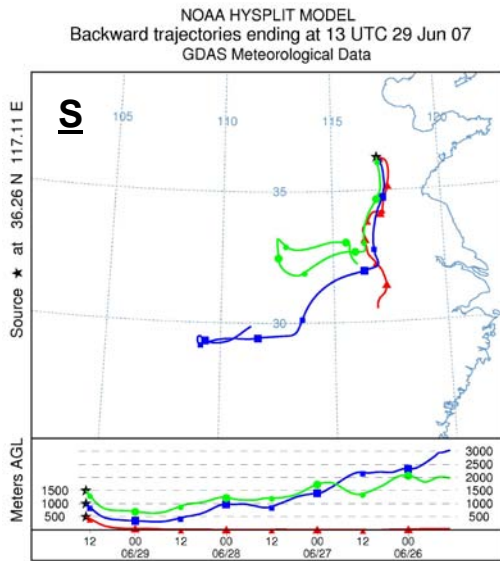
In this chapter, data from Mt. Tai and Mt. Waliguan are examined to study the impact of air masses from different source regions. The high elevation of the two sites makes them more suitable for this kind of study than the surface sites. As has been mentioned, these two high altitude sites represent the polluted eastern part and clean western part of China, respectively.

8.1. Eastern China

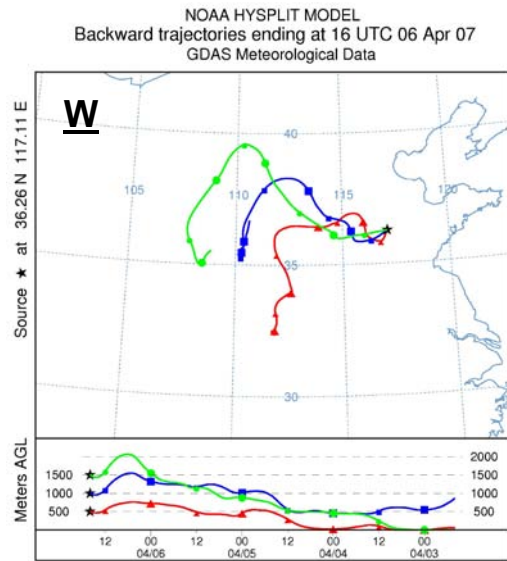
About 450 back trajectories (see Section 4.3) were obtained for the two phases of the Mt. Tai (TS) studies. The air masses reaching the TS site were classified into six main categories for the spring study and seven main categories for the summer study. According to the origins, paths, and altitudes of the trajectories, the definitions of the categories are summarized as follows. The S group denotes air masses passing over eastern China and arriving at the site from the southeast or south; the W group indicates air masses originating in central China and arriving at the site from the southwest or west; the NW group denotes continental air masses from northwest; the N group refers to air masses coming from the north; the NE group comprises air masses originating in the Northeast Plains (spring only); the LP group encompasses air masses moving slowly or with a loopy trajectory over the North China Plains; the EA group comprises air

masses passing over the Korean Peninsula and Japan (summer only); and the ME group denotes maritime air masses making relatively short journeys over the eastern coastal areas of China (summer only).

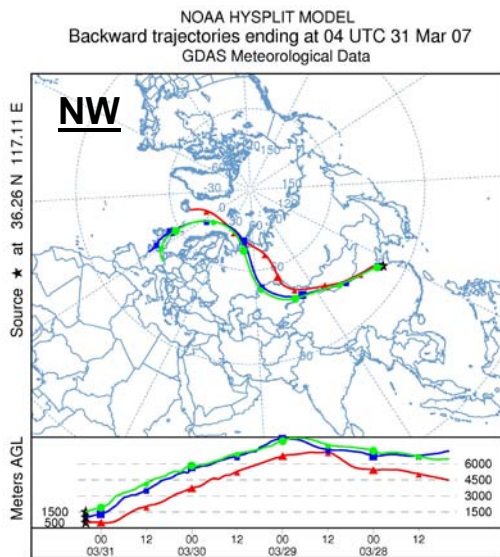
The typical pathways for each category are shown in Figure 8-1a-h. In the spring study, continental air masses were the most abundant type, accounting for 29% of the total (NW 15% and N 14%), followed by the S (25%), LP (19%), W (18%), and NE (9%) groups. The transport characteristics in summer were different from those in spring, which is consistent with previous studies (e.g., Gao et al., 2005). Air masses from the eastern regions had a larger impact, with the LP group having the largest proportion (30%), followed by the EA (20%), ME (16%), S (11%), N (8%), W (5%), and NW (3%) groups. Six percent of the trajectories in the TS Summer study were not classified.



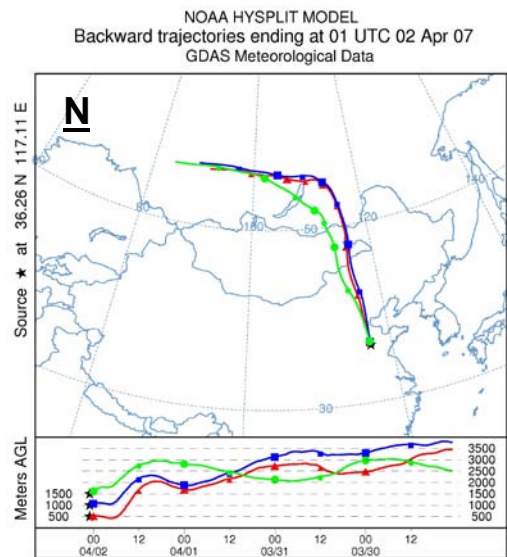
(a)



(b)



(c)



(d)

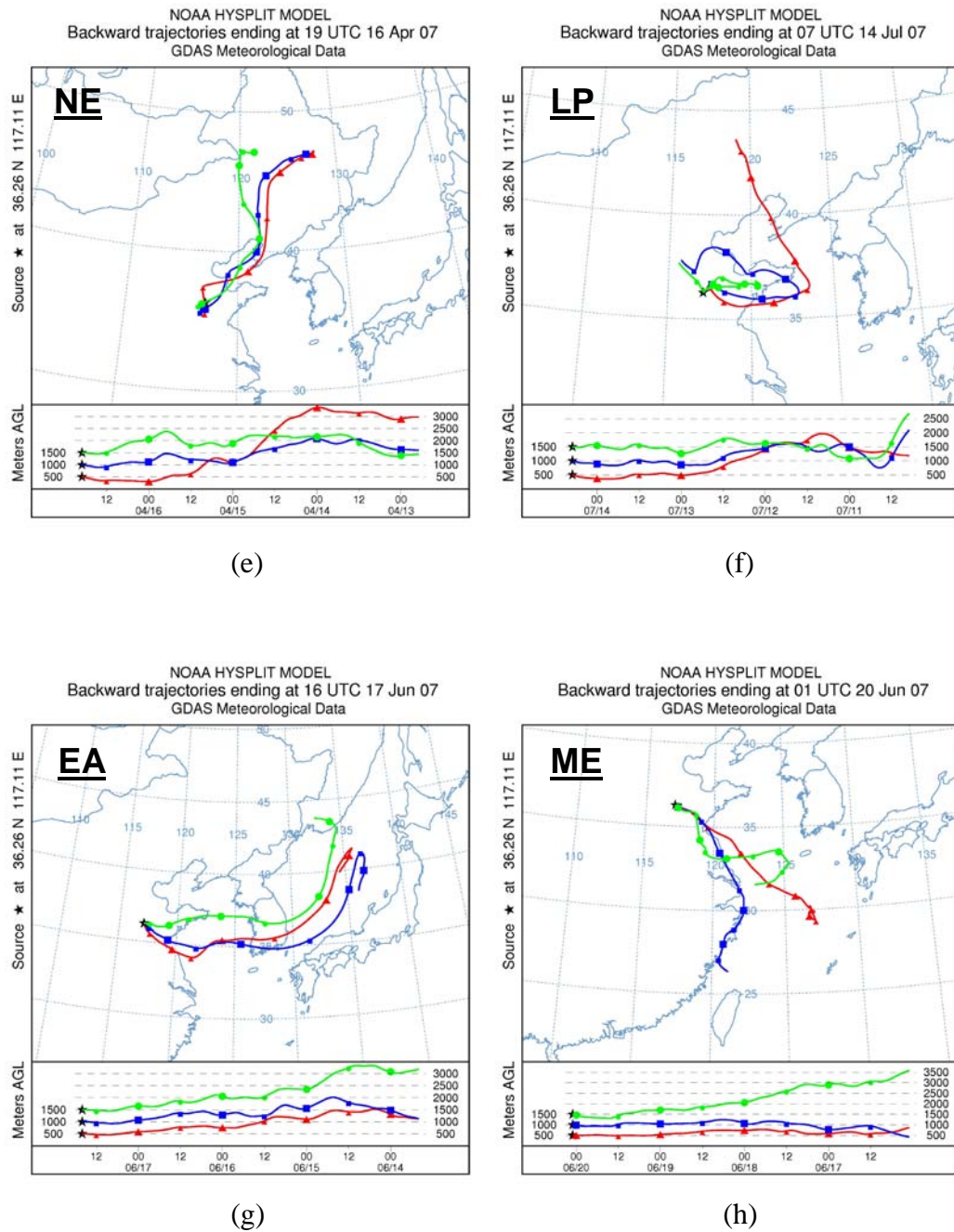


Figure 8-1. Examples of the eight types of air masses classified by the back trajectories: (a) south originating passing through eastern China (S) on June 29 at 2100 BJT; (b) west originating passing through central China (W) on Apr 7 at 0000 BJT; (c) continental originating (NW) on Mar 31 at 1200 BJT; (d) north originating (N) on Apr 2 at 0900 BJT; (e) northeast originating passing through the Northeast Plains (NE) on Apr 17 at 0300 BJT; (f) loop trajectories (LP) on July 14 at 1500 BJT; (g) eastern Asia originating (EA) on June 18 at 0000 BJT; and (h) marine originating (ME) on June 20 at 0900 BJT.

To determine the relationship between PAN concentrations and the origins of the air masses at TS and to reveal the photochemical pollution status of the different regions under study, the PAN and other trace gas statistics were calculated for the eight categories of air masses (see Table 8-1). As the trajectories were calculated every three hours, the mixing ratios of PAN and the other gases were averaged over a three-hour period centered at the termination time of each trajectory.

Table 8-1. Statistical data on PAN, O₃, CO, NO_y, Total N, and SO₂ in each air mass category captured at Mt. Tai^a.

	Mean (standard deviation) ^b						n ^c
	PAN	O ₃	CO	NO _y	Total N	SO ₂	
<i>TS Spring</i>							
S	1.42 (0.47)	67 (8)	526 (185)	32.9 (11.1)	25.6 (8.9)	21.2 (10.2)	58
W	1.16 (0.47)	65 (12)	502 (174)	26.9 (10.5)	20.1 (8.8)	17.0 (9.9)	40
NW	0.66 (0.28)	58 (7)	271 (131)	13.0 (11.1)	10.0 (10.2)	6.2 (5.7)	34
N	0.75 (0.26)	51 (8)	276 (83)	13.8 (7.1)	8.6 (5.9)	9.4 (7.2)	32
NE	1.43 (0.35)	62 (8)	439 (79)	33.4 (15.6)	28.3 (12.3)	14.2 (9.5)	20
LP	1.45 (0.50)	62 (12)	612 (255)	35.7 (25.7)	28.8 (25.2)	16.3 (14.8)	44
<i>TS Summer</i>							
S	0.75 (0.35)	75 (15)	434 (126)	24.4 (12.0)	21.5 (11.2)	3.5 (3.6)	27
W	0.72 (0.28)	79 (16)	426 (181)	27.1 (7.5)	24.0 (7.4)	6.6 (7.4)	12
NW	0.07 (0.03)	65 (5)	135 (34)	6.0 (2.4)	5.4 (2.0)	0.5 (0.7)	8
N	0.97 (0.48)	82 (13)	398 (99)	25.7 (8.8)	22.0 (7.6)	6.2 (4.7)	20
LP	0.75 (0.40)	72 (13)	495 (227)	23.5 (11.5)	20.2 (11.0)	8.7 (7.8)	71
EA	1.28 (0.74)	80 (22)	414 (180)	26.2 (12.1)	22.8 (10.8)	15.4 (12.5)	49
ME	0.36 (0.22)	52 (12)	440 (196)	15.5 (9.9)	14.2 (9.2)	5.3 (6.7)	38

^aS: air masses passing over eastern China arriving at the site from the southeast or south; W: air masses originating from central China arriving at the site from the southwest or west; NW: continental air masses from the northwest; N: air masses coming from the north; NE: air masses originating in the Northeast Plains; LP: loopy trajectories over the North China Plains; EA: air masses passing over the Korean Peninsula and Japan; ME: maritime air masses making relatively short journeys over the eastern coastal areas of China.

^bThe means (standard deviations) are in ppbv.

^cn is the number of three-hour data of PAN.

In the spring study, the mean PAN mixing ratio (1.45 ± 0.50 ppbv) in the LP group was the highest among the six categories, which can be explained by the slow movement of air passing over the North China Plains with strong anthropogenic emissions. In the S and NE categories, the levels of PAN (1.42 ± 0.47 ppbv in the S group and 1.43 ± 0.35 ppbv in the NE group) were comparable to those in the LP group. These results indicate that pollutants emitted from the highly urbanized regions of eastern China, and especially the Yangtze River delta and the highly industrialized region of the Northeast Plains, contribute greatly to the high levels of PAN in the air masses arriving at the summit of Mt. Tai. The similarly high concentrations of PAN in the NE, LP, and S categories reflect the severe pollution in coastal China, with no significant difference between regions in the north and south.

The air masses from the northwest and north contained relatively low levels of PAN, with mean values of 0.66 ppbv (± 0.28) and 0.75 ppbv (± 0.26) in the NW group and N group, respectively. Figure 8-1 indicates that the air masses in the NW group mostly come from the upper troposphere (at about 6 km above ground level (AGL)) over the remote Arctic and Siberian regions, whereas the air masses in the N group generally originate from the remote central Eurasian continent and travel at a high speed, suggesting relatively short residence times over highly polluted northern China.

Other trace gases also occurred at their highest levels in the LP or S groups and at their lowest levels in the NW or N groups. In addition, the comparably high concentrations of O₃, CO, and SO₂ in the W group indicate the impact of emissions from central China, probably from the industrial areas in the highlands of Shanxi province.

In the summer study, the air masses in the S, W, and LP groups showed evidence of photochemical pollution in the industrialized and urbanized regions of China, with mean PAN mixing ratios of 0.75 ppbv (± 0.35), 0.72 ppbv (± 0.28), and 0.75 ppbv (± 0.40), respectively, for the three groups. Consistent with the spring study, the air masses in the NW group contained the lowest level of PAN (0.07 ± 0.03 ppbv), although this category accounts for only 3% of the trajectories in summer. Although the air masses in the ME category pass over the eastern coastal regions, the PAN concentration (0.36 ± 0.22 ppbv) was much lower than in the S and LP categories, mainly due to the faster traveling speed and the shorter residence time of these air masses over the polluted coastal areas.

The mean PAN mixing ratio of the N group in the summer (0.97 ± 0.48 ppbv) was higher than those of the S, W, and LP groups, which is the opposite of the spring results. Moreover, O₃ had the highest average concentration (82 ± 13 ppbv) in the N group in summer. Careful inspection of the trajectories reveals that the air masses in summer travel much more slowly and originate at a lower

altitude (figure not shown). Stronger convective activities in the summer further result in an increase in the influence of emissions from northern China, and especially from Beijing, Tianjin, and Ji'nan, which are located along the pathways of the air masses in the N group.

One of the interesting findings of the TS Summer study was that the EA category, which accounts for 20% of the total trajectories, had the highest mean PAN concentration (1.28 ± 0.74 ppbv) among the seven categories, and the levels of other trace gases in this category were also high (see Table 8-1). This may indicate a significant contribution of pollution from Korea or Japan. Nevertheless, it must be remembered that back trajectory analysis is a simple tool for exploring the sources of pollutants that has limitations when considering vertical mixing or dispersion processes. It seems doubtful that long-range transport over about 600 km could cause such high concentrations of these trace gases. Additional analyses with more meteorological modeling are thus needed to verify the results of the back trajectory analysis.

8.2. Western China

8.2.1. Overall results

As mentioned in Chapter 5 (see Figure 5-4), three major types of air masses were sampled in the WLG study. The first type was characterized by high

concentrations of O₃ and low concentrations of PAN and of primary gases, and was identified between July 24 and 27. The back trajectory analysis revealed that the first type of air masses mainly came from the northwest, and had the characteristics of upper tropospheric air. The second type was marked by relatively higher levels of PAN, CO, and NO_y, and was measured in the first few days of August. The back trajectory analysis indicated that this type of air mass mainly came from the northeast. The third type was rather complicated. The air mainly came from the east and southeast and contained moderate concentrations of PAN, CO, and NO_y and lower concentrations of O₃. The six regional transport cases all occurred with this type of air masses. A detailed explanation of these cases is given in Section 8.2.2.

About 200 back trajectories (see Section 4.3) were calculated for the study period at WLG, and were classified into three categories: the NWW group, which comprises air masses originating from central Asia, passing over Xinjiang province of China at a high speed, and arriving at the site from west or northwest; the NNE group, which refers to air masses coming from the north or northeast that originated from Mongolia and moved over Inner Mongolia and Gansu province of China; and the SE group, which consists of air masses coming from the east or south that passed through the PBL over southern and central China. The SE category accounts for 51% of the total trajectories, followed by the NWW (22%) and NNE (20%) categories. Seven percent of the trajectories in the

WLG study are not classified.

Mixing ratios of PAN and other trace gases were averaged to three-hour concentrations, and results for the classification are summarized in Table. Air masses from the eastern region contained the highest levels of PAN, which showed the impact of pollution transport from urbanized areas of China, whereas air masses from the western region contained the lowest. The average PAN mixing ratios were 0.36 (\pm 0.07) ppbv in the NWW group, 0.43 (\pm 0.09) ppbv in the NNE group, and 0.49 (\pm 0.13) ppbv in the SE group. The values in the SE group were higher than those in the NNE group with a larger standard deviation, which is in accordance with the occurrence of the transport cases.

Table 8-2. Statistical data on PAN, O₃, CO, and NO_y in each air mass category captured at WLG^a.

	Mean (standard deviation) ^b				n ^c
	PAN	O ₃	CO	NO _y	
NWW	0.36 (0.07)	64 (4)	120 (35)	1.1 (0.5)	42
NNE	0.43 (0.09)	62 (7)	147 (40)	1.5 (0.6)	38
SE	0.49 (0.13)	56 (7)	168 (50)	1.6 (0.6)	96

^aNWW: air masses coming from west or northwest; NNE: air masses coming from north or northeast; SE: air masses coming from south or east.

^bThe means (standard deviations) are in ppbv.

^cn is the number of three-hour data of PAN.

Consistent with the results of PAN, primary pollutants (CO and NO_y) also showed highest concentrations in the SE category, while lowest concentrations in the NWW category. On the contrary, O₃, which has natural source, showed

opposite results with highest levels in the NWW group and lowest levels in the SE group. This is mainly due to the descending transport of O₃-rich air from upper troposphere. These results demonstrate that PAN is a much better indicator of photochemical pollution, comparing with O₃.

8.2.2. Case study of pollution transport to Mt. Waliguan

Although the presence of trace gases at WLG is strongly influenced by air masses from remote places in western China and Central Asia, regional pollution from the east can also affect the air composition over WLG (Wang et al., 2006b). During the study in 2006 summer, this impact was evident. The six cases of regional transport marked in Figure 5-4 are shown in detail in Figure 8-2. In four of the six cases, that is, in all except those on Aug 7 and 8, air masses containing highly elevated PAN concentrations arrived at the site at around 2000 BJT, a time of a day when the in situ formation of PAN can be excluded. The other gases also increased sharply in concentration along with PAN. These plumes lasted for 2 to 6 hours, corresponding to a plume width of 36 - 108 km at an average wind speed of 5 m/s. This suggests that the plumes originated in large area sources and had experienced relatively weak dispersion and mixing since emission. On Aug 7, the plumes arrived at the site in the morning, and on Aug 8 they arrived at night. In both cases, they lasted for more than 8 hours, which suggests a longer transport time or stronger dispersion since their emission from the sources.

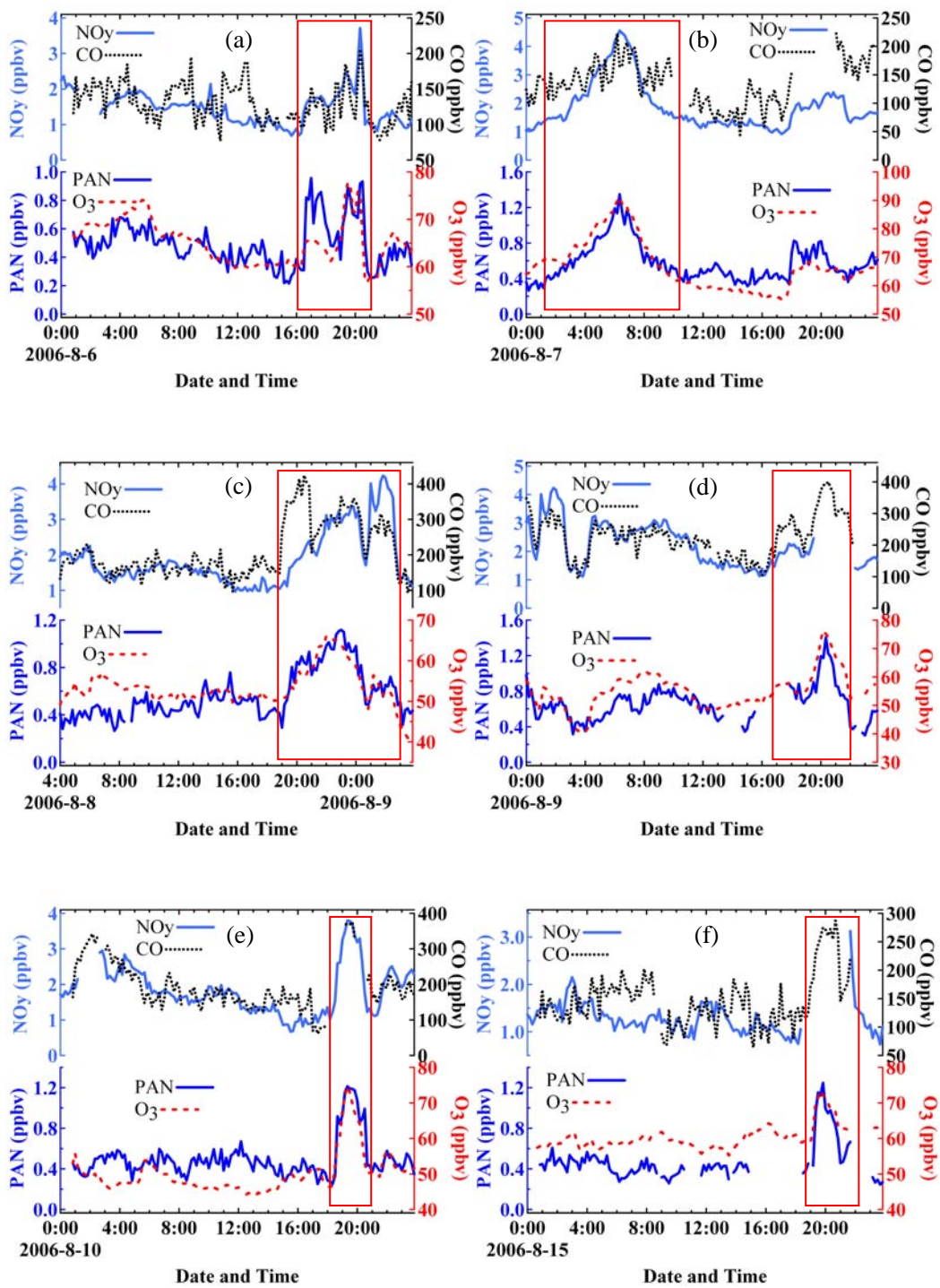


Figure 8-2. 10-min data for PAN, O₃, CO, and NO_y measured at WLG on (a) Aug 6, (b) Aug 7, (c) Aug 8, (d) Aug 9, (e) Aug 10, and (f) Aug 15.

To elucidate the source regions of the transport cases, 48-h back trajectories were calculated (see Section 4.3). Consistent with the foregoing discussion, the results of the back trajectory analysis (see Figure 8-3) showed that during all six periods of the regional transport cases, the majority of the air mass trajectories passed over the Lanzhou urban area from the east, reflecting the predominant contribution of Lanzhou urban emissions to the remote study site at WLG.

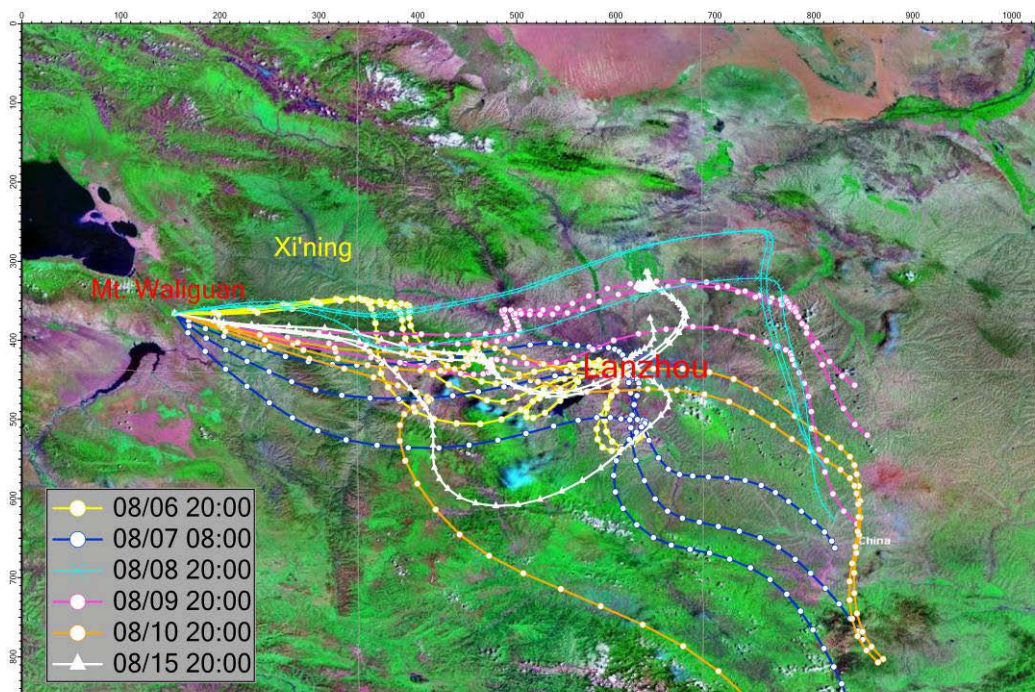


Figure 8-3. Back trajectories showing the impact of LZ on WLG in six cases.

(HYSPLIT 48-hour trajectory, GDAS data: 100 km, 3-h)

Figure 8-4a-f shows the distributions of the particle plumes as calculated from the Lagrangian backward dispersion simulation (see Section 4.3) at the time of the peaks on Aug 7, 8, and 10. In the figure, the transport times (ages) of the particles before arrival at the WLG receptor are color-coded to indicate the history of the observed air masses, with red denoting the oldest particles. The left panel shows the results for all of the vertical levels and the right panel shows the results for altitudes below 1 km (AGL) to indicate the transport and dispersion of particles in the PBL. In accordance with Figure 8-3, Figure 8-4 confirms that the plumes measured at WLG in these three cases can all be traced back to Lanzhou, but rarely passed over Xining, the second largest source area in the region that is in fact closer to WLG than LZ. This may be attributable to the blocking effect of the mountains between Mt. Waliguan and Xining (see the topographical map in Figure 4-2).

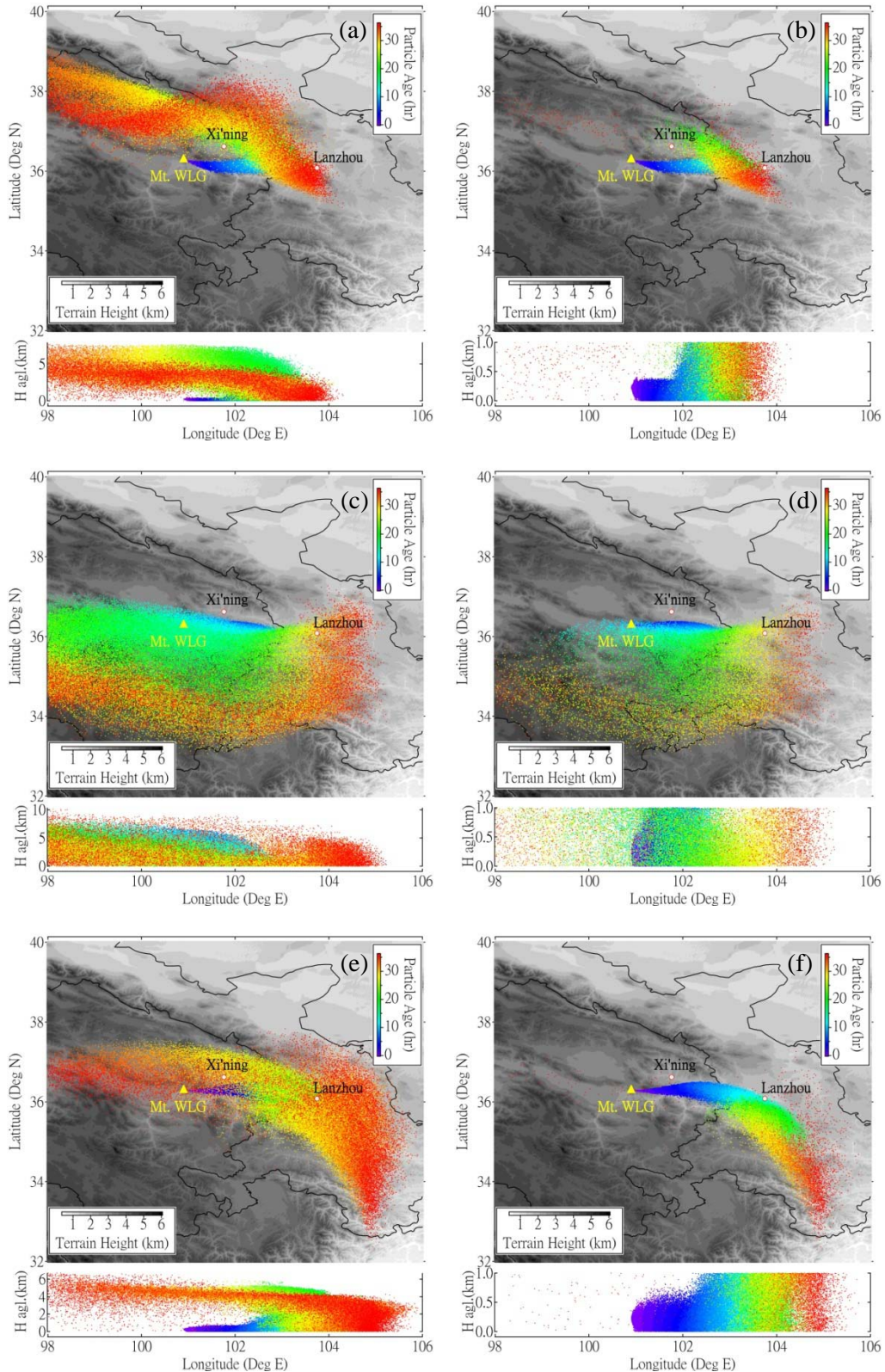


Figure 8-4. Horizontal and vertical distribution of 36-h backward Lagrangian particle plumes at the peak hour of episodes on (a and b) Aug 7, (c and d) Aug 8, and (e and f) Aug 10, 2006. The particles are color-coded by age to show their historical distribution. The left panel shows the results for all vertical levels and the right panel shows the results for altitudes below 1 km (AGL).

A closer examination of Figure 8-4 indicates different transport and dispersion characteristics in the three cases. In the Aug 7 case, the air mass had a long residence time over Lanzhou before arriving at WLG from the east, as indicated by the numerous particles around the city shown in Figure 8-4a and b. The transport time from LZ to WLG was about 1 day. In contrast, the air in the Aug 8 case came from the east in the PBL and mixed with remote air over the southeastern mountain areas, as indicated by the large spread of particles in Figure 8-4c and d. The transport time from LZ was over 30 hours. The longer transport time from LZ and the stronger mixing on Aug 8 explains the more moderate peaks of PAN and O₃ and the less well-defined plume compared with the case on Aug 7. In the Aug 10 case, the air masses had a similar transport history to the Aug 7 case, but had a much faster transport speed and a poorer dispersion in the PBL (indicated by the tight particle distribution in Figure 8-4e and f), which is consistent with the much narrower plume observed on this day.

For the other three cases shown in Figure 8-2, the particle simulation results (figures not shown) were similar to those for Aug 10, indicating fast transport from the east and poorer dispersion, which is again consistent with the observed sharp peaks of trace gases observed around 2000 BJT on these days at WLG. Weather charts show that these cases were mostly associated with a band of high pressure located in the north that caused strong easterly winds in the lower troposphere (figure not shown).

CHAPTER 9: CONCLUSIONS

9.1. Summary of the major scientific findings

Peroxyacetyl nitrate, in conjunction with ozone and other trace gases, was continuously measured at an urban site (in Hong Kong, HK), a suburban site (in Lanzhou, LZ), a rural site (Mt. Tai, TS), and a remote site (Mt. Waliguan, WLG) in different regions of China in 2006 and 2007. The results provide useful insights into photochemical pollution in industrialized regions of China, pollution transport between areas, and the background chemistry over the remote Qinghai-Tibet Plateau. The main findings are summarized as follows.

- (1) The measurements in Lanzhou showed rather serious photochemical pollution, with a maximum PAN value of 9.13 ppbv and a peak O₃ value of 161 ppbv. In comparison, peak concentrations of PAN as high as 7.44 ppbv were detected in Hong Kong during photochemical episodes. Spring and summer studies at Mt. Tai reflected severe regional air pollution in eastern China, with mean concentrations of PAN and other trace gases all higher than those measured at Lanzhou. The concentrations of PAN were much higher in spring than in summer, with average values of 1.17 ± 0.55 ppbv in the former and 0.78 ± 0.58 ppbv in the latter. Summertime baseline concentrations of PAN in western

China were observed at WLG to have an average mixing ratio of 0.44 (\pm 0.16) ppbv.

(2) PAN exhibited a strong diurnal pattern at Lanzhou, peaking at noon due to intense local photochemical production. Diurnal variations in PAN typical to urban areas were also observed in HK, with elevated concentrations in the early afternoon. In the Mt. Tai studies, the PAN and O₃ concentrations revealed photochemical production in the regional air masses, with afternoon peaks in both phases. The possible transport of pollutants emitted from southwestern sources in spring was indicated by a second peak for PAN and other gases in the evening. At WLG, the elevated concentrations of PAN in the evening suggest the transport of regional pollution.

(3) The daily maximum values of PAN and O₃ showed a strong correlation ($r^2 = 0.91$) in Lanzhou, with a slope of PAN/O₃ of 0.091 ppbv ppbv⁻¹ that implies that, on average, 9 PAN molecules are produced for every 100 O₃ molecules formed in the Lanzhou airshed. The relatively high PAN/O₃ ratios imply abundant PAN precursors in the VOCs in Lanzhou. The regression slope of the PAN daily maximum/O₃ daily maximum was 0.059 ppbv ppbv⁻¹ in the HK 07 study ($r^2 = 0.70$), which reflects the moderate level of PAN precursors in Hong Kong. In contrast to those for

Lanzhou, the slopes for the TS studies were further reduced to 0.034 ppbv ppbv⁻¹ ($r^2 = 0.29$) and 0.026 ppbv ppbv⁻¹ ($r^2 = 0.66$) in spring and summer, respectively, implying that approximately 3 PAN molecules are produced for every 100 O₃ molecules in the air masses arriving at the summit of Mt. Tai. These ratios in the TS studies indicate that the VOC precursors of secondary pollutants are mainly O₃ precursors, and the photochemical transformation of primary pollutants in eastern China appears not to favor the formation of PAN.

(4) A nitrogen budget analysis at Mt. Tai revealed that Total N (sum of HNO₃ and p-NO₃⁻) contributed 78% and 87% to the total NO_y in spring and summer, respectively, whereas PAN contributed only 4.4% and 3.3%. This implies that inorganic chemistry has a more dominant role in the polluted atmosphere of the North China Plains. In contrast, a much higher contribution of PAN was found at WLG (32%), which is comparable to other studies at high altitudes over continental areas and indicates that PAN is an important reservoir of NO_y in the troposphere in remote areas.

(5) Back trajectory analysis at Mt. Tai showed that air masses originating and passing over coastal regions of China contained higher concentrations of PAN in both spring and summer, whereas the

descending continental air from the northwest was the cleanest. Air masses traveling from the north in the summer indicate the possible contribution of pollutants from Beijing, Tianjin, and Ji'nan at the summit of Mt. Tai. The highest PAN concentrations (1.28 ± 0.74 ppbv on average) in the summertime trajectories appeared in the EA group, which comprises air masses passing over the Korean Peninsula or Japan.

(6) Results of back trajectory analysis at WLG show that PAN is a better indicator of photochemical pollution in remote areas, compared with O₃. Air masses from polluted eastern regions had the highest PAN, while O₃ was highest in the air masses from remote western areas. The transport of photochemically aged air masses to WLG from Lanzhou in the east was observed in six well-identified cases in which PAN and other trace gases (O₃, CO, and NO_y) all occurred in greatly elevated concentrations over their respective background levels. Particle release simulation proved to be useful in tracing the possible source area of the polluted air masses observed at the remote WLG site.

9.2. Suggestions for future work

Field study

In this project, PAN data were obtained in field studies at four sites in three

major regions of China. The measurements were taken for durations of between one and three months on each site. In future, it would be interesting to obtain more information on seasonal and annual variations in PAN in China, and it is recommended that long-term field studies be carried out for this purpose.

For the HK site, it is suggested that other trace gases, such as O₃, CO, and NO_y, be measured concurrently with PAN in future to obtain knowledge of the relationships between PAN and these gases in HK and for comparison with the results from the LZ, TS, and WLG studies.

Chemical and meteorological modeling

As PAN occurred in different concentrations, patterns, and relationships with O₃ and other gases in the different environments, modeling might be a useful and convenient tool for further exploring the mechanisms of PAN formation, transformation, and decomposition. The parameters of such chemical models could be set for various conditions to study the major factors affecting PAN characteristics, such as the PAN/O₃ ratio.

The results of such modeling could also be compared with ambient data from field studies. Satellite data including NO or NO₂ and emission inventory data such as CO can be used directly or can be input into chemical and transport models to provide independent validation of the key findings of the present work.

Meteorological data and other modeling tools could also be used to further study the sources of high PAN concentrations in the “East Asian” air masses in the summer study at Mt. Tai.

REFERENCES

- Altshuller, A.P., 1983. Measurements of the products of atmospheric photochemical reactions in laboratory studies and in ambient air-relationships between ozone and other products. *Atmospheric Environment* 17, 2383-2427.
- Beine, H.J., Krognes, T., 2000. The seasonal cycle of peroxyacetyl nitrate (PAN) in the European Arctic. *Atmospheric Environment* 34, 933-940.
- Bottenheim, J.W., Barrie, L., Atlas, A.E., 1993. The partitioning of nitrogen oxides in the lower Arctic troposphere during spring 1988. *Journal of Atmospheric Chemistry* 17, 15-27.
- Bottenheim, J.W., Sirois, A., Brice, K.A., Gallant, A.J., 1999. Five years of continuous observations of PAN and ozone at a rural location in eastern Canada. *Journal of Geophysical Research* 99, 5333-5352.
- Brasseur, G.P., Orlando, J.J., Tyndall, G.S., 1999. *Atmospheric Chemistry and Global Change*. Oxford University Press, New York, USA.
- Bridier, I., Caralp, F., Loirat, H., Lesclaux, R., Veyret, B., Becker, K.H., Reimer, A., Zabel, F., 1991. Kinetic and theoretical studies of the reaction $\text{H}_3\text{CC}(\text{O})\text{O}_2 + \text{NO}_2 + \text{M} \leftrightarrow \text{H}_3\text{CC}(\text{O})\text{O}_2\text{NO}_2 + \text{M}$ between 248 and 393 K and between 30 and 760 torr. *Journal of Physical Chemistry* 95, 3594-3600.
- Calvert, J.G., Lazfus, A., Kok, G.L., Heikes, B.G., Walega, J.G., Ling, J., Cantrell, C.A., 1985. Chemical mechanisms of acid generation in the troposphere, *Nature* 317, 27.
- Cox, R.A., Roffey, M.J., 1977. Thermal decomposition of peroxyacetyl nitrate in the presence of nitric oxide. *Environmental Science and Technology* 11, 900-906.
- Dassau, T.M., Shepson, P.B., Bottenheim, J.W., Ford, K.M., 2004. Peroxyacetyl nitrate photochemistry and interactions with the Arctic surface. *Journal of Geophysical Research* 109, D18302, doi: 10.1029/2004JD004562.
- Ding, A.J., Wang, T., Zhao, M., Wang, T.J., Li, Z.K., 2004. Simulation of sea-land breezes and a discussion of their implications on the transport of air pollution during a multi-day ozone episode in the Pearl River Delta of China. *Atmospheric Environment* 38, 6737-6750.
- Ding, A., Wang, T., 2006. Influence of stratosphere-to-troposphere exchange on the seasonal cycle of surface ozone at Mount Waliguan in western China, *Geophysical Research Letters*, 33, L03803, doi:10.1029/2005GL024760.

-
- Ding, A.J., Wang, T., Thouret, V., Cammas, J.-P., Nédélec, P., 2008. Tropospheric ozone climatology over Beijing: Analysis of aircraft data from the MOZAIC program. *Atmospheric Chemistry and Physics* 8, 1-13.
- Draxler, R.R., Hess, G.D., 1997. Description of the HYSPLIT_4 modeling system, NOAA Technical Memorandum ERL ARL-224, Air Resource Laboratory, Silver Spring, Maryland.
- Finlayson-Pitts, B.J., Pitts, J.N.Jr., 1986. *Atmospheric Chemistry: Fundamentals and Experimental Techniques*, Wiley Interscience, John Wiley and Sons, New York.
- Ford, K.M., Campbell, B.M., Shepson, P.B., Bertman, S.B., Honrath, R.E., Peterson, M., Dibb, J.E., 2002. Studies of peroxyacetyl nitrate (PAN) and its interaction with the snowpack at Summit, Greenland. *Journal of Geophysical Research* 107, D10, 4102, 10.1029/2001JD000547.
- Gaffney, J.S., Marley, N.A., Prestbo, E.W., 1989. Peroxyacyl nitrates (PANs): Their physical and chemical properties. In *The Handbook of Environmental Chemistry*, Hutzinger, O., Ed, Springer-Verlag: Berlin, Vol. 4, Part B, 1-38.
- Gaffney, J.S., Marley, N.A., Prestbo, E.W. 1993. Measurements of peroxyacetyl nitrate at a remote site in the southwestern United States: Tropospheric implications. *Environmental Science and Technology* 27, 1905-1910.
- Gaffney, J.S., Bornick, R.M., Chen, Y.-H., Marley, N.A., 1998. Capillary gas chromatographic analysis of nitrogen dioxide and PANs with luminal chemiluminescent detection. *Atmospheric Environment* 32, 1145-1154.
- Gaffney, J.S., Marley, N.A., Cunningham, M.M., Doskey, P.V., 1999. Measurements of peroxyacyl nitrates (PANs) in Mexico City: Implications for megacity air quality impacts on regional scales. *Atmospheric Environment* 33, 5003-5012.
- Gao, H., Zhou, L., Ma, M.Q., Chen, X.G., Hu, Z.D., 2004. Composition and source of unknown organic pollutants in atmospheric particulates of the Xigu District, Lanzhou, People's Republic of China. *Bulletin of Environmental Contamination and Toxicology* 72, 923-930.
- Gao, J., Wang, T., Ding, A.J., Liu, C.B., 2005. Observational study of ozone and carbon monoxide at the summit of Mount Tai (1534 m a.s.l.) in central-eastern China. *Atmospheric Environment* 39, 4779-4791.
- Glavas, S., Moschonas, N., 2001. Determination of PAN, PPN, PnBN and selected pentyl nitrates in Athens, Greece. *Atmospheric Environment* 35, 5467-5475.

-
- Grosjean, D., 1988. Aldehydes, carboxylic acids and inorganic nitrate during NSMCS. *Atmospheric Environment* 22, 1637-1648.
- Grosjean, D., 2003. Ambient PAN and PPN in southern California from 1960 to the SCOS97-NARSTO. *Atmospheric Environment* 37, S221-238.
- Grosjean, E., Grosjean, D., Woodhouse, L.F., 2001. Peroxyacetyl nitrate and peroxypropionyl nitrate during SCOS 97-NARSTO. *Environmental Science and Technology* 35, 4007-4014.
- Grosjean, E., Grosjean, D., Woodhouse, L.F., Yang, Y.J., 2002. Peroxyacetyl nitrate and peroxypropionyl nitrate in Porto Alegre, Brazil. *Atmospheric Environment* 36, 2405-2419.
- Guicherit, R., 1988. Ozone on an urban and regional scale – with special reference to the situation in the Netherlands. In: Isaksen ISA, editor. *Tropospheric Ozone: Regional and Global Scale Interactions NATO ASI Series C: Mathematical and Physical Sciences*. Dordrecht: D. Reidel, 49-62.
- Ho, K.F., Lee, S.C., Louie, P.K.K., and Zou, S.C., 2002. Seasonal variation of carbonyl compound concentration in urban area of Hong Kong. *Atmospheric Environment* 36, 1259 – 1265.
- Jacobi, H.-W., Weller, R. Jones, A.E., Anderson, P.S., Schrems, O., 2000. Peroxyacetyl nitrate (PAN) concentrations in the Antarctic troposphere measured during the photochemical experiment at Neumayer (PEAN'99). *Atmospheric Environment* 34, 5235-5247.
- Kligerman, A.D., Mottus, K., Erexson, G.L., 1995. Cytogenetic analyses of the in vitro and in vivo responses of murine cells to peroxyacetyl nitrate (PAN), *Mutat. Res.* 341, 199-206.
- Kourtidis, K.A., Fabian, P., Zerefos, C., Rappenglück, B., 1993. Peroxiacetyl nitrate (PAN), peroxypropionyl nitrate (PPN) and PAN/ozone ratio measurements at three sites in Germany. *Tellus* 45B, 442-457.
- Lin, J.K., Chen, K.J., Liu, G.Y., Chu, Y.R., Lin-Shiau, S.Y., 2000. Nitration and hydroxylation of aromatic amino acid and guanine by the air pollutant peroxyacetyl nitrate. *Chemico-Biological Interactions* 127, 219-236.
- Logan, J.A., 1989. Ozone in rural-areas of the United States. *Journal of Geophysical Research* 94 (D6), 8511-8532.
- Lonneman, W.A., Bufalini, J.J., Seila, R.L., 1976. PAN and oxidant measurement in ambient

-
- atmospheres. *Environmental Science and Technology* 10, 374-381.
- Louie, P.K.K., Chow, J.C., Chen, L.W.A., Watson, J.G., Leung, G., Sin, S.W.M., 2005. PM_{2.5} chemical composition in Hong Kong: Urban and regional variations, *Science of the Total Environment* 338, 267 – 281.
- Lovelock, J.E., 1977. PAN in the natural environment: Its possible significance in the epidemiology of skin cancer. *Ambio* 6, 131-133.
- Marley, N.A., Gaffney, J.S., Ramos-Villegas, R., Cárdenas González, B., 2007. Comparison of measurements of peroxyacyl nitrates and primary carbonaceous aerosol concentrations in Mexico City determined in 1997 and 2003. *Atmospheric Chemistry and Physics* 7, 2277-2285.
- McFadyen, G.G., Cape, J.N., 1999. Physical and chemical influences on PAN concentrations at a rural site. *Atmospheric Environment* 33, 2929-2940.
- McFadyen, G.G., Cape, J.N., 2005. Peroxyacetyl nitrate in eastern Scotland. *Science of the Total Environment* 337, 213-222.
- Muthuramu, K., Shepson, P.B., Bottenheim, J.W., Jobson, B.T., Niki, H., Anlauf, K.G., 1994. Relationships between organic nitrates and surface ozone destruction during Polar Sunrise Experiment 1992. *Journal of Geophysical Research* 99, 25369-25378.
- Müller, K.P., Rudolph, J., 1992. Measurements of peroxyacetyl nitrate in the marine boundary layer over the Atlantic. *Journal of Atmospheric Chemistry* 15, 361-367.
- Orlando, J.J., Tyndall, G.S., Calvert, J.G., 1992. Thermal decomposition pathways for peroxyacetyl nitrate (PAN): Implications for atmospheric methyl nitrate levels. *Atmospheric Environment* 26, 3111-3118.
- Peak, M.J., Belser, W.L., 1969. Some effects of the air pollutant, peroxyacetyl nitrate, upon deoxyribonucleic acid and upon nucleic acid bases. *Atmospheric Environment* 3, 385-397.
- Penkett, S.A., Brice, K.A., 1986. The spring maximum in photo-oxidants in the northern hemisphere troposphere. *Nature* 319, 655-657.
- Prestbo, E.W., 1992. Atmospheric chemistry and long-term measurements of peroxyacetyl nitrate and ozone at a remote location in Northern New Mexico. Thesis (Ph.D.), University of Washington, USA.
- Rappenglück, B., Kourtidis, K., Fabian, P., 1993. Measurements of ozone and peroxyacetyl nitrate (PAN) in Munich. *Atmospheric Environment* 27B, 293-305.

-
- Rappenglück, B., Melas, D., Fabian, P., 2003. Evidence of the impact of urban plumes on remote sites in the Eastern Mediterranean. *Atmospheric Environment* 37, 1853-1864.
- Rembges, D., Duane, M., Hjorth, J., Bloem, H., Zaiman, W., Larsen, B.R., 2001. PAN and air quality in northern Italy: Diurnal variation and longterm trends. In: Hjorth, J., Raes, F., Angeletti, G., editors, *A Changing Atmosphere*. Torino: JRC Ispra, A71.
- Renzetti, N.A., Ryan, R.J., 1961. Atmospheric sampling for aldehydes and eye irritation in Los Angeles smog 1960. *Journal of the Air Pollution Control Association* 17, 454-459.
- Roberts, J.M., Flocke, F., Weinheimer, A., Tanimoto, H., Jobson, B.T., Riemer, D., Apel, E., Atlas, E., Donnelly, S., Stroud, V., Johnson, K., Weaver, R., Fehsenfeld, F.C., 2001. Observations of APAN during TexAQS 2000. *Geophysical Research Letters* 28, 4195-4198.
- Roberts, J.M., Flocke F., Stroud, C.A., Hereid, D., Williams, E., Fehsenfeld, F., Brune, W., Martinez, M., Harder, H., 2002. Ground-based measurements of peroxy-carboxylic nitric anhydrides (PANs) during the 1999 Southern Oxidants Study Nashville Intensive. *Journal of Geophysical Research* 107, D21, 4554, doi:10.1029/2001JD000947.
- Roberts, J.M., Jobson, B.T., Kuster, W., Goldan, P., Murphy, P., Williams, E., Frost, G., Riemer, D., Apel, E., Stroud, C., Wiedinmyer, C., Fehsenfeld, F., 2003. An examination of the chemistry of peroxy-carboxylic nitric anhydrides and related volatile organic compounds during Texas Air Quality Study 2000 using ground-based measurements. *Journal of Geophysical Research* 108, D16, 4495, doi:10.1029/2003JD003383.
- Rubio, M.A., Oyola, P., Gramsch, E., Lissi, E., Pizarro, J., Villena, G., 2004. Ozone and peroxyacetyl nitrate in downtown Santiago, Chile. *Atmospheric Environment* 38, 4931-4939.
- Russo, R.S., Talbot, R.W., Dibb, J.E., Scheuer, E., Seid, G., Jordan, C.E., Fuelberg, H.E., Sachse, G.W., Avery, M.A., Vay, S.A., Blake, D.R., Blake, N.J., Atlas, E., Fried, A., Sandholm, S.T., Tan, D., Singh, H.B., Snow, J., Heikes, B.G., 2003. Chemical composition of Asian continental outflow over the western Pacific: Results from Transport and Chemical Evolution over the Pacific (TRACE-P). *Journal of Geophysical Research* 108 (D20), 8804, doi: 10.1029/2002JD003184.
- Sandholm, S., Olsen, J., Bradshaw, J., Talbot, R., Singh, H., Gregory, G., Blake, D., Anderson, B., Sachse, G., Barrick, J., Collins, J., Klemm, K., Lefer, B., Klemm, O., Gorzelska, K., Herlth, D., O'Hara, D., 1994. Summertime partitioning and budget of NO_y compounds in the troposphere over Alaska and Canada: ABL3B. *Journal of*

Geophysical Research 99, 1837-1861.

Schmitt, R., Volz-Thomas, A., 1997. Climatology of ozone, PAN, CO and NMHC in the free troposphere over the Southern North Atlantic. *Journal of Atmospheric Chemistry* 28, 245-262.

Schrimpf, W., Lienaerts, K., Müller, K.P., Koppmann, R., Rudolph, J., 1998. Peroxyacetyl nitrate (PAN) measurements during the POPCORN Campaign. *Journal of Atmospheric Chemistry* 31, 139-159.

Seinfeld, J.H., Pandis, S.N., 1998. *Atmospheric Chemistry and Physics: From Air Pollution to Climate Change*, Wiley Interscience, John Wiley and Sons, New York, 294-295.

Senum, G.I., Lee, Y.N., Gaffney, J.S., 1984. Ultraviolet absorption spectrum of peroxyacetyl nitrate and peroxypropionyl nitrate. *Journal of Physical Chemistry* 88, 1269-1270.

Singh, H.B., 1987. Reactive nitrogen in the troposphere. *Environmental Science and Technology* 21, 320-327.

Singh, H.B., Salas, L. J., 1989. Measurements of peroxyacetyl nitrate (PAN) and peroxypropionyl nitrate (PPN) at selected urban, rural, and remote sites. *Atmospheric Environment* 23, 231-238.

Sirois, A., Bottenheim, J.W., 1995. Use of backward trajectories to interpret the 5-year record of PAN and O₃ ambient air concentrations at Kejimikujik National Park, Nova Scotia. *Journal of Geophysical Research* 100:2867-2881.

Spicer, C.W., Holdren, M.W., Keigley, G.W., 1983. The ubiquity of peroxyacetyl nitrate in the continental boundary layer. *Atmospheric Environment* 17, 1055-1058.

Stephens, E.R., Hanst, P.L., Dörr, R.C., Scott, W.E., 1956. Reactions of nitrogen dioxide and organic compounds in air. *Industrial and Engineering Chemistry* 48, 1498-1504.

Stephens, E.R., 1969. The formation, reactions and properties of peroxyacyl nitrates (PANs) in photochemical air pollution. *Advances in Environmental Sciences and Technology* 1, 119-146.

Stohl, A., Foster, C., Eckhardt, S., Spichtinger, N., Huntrieser, H., Heland, J., Schlager, H., Wilhelm, S., Arnold, F., Cooper, O., 2003. A backward modeling study of intercontinental pollution transport using aircraft measurements, *Journal of Geophysical Research*, 108, D12, 4370, doi:10.1029/2002JD002862.

Streets, D.G., Zhang, Q., Wang, L.T., He, K.B., Hao, J.M., Wu, Y., Tang, Y. H., Carmichael, G. R., 2006. Revisiting China's CO emissions after the transport and chemical

-
- evolution over the Pacific (TRACE-P) mission: Synthesis of inventories, atmospheric modeling, and observations. *Journal of Geophysical Research*, 111, D14, D14306.
- Talukdar, R.K., Burkholder, J.B., Schmoltner, A.M., Roberts, J.M., Wilson, R.R., Ravishankara, A.R., 1995. Investigation of the loss processes for peroxyacetyl nitrate in the atmosphere: UV photolysis and reaction with OH. *Journal of Geophysical Research* 100, 14163-14173.
- Tanimoto, H., Furutani, H., Kato, S., Matsumoto, J., Makide, Y., Akimoto, H., 2002. Seasonal cycles of ozone and oxidized nitrogen species in northeast Asia – 1. Impact of regional climatology and photochemistry observed during RISOTTO 1999-2000. *Journal of Geophysical Research* 107, D24, 4747, doi:10.1029/2001JD001496.
- Tsalkani, N., Mellouki, A., Poulet, G., Toupance, G., LeBras, G., 1988. Rate constant measurement for the reactions of OH and Cl with peroxyacetyl nitrate at 298 K. *Journal of Atmospheric Chemistry* 7, 409-419.
- US Department of Health Education and Welfare, 1970. Air Quality criteria for photochemical oxidants. Washington, DC, US DHEW (National Air Pollution Control Administration Publication No. AP 63).
- Wang, T., Poon, C.N., Kwok, Y.H., Li, Y.S., 2003. Characterizing the temporal variability and emission patterns of pollution plumes in the Pearl River Delta of China. *Atmospheric Environment* 37, 3539-3550.
- Wang, T., Ding, A.J., Gao, J., Wu, W.S., 2006. Strong ozone production in urban plumes from Beijing, China. *Geophysical Research Letters* 33, L21806, doi: 10.1029/2006GL027689.
- Wang, T., Wong, H.L.A., Tang, J., Ding, A., Wu, W.S., Zhang, X.C., 2006. On the origin of surface ozone and reactive nitrogen observed at a remote mountain site in the northeastern Qinghai-Tibetan Plateau, western China. *Journal of Geophysical Research* 111, D08303, doi:10.1029/2005JD006527.
- Watanabe, I., Nakanishi, M., Tomita, J., Hatakeyama, S., Murano, K., Mukai, H., Bandou, H., 1998. Atmospheric peroxyacetyl nitrates in urban/remote sites and the lower troposphere around Japan. *Environmental Pollution* 102, 253-261.
- Whalley, L.K., Lewis, A. C., McQuaid, J.B., Purvis, R. M., Lee, J.D., Stemmler, K., Zellweger, C., Ridgeon, P., 2004. Two high-speed, portable GC systems designed for the measurement of non-methane hydrocarbons and PAN: Results from the Jungfrauoch High Altitude Observatory. *Journal of Environmental Monitoring* 6, 234-241.

-
- Williams, E.J., Grosjean, E., Grosjean, D., 1993. Ambient levels of the peroxyacylnitrates PAN, PPN, and MPAN in Atlanta Ga. *Journal of Air Waste Management Association* 43, 873-879.
- Williams, J., Roberts, J.M., Bertman, S.B., Stroud, C.A., Fehsenfeld, F.C., Baumann, K., Buhr, M.P., Knapp, K., Murphy, P.C., Novick, M., Williams, E.J., 2000. A method for the airborne measurement of PAN, PPN and MPAN, *Journal of Geophysical Research* 105, 28943-28960.
- Wong, H.L.A., Wang, T., Ding, A., Blake, D.R., Nam, J.C., 2007. Impact of Asian continental outflow on the concentrations of O₃, CO, NMHCs and halocarbons on Jeju Island, South Korea during March 2005. *Atmospheric Environment* 41, 2933-2944.
- Zellweger C., Ammann, M., Buchmann, B., Hofer, P., Lugauer, M., Rüttimann, R., Streit, N., Weingartner, E., Baltensperger, U., 2000. Summertime NO_y speciation at the Jungfraujoch, 3580 m above sea level, Switzerland. *Journal of Geophysical Research* 105, 6655-6667.
- Zellweger, C., Forrer, J., Hofer, P., Nyeki, S., Schwarzenbach, B., Weingartner, E., Ammann, M., Baltensperger, U., 2002. Partitioning of reactive nitrogen (NO_y) and dependence on meteorological conditions in the lower free troposphere. *Atmospheric Chemistry and Physics Discussions* 2, 2259-2296.
- Zhang, J., Wang, T., Chameides, W.L., Cardelino, C., Kwok, J., Blake, D.R., Ding, A., So, K.L., 2007. Ozone production and hydrocarbon reactivity in Hong Kong, Southern China. *Atmospheric Chemistry and Physics* 7, 557-573.
- Zhang, J.B., Tang, X.Y., 1994. Atmospheric PAN measurements and the formation of PAN in various systems. *Environmental Chemistry* 13, No. 1, 30-39.
- Zhang, L., Chen, C.H., Li, S.X., Zhang, F., 2000. Air pollution and potential control schemes in Lanzhou. *Research of Environmental Sciences* 13, 18-21.
- Zhou, L.X., Tang, J., Wen, Y.P., Li, J.L., Yan, P., Zhang, X.C., 2003. The impact of local winds and long-range transport on the continuous carbon dioxide record at Mount Waliguan, China. *Tellus* 55B, 145-158.